

Calixarene-based amphiphiles: Synthesis, Self-assembly and Interaction with DNA

Inauguraldissertation

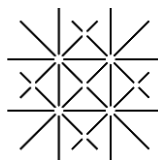
zur

Erlangung der Würde eines Doktors der Philosophie

vorgelegt der

Philosophisch-Naturwissenschaftlichen Fakultät

der Universität Basel



U N I
B A S E L

von

Vanessa Rullaud

Aus France

Basel, 2015

Original document stored on the publication server of the University of Basel

edoc.unibas.ch



This work is licenced under the agreement

„Attribution Non-Commercial No Derivatives – 3.0 Switzerland“ (CC BY-NC-ND 3.0 CH). The complete text
may be reviewed here:

creativecommons.org/licenses/by-nc-nd/3.0/ch/deed.en

Genehmigt von der Philosophisch-Naturwissenschaftlichen Fakultät auf
Antrag von

Prof. Dr. Patrick Shahgaldian

Prof. Dr. Thomas Ward

Prof. Dr. Wolfgang Meier

Basel, den 9 Dezember 2014

Prof. Dr. Jörg Schibler

Dekan



Namensnennung-Keine kommerzielle Nutzung-Keine Bearbeitung 3.0 Schweiz
(CC BY-NC-ND 3.0 CH)

Sie dürfen: **Teilen** — den Inhalt kopieren, verbreiten und zugänglich machen

Unter den folgenden Bedingungen:



Namensnennung — Sie müssen den Namen des Autors/Rechteinhabers in der von ihm festgelegten Weise nennen.



Keine kommerzielle Nutzung — Sie dürfen diesen Inhalt nicht für kommerzielle Zwecke nutzen.



Keine Bearbeitung erlaubt — Sie dürfen diesen Inhalt nicht bearbeiten, abwandeln oder in anderer Weise verändern.

Wobei gilt:

- **Verzichtserklärung** — Jede der vorgenannten Bedingungen kann **aufgehoben** werden, sofern Sie die ausdrückliche Einwilligung des Rechteinhabers dazu erhalten.
- **Public Domain (gemeinfreie oder nicht-schützbar Inhalte)** — Soweit das Werk, der Inhalt oder irgendein Teil davon zur Public Domain der jeweiligen Rechtsordnung gehört, wird dieser Status von der Lizenz in keiner Weise berührt.
- **Sonstige Rechte** — Die Lizenz hat keinerlei Einfluss auf die folgenden Rechte:
 - Die Rechte, die jedermann wegen der Schranken des Urheberrechts oder aufgrund gesetzlicher Erlaubnisse zustehen (in einigen Ländern als grundsätzliche Doktrin des **fair use** bekannt);
 - Die **Persönlichkeitsrechte** des Urhebers;
 - Rechte anderer Personen, entweder am Lizenzgegenstand selber oder bezüglich seiner Verwendung, zum Beispiel für **Werbung** oder Privatsphärenschutz.
- **Hinweis** — Bei jeder Nutzung oder Verbreitung müssen Sie anderen alle Lizenzbedingungen mitteilen, die für diesen Inhalt gelten. Am einfachsten ist es, an entsprechender Stelle einen Link auf diese Seite einzubinden.

Contents

<i>Abbreviations and Acronyms</i>	1
<i>Aim</i>	3
1 <i>Introduction</i>	7
1.1 <i>Supramolecular Chemistry</i>	7
Background.....	7
Biological Self-Assembly: Functions and Informations.....	8
Bio-Inspired Self-Assembly	11
Supramolecular Self-Assembly of Macrocycles	15
1.2 <i>Self-Assembly of Amphiphilic Calixarenes as Langmuir Films at the Air-Water Interface</i>	20
Interaction with Ions	24
Interaction with Transition Metal Ions	25
Interaction with Pharmaceutical Molecules.....	26
Calixarene Langmuir Films: Protein Interactions.....	27
Calixarene Langmuir Films: DNA Binding	29
1.3 <i>Gene Therapy</i>	31
Viral Vectors	32
Non-Viral Vectors	32

1.4 Self-Assembly of Calixarenes in Aqueous Solution	34
Amphiphilic Calixarenes and Self-Assembly as Nanoparticles	34
Interaction with Proteins.....	36
Interaction with DNA Molecules	37
1.5 Layer-by-Layer Self-Assembly.....	45
Core-Shell Nanoparticles as DNA Vectors	48
References.....	50
2 <i>Synthesis and Characterization of Calixarene Derivatives...</i>	67
2.1 Upper Rim Functionalization	68
Synthesis of 5,11,17,23-tetra(guanidinium)-25,26,27,28-tetra(dodecyloxy)-calix[4]arene (GC12).....	68
Synthesis of <i>p</i> -amino-25,26,27,28-tetra(dodecyloxy)-calix[4]arene derivatives.....	71
2.2 Lower Rim Functionalization	75
Tetrasubstitution of <i>p</i> -acyl-calix[4]arene	75
Selective Disubstitution of <i>p</i> -diacyl-calix[4]arene	77
Conclusions	79
References.....	80
3 <i>Calixarene Langmuir Films: Self-Assembly and DNA Interaction Study.....</i>	83
3.1 GC12 Self-Assembly as Langmuir Monolayer and DNA Interaction	84

3.2 Amino-Calix[4]arene Derivatives Self-Assembly as Langmuir Monolayers and DNA Interaction	93
Conclusions	99
References.....	101
4 Calixarene-Based Nanoparticles: DNA-Binding Study	103
4.1 Calixarene-Based Nanoparticles: Preparation and Characterization	104
4.2 Calixarene-Based Nanoparticles: Interaction with DNA ..	111
Ethidium Bromide Displacement Assay	111
Circular Dichroism Spectroscopy (CD)	117
Isothermal Titration Calorimetry (ITC)	120
4.3 Calixarene-Based Nanoparticles: Layer-by-Layer Coating	122
4.4 Calixarene-DNA Complexes: Self-Assembled Lipoplexes.	125
Conclusions	128
References.....	130
5 Transfection Tests	133
6 Conclusions and Outlook	139
7 Experimental Section.....	145
7.1 Methodology.....	145
General	145
General Procedure for the Ipso Nitration.....	147

Contents

General Procedure for the Reduction of the Nitro Groups into Amine.....	151
General Procedure for the Protonation of the <i>p</i> -Amino Calix[4]arene Derivatives	154
General Procedure for the Diacylation.....	157
General Procedure for the <i>o</i> -Alkylation	158
Langmuir Monolayer Experiments	158
Spectroscopic Ellipsometry	159
Nanoparticules Preparation and Characterization	159
DNA-Binding Experiments and Characterization.....	161
Transfection Protocol	164
7.2 Results.....	165
References.....	175
8 Acknowledgements.....	177
9 Curriculum Vitae	179

Abbreviations and Acronyms

^1H NMR	Proton Nuclear Magnetic Resonance
^{13}C NMR	Carbon Nuclear Magnetic Resonance
Å	Ångström
AC ₅₀	Concentration at 50 % of the fluorescence intensity
BAM	Brewster Angle Microscope
Boc	<i>tert</i> -Butyloxycarbonyl
CD	Circular Dichroism
DMF	<i>N,N</i> -Dimethylformamide
DMSO	Dimethyl sulfoxide
DNA	Deoxyribonucleic acid
EtBr	Ethidium bromide
EtOH	Ethanol
MS (ESI)	Electrospray Ionization Mass Spectrometry
eV	Electron volt
HEPES	2-[4-(2-Hydroxyethyl)piperazin-1-yl]ethanesulfonic acid
ITC	Isothermal Titration Calorimetry
M	Molar (mol L^{-1})
mM	Millimolar (mmol L^{-1})
μM	Micromolar ($\mu\text{mol L}^{-1}$)
MW	Molecular Weight
nm	Nanometer
ppm	Parts per million
R _f	Retardation factor
rpm	Revolutions per minute
THF	Tetrahydrofuran
TLC	Thin Layer Chromatography

Aim

The aim of my thesis is to design and study the ability of amphiphilic calixarenes to self-assemble as nanoparticles able to interact with DNA for therapeutic purposes.

The present doctoral thesis focused on the synthesis of amphiphilic calix[4]arenes, the study of their self-assembly properties at the air-water interface as Langmuir monolayers or in solution as nanoparticles and on the DNA-binding properties of the resulting self-assembled structures. The objective is to improve the understanding of the interaction of amphiphilic calixarene-based nanoparticles with DNA molecules, and to improve the comprehension of the effect of the calixarene structure: on the self-assembly of the amphiphilic calixarene as nanoparticles and on the interaction of the calixarene-based nanoparticles with DNA.

My PhD work can be divided in three distinct parts:

First, my work aimed at the synthesis of amphiphilic calix[4]arenes locked in the cone conformation. A water-insoluble 5,11,17,23-tetra(guanidinium)-25,26,27,28-tetra(dodecyloxy)-calix[4]arene, named **GC12**, bearing at the upper rim four guanidino recognition moieties and at the lower rim hydrophobic functions (four dodecyloxy chains), has been synthesized. To study the influence of the number of recognition moieties on the self-assembly and on the interaction with DNA, mono-, di-, tri- and tetraamino calix[4]arene derivatives bearing four dodecyloxy chains at the lower rim have been synthesized: The 5-mono(amino)-25,26,27,28-tetra(dodecyloxy)-calix[4]arene (**1NH₂4C₁₂**), the 5,11-di(amino)-25,26,27,28-tetra(dodecyloxy)-calix[4]arene (**1,2NH₂4C₁₂**), the 5,17-di(amino)-25,26,27,28-tetra(dodecyloxy)-calix[4]arene (**1,3NH₂4C₁₂**), the 5,11,17-tri(amino)-25,26,27,28-tetra(dodecyloxy)-calix[4]arene (**3NH₂4C₁₂**) and the 5,11,17,23-tetra(amino)-25,26,27,28-tetra(dodecyloxy)-calix[4]arene (**4NH₂4C₁₂**).

The second part presents the study of the synthesized cationic calix[4]arenes self-assembled as Langmuir monolayers at the air-water interface. The DNA-binding ability at this interface has been investigated with three model 30-mer oligonucleotides, two homooligonucleotides **AT** (dA₃₀-dT₃₀), **GC** (dG₃₀-dC₃₀) and one heterooligonucleotide **ATGC** containing 50 % **AT** and 50 % **GC**. The Langmuir monolayer experiments indicated that the interaction with DNA is dependent on the DNA sequence.

The third part of my PhD work concerns the study of the self-assembly of the amphiphilic calixarene in solution as nanoparticle and the binding mechanism of the calixarene-based nanoparticles to the double helix of the DNA molecules. The binding mechanism has been studied by fluorescence spectroscopy, circular dichroism (CD) and isothermal titration calorimetry (ITC). The results indicate that **GC12** and the **4NH₂4C₁₂**-based nanoparticles interact with the DNA double helix not only via electrostatic interaction but also via a groove-binding mechanism. While the fluorescence displacement assay performed with **1NH₂4C₁₂**, **1,2NH₂4C₁₂**, **1,3NH₂4C₁₂** and **3NH₂4C₁₂** derivatives indicates most likely an electrostatic interaction mechanism between the calixarene-based nanoparticles and the DNA molecules.

The results reported in my PhD dissertation highlight the influence of the calixarene structure, on their self-assembly as Langmuir monolayer at the air-water interface and as nanoparticles in water. Moreover the binding mechanism between the DNA phosphodiester backbone and the self-assembled calix[4]arene is dependent of the number of recognition moieties but is also governed by a sequence dependent interaction mechanism.

1 Introduction

1.1 Supramolecular Chemistry

Background

At the interface between physics, chemistry and biology, supramolecular chemistry has become a major scientific field over the past 25 years. The concept of “supramolecular chemistry” was coined by Jean-Marie Lehn who, with Donald J. Cram and Charles J. Pedersen, received the 1987 Nobel Prize in Chemistry for their achievements in the field of supramolecular chemistry.¹⁻³ Lehn defined supramolecular chemistry as “the chemistry beyond the molecule”.²

Beyond molecular chemistry, based on the covalent bond, supramolecular chemistry relies on molecular interactions and intermolecular bonding. Molecular self-assembly is the spontaneous organization of molecules into two or three-dimensional structures,⁴⁻⁵ governed by non-covalent forces such as hydrogen bonding, van der Waals forces, π - π interactions or electrostatic effects. Those non-covalent interactions can form well-defined structure in a reversible and accurate fashion. Self-assemblies are processes that require the reversibility of all the stages of the self-assembly, in order to achieve the most stable energy state: the formation of self-assembled structures is thermodynamically driven. Self-assembly is ubiquitous in chemistry and biology. For example, it generates much of the functionality of living cells: DNA, protein, cells or viruses are biological structures with a precise organization at a level below the nanometer formed by self-assembly.

Biological Self-Assembly: Functions and Informations

Natural self-assemblies such as the folding of polypeptide chains into proteins, the self-assembly of DNA strands into a double helix, and the bilayer membranes of cells formed by the self-assembly of lipids, have been extensively studied.

DNA is well known as the molecule bearing genetic information. All living organisms are composed of cells, whether prokaryotic or eukaryotic cells and each cell possess all the genetic information that determines the development and functioning of an organism.

DNA is composed of two complementary strands bound together via hydrogen bonding and π - π stacking to form a supramolecular structure: a stable, flexible double helix that can adapt rapidly to the effects of the environment (for example, pH, temperature, ions). DNA's ability to store information lies in a code made from four nucleobases: A (adenine), T (thymine), G (guanine) and C (cytosine). DNA can store large amounts of information. This information depends on the sequence of the four bases. Modifications of the DNA: change in the sequence of the base pairs or chemical modification to the DNA that affects the way the molecule is shaped such as methylation can modify the information transmitted by the DNA.

For example, in nature, DNA methylation defines honeybee behavior. Herb et al. reported on the relationship between the function of the bees in the hive and reversible DNA modification.⁶ Different types of worker bees exist. Herb et al. studied the nurses, nursing and feeding the queen and larvae, and the foragers that travel to collect nectar or pollen. It is known that these two types of worker bees (nurses and foragers) differ in their bodies, mental abilities, and behavior. Herb et al. removed all the nurses from a hive and found that half of the forager bees could become nurses to compensate this loss. This role change is due to a chemical modification involving epigenetic modifications by DNA methyltransferases. A methyl group is added to specific cytosine bases of the DNA. This enzymatic process, called DNA methylation, is a modification of the DNA structure that affects the way the DNA molecule is shaped and, consequently, affects the regulation of genetic activity.

Introduction

DNA methylation induces a change of information transmitted by the DNA sequence; this process is reversible.

A second example of natural self-assembly is the folding of proteins. Proteins are chains of amino acids that fold into a three-dimensional shape. There are four levels of protein structure. The primary structure is a linear sequence of amino acids in the polypeptide chain. The secondary structure corresponds to the arrangement of the polypeptide chain via hydrogen bonding between the amino acids into α -helices or β -sheets. The tertiary structure corresponds to the three-dimensional structure of the protein, and the quaternary structure is the arrangement of two or more polypeptide chains by non-covalent bonds. Protein folding is a precise self-assembly which defines proteins' shapes and functionalities. In some neurodegenerative diseases such as Alzheimer's and Parkinson's, the cause of the disease is believed to be proteins misfolding. In a normal protein, hydrophobic amino acids bury themselves inside the protein. However, if the protein fails to self-assemble properly these hydrophobic amino acids are exposed and they rapidly seek out and bind to hydrophobic groups on other protein molecules, forming insoluble aggregates or plaques that are found in the brain of patients with neurodegenerative diseases.⁷

Another example of the transmission of information by self-assembled structure is the contraction-extension of muscles. Muscle movement is controlled and coordinated by thousands of proteins that function individually over distances of the order of a nanometer.

Skeleton, smooth and cardiac muscles are composed of two major proteins (myosin and actin) organized into filaments forming a repeating structure. Myosin filaments are thick filaments in which the myosin proteins are arranged in a cylinder and actin filaments are thin filaments arranged in a double helix. When muscles contract, the actin filaments slide over the myosin filaments. In the presence of calcium the active sites of the actin proteins are accessible and the actin recognition sites of the myosin proteins bind spontaneously. Once the proteins are bound, the myosin undergoes a conformational change: the movement of the myosin causes the thin film to move. Muscle contraction occurs when the thousands of proteins composing the filaments slide over one another in a series of repetitive and perfectly coordinated events.⁸

Bio-Inspired Self-Assembly

Over time, evolution has led to some incredible developments, from the photosynthetic machinery in plants to the human eye. Scientists have developed technologies that seek to mimic some of life's unique innovations. A few examples of natural self-assemblies that inspired researchers will be discussed in this paragraph.

The structure of the shark's skin is composed of tiny scales called "dermal denticles" (skin teeth) aligned in the direction of the water flow (Figure 1a). These tiny denticles reduce friction between the shark skin and the water surrounding it, thereby diminishing surface resistance when moving at high speed. Drag reduction in fluid flow is of interest in various commercial applications. Nanomaterial-based paint mimicking shark skins

Introduction

have been studied for their ability to reduce drag in pipelines^{9, 10} and limit drag in aircraft¹¹ to decrease fuel consumption.

Moreover, bacterial colonies cannot develop because the spacing between these dermal denticles is such that microscopic organisms have difficulty adhering.¹²

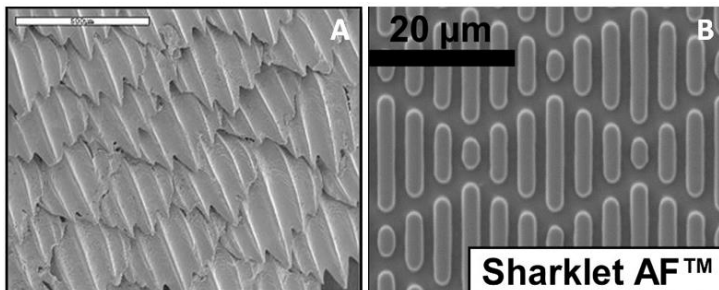


Figure 1. a) Galapagos sharkskin and b) Sharklet micropattern. [Reprinted with permission from ref. 8. Copyright (2009) American Chemical Society].

A shark skin-like material called “Sharklet”, developed by Brennan and co-workers, prevents bacterial contaminations.¹²⁻¹³ Brennan and co-workers compared two types of infection-causing bacteria, methicillin-resistant and susceptible *Staphylococcus aureus* (MRSA and MSSA) on three surfaces, the Sharklet micropattern (Figure 1b), a commonly used copper alloy, and a smooth control surface.¹² They discovered that the Sharklet micropattern reduced transmission of MSSA by 97 % compared to the smooth control surface. The Sharklet surface had 94 % less MRSA bacteria than the control surface, while the copper had 80 % less. Sharklet material could be used in hospitals to prevent bacteria growth.

A second example of bio-inspired material is based on a gecko's toes. Geckos' toes are covered by arrays of hair-like structures called setae, which increase the effective surface area between the foot and the surface on which it rests, thus increasing adhesive force. Irschick and Crosby developed an adhesive pad called "Geckskin", composed of polyurethane or polydimethylsiloxane (Figure 2a).

The gecko-like adhesive exhibits a high shear adhesive force capacity of 300 kg per 100 cm² and the adhesive can be removed easily (<1 kg in peel) without leaving residues. Furthermore, the adhesive can be applied and reapplied on a variety of surfaces without losing its stickiness.¹⁴⁻¹⁵ Geckskin technology can be used in a range of applications as it can easily attach and detach everyday life objects such as televisions and computers to walls, as well as medical and industrial equipment (Figure 2b).

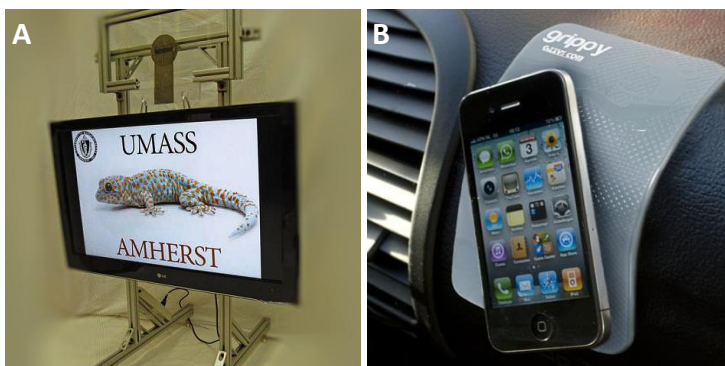


Figure 2. a) Geckskin holding a 42-inch television¹⁴ and b) "Grippy Pad" based on Geckskin technology. [Adapted from ref. 9. Copyright (2012), John Wiley and Sons].

Introduction

Last example, the scyllarus shrimp, also called the mantis shrimp, is the only species of shrimp able to break the shells of its prey with a club that accelerates underwater at around $10\,400\text{ g}$ ($102\,000\text{ m s}^{-2}$). The club is a highly complex structure: it has several regions, including layers of chitin fibers each layer of chitin fibers is rotated by a small angle with respect to the layer below, forming a helicoidal composite that act as shock absorbers (Figure 3).

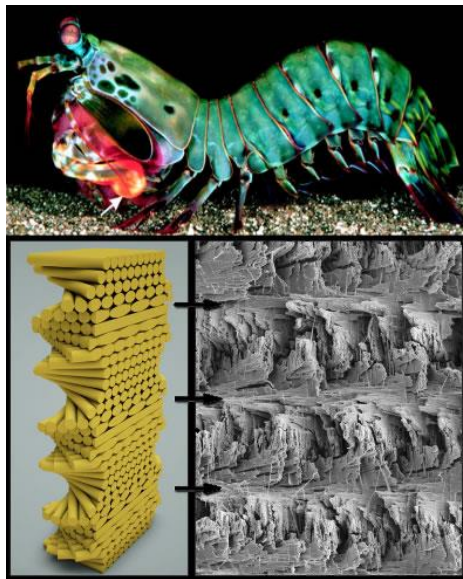


Figure 3. Mantis shrimp and the helicoidal structure of the club. [from <http://www.engr.ucr.edu/> Copyright (2013)].

The mantis shrimp moves its club so quickly that the club produces destructive bubbles that collapse quickly and therefore release energy; this process is called cavitation. Cavitation can cause serious damage; it is known to destroy ship propellers, pumps and turbines.

The strength of the club lies in its helicoidal structure that propagates the crack between the fiber rather than breaking them. Nevertheless, the shrimps regularly molt to replace the worn out appendages.

Kisailus and co-workers designed carbon fiber-epoxy composites mimicking the helical structure of the mantis club. The carbon fiber-epoxy composites was produced with different fibers layers rotation angles (7.8° , 16.3° , and 25.7°) and the composites were compared to conventional composites used in aerospace industry in which all the fibers are aligned in parallel (unidirectional) or have fiber layers oriented at 0° , $\pm 45^\circ$, and $\pm 90^\circ$ directions angles (quasi-isotropic structures) (Figure 3).¹⁶ They found that the carbon fiber-epoxy composites helicoids structure is more resistant to external damage than the structures commonly used in the aerospace industry. The dent depth damage to the helicoidal samples was 20 to 50 percent less than the quasi-isotropic samples. In compression tests, helicoidal samples displayed a 15 to 20 percent increase in residual strength after impact compared to the quasi-isotropic samples. Potential applications for such a material could include aircraft and automotive panels, athletic helmets and military body armor.

Supramolecular Self-Assembly of Macrocycles

Many examples of self-assembly can be found in nature: it often displays a great sophistication in structure and in function. Since Lehn, Pederson and Cram's Nobel Prize in 1987 the use of supramolecules to form self-assembled structures has gained much attention and allowed a better understanding of natural self-assembly processes.

Among the various molecular platforms that can be used for the construction of self-assembled structures, macrocycles such as crown-ethers, cryptands,¹⁷ resorcinarenes, cyclodextrins,¹⁸ cryptophanes¹⁹ and calixarenes have largely been developed during the last decades. A few examples of the self-assembly of macrocycles will be discussed in this paragraph.

Crown-ethers are among the simplest macrocycles: they are cyclic polyethers discovered by Charles Pedersen in 1967 (Figure 4).²⁰ The important complexation ability of crown-ethers toward alkali and alkaline earth metal ions has been applied to sensors,²¹ ion channel model systems,²² and membrane formation.²¹

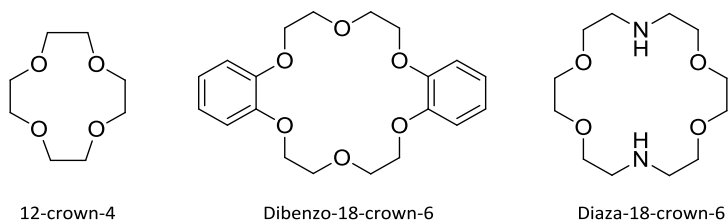


Figure 4. Examples of crown-ethers.

The intrinsic affinity of crown-ethers for cations has been used by Clark et al.,²³ to design a daisy chain molecule with an ammonium binding site and crown-ether recognition moieties, separated by a rigid biphenyl linker. Clark et al. studied the recognition between an ammonium cation and an aromatic crown-ether (Figure 5).

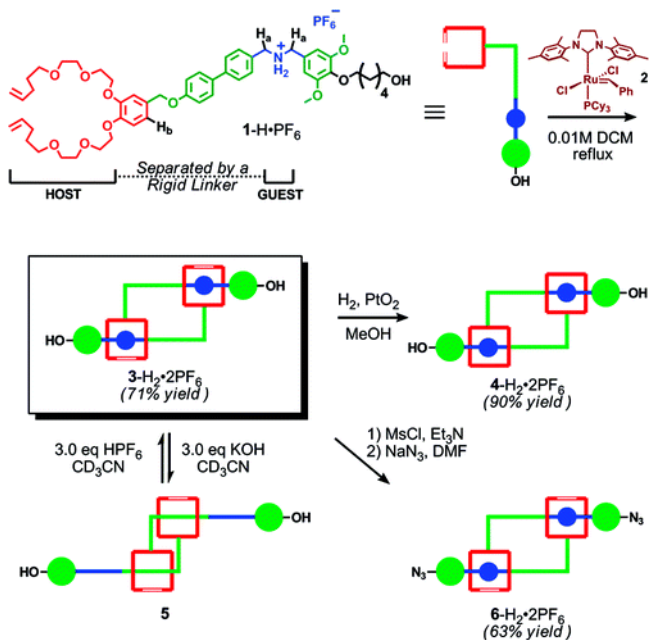


Figure 5. Graphic representation of the binding and switching of the daisy chain. [Reprinted with permission from ref. 18. Copyright (2009) American Chemical Society].

Under basic conditions, the crown-ether molecule moves away from the ammonium and interacts with the biphenyl. Upon protonation of the ammonia group, the crown-ether returns to its original conformation (Figure 5). This work tends to mimic the extension-contraction of natural fibers.

Shortly after the discovery of crown-ethers, Lehn achieved the synthesis of a cage-like molecule called cryptand in 1967 (Figure 6).

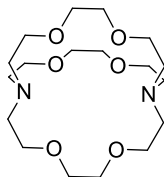


Figure 6. Chemical structure of a cryptand.

Transport of ions or small molecules plays an important role in a wide range of biological processes in nature. Achieving transport of ions by synthetic receptors involved the design of molecules that had a selective recognition site. As crown-ethers, cryptands are used to complex ionic molecules. Cryptands are three-dimensional equivalents of crown-ethers, but they form stronger complexes with higher selectivity and specificity than crown-ethers.²⁴ For example, it is known that the binding constant of potassium ions is 10^4 higher for [2, 2, 2]cryptand than for 18-crown-6.²⁵

Most macrocycles are synthetic and do not occur naturally. Cyclodextrins are natural macrocycles that result from the degradation of starch by bacteria, composed of 6, 7 or 8 glucose units named α -, β -, and γ -cyclodextrins, respectively (Figure 7). Due to their molecular structures and shapes, cyclodextrins possess a ability to act as molecular containers by entrapping guest molecules in their internal cavities.²⁴

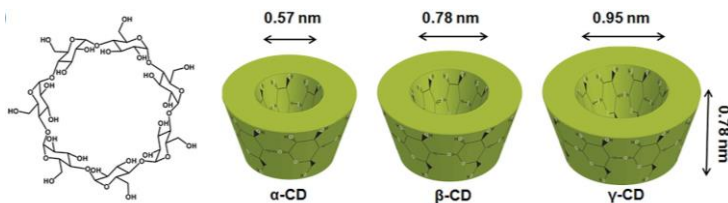


Figure 7. Structure of natural cyclodextrins.²⁶ [Adapted with permission from ref. 21. Copyright (2013) American Chemical Society].

The resulting inclusion complexes are used in the food industry to prepare cholesterol-free products,²⁷ as a flavor enhancer in chewing-gums,²⁸ in cosmetics,²⁹ and in medicine.³⁰⁻³¹

Calixarenes are macrocyclic molecules formed by the condensation of phenols with formaldehyde. The general structure is shown in Figure 8.³²⁻³³

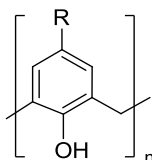


Figure 8. Structure of calix[n]arene.

Calixarene are considered to be the third generation of macrocycles after cyclodextrins and crown-ethers.³⁴ The chemistry of calixarenes has been applied in diverse areas such as host-guest chemistry,³⁵ selective membranes,³⁶ HPLC stationary phases, selective ion transport³⁷ and as mimics of biological processes.^{33, 38-39}

Supramolecular chemistry has become a rapidly growing field. In life science, the concept of self-assembled structure by non-covalent interactions is a crucial for understanding many biologically important structures. In material science the self-assembly opens new perspectives and allows for the design of smart materials by controlling their self-assembly.

1.2 Self-Assembly of Amphiphilic Calixarenes as Langmuir Films at the Air-Water Interface

Lipids are an important class of molecules as they are the main component of the bilayer cell membranes of all living organisms that allow the selective diffusion of ions and small molecules in and out of the cells. Surfactant molecules can self-assemble as a monolayer at the air-water interface to mimic a membrane. The hydrophilic moieties of the amphiphilic molecules are immersed in water and the hydrophobic parts face the air as represented in Figure 9.

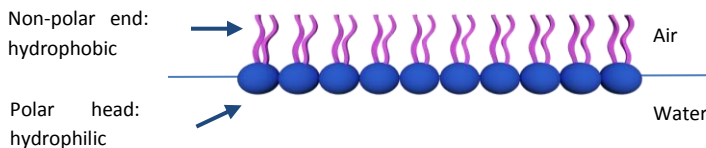


Figure 9. Schematic representation of amphiphilic molecules self-assembled at the air-water interface.

In 1917, Irving Langmuir introduced new theoretical concepts and experimental methods to investigate the film formation on water interfaces. In 1932 he was awarded the Nobel Prize in Chemistry for his discoveries and investigations in surface chemistry. Insoluble monolayers at the air-water interface are named Langmuir films. Irving Langmuir and Katherine Blodgett developed a technique to transfer insoluble monolayers onto substrates. This transfer is called a Langmuir-Blodgett transfer and the generated films Langmuir-Blodgett films. Langmuir monolayers provide a simple way to study interactions in two-dimensional arrangements of amphiphilic molecules. The effect of pH, temperature and ions on the amphiphilic molecules and the interaction with biomolecules such as proteins, peptides or DNA can be studied. Direct studies at the air-water interface can be performed using optical methods such as fluorescence microscopy,⁴⁰ Brewster angle microscopy,⁴¹ X-ray reflectivity,⁴² PM-IRRAS,⁴³⁻⁴⁵ and ellipsometry.⁴⁶⁻⁴⁷ The Langmuir monolayer technique is a sensitive technique that provides quantitative information about the density and orientation of the amphiphiles at the air-water interface.

Due to their conical shape and easy functionalization, calixarenes are ideal molecules for the design of complexes amphiphile able of molecular recognition. Indeed, amphiphilic calixarenes have gained attention in Langmuir films as calixarene molecules exhibit self-assembly properties at the air-water interface.^{39, 48}

Introduction

Calixarene macrocycles, mentioned in Chapter 1 (Supramolecular self-assembly of macrocycles page 14) are prepared by the base-catalyzed condensation of *para*-substituted phenols and formaldehyde.³² Calixarenes are macrocycles composed of phenolic units arranged in cyclic arrays and linked by methylene bridges. The name was coined by Gutsche, as the three-dimensional structure of the molecule looks like a “calix crater”, an ancient Greek vase. The term “arene” denotes the presence of aromatic moieties and the “[n]”, indicates the number of phenolic units. The most common calixarenes, represented in Figure 10, are the calix[4]arene, calix[6]arene and calix[8]arene, but the number of phenolic units can be up to 20.⁴⁹

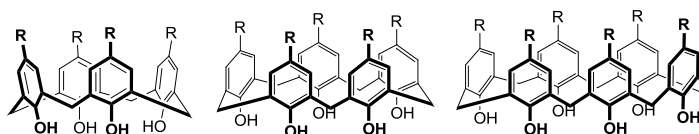


Figure 10. Examples of calix[n]arenes.

Furthermore, calixarenes are composed of three parts, a wide upper rim, a narrow lower rim and a central annulus (Figure 11) that can be functionalized to design complex molecules.³³

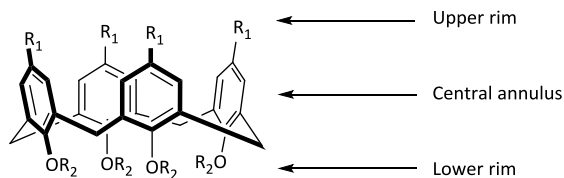


Figure 11. Structure of the calix[4]arene.

Calix[n]arenes exist in different conformations depending on their functionalization and the solvent used to solubilize them as the phenolic units of the calix[4]arene can rotate along the methylene bridge. Calix[4]arenes exist in four conformational isomers – the cone, partial cone, 1,2-alternate and 1,3-alternate – as shown in Figure 12. The cone conformation is the most stable conformation amongst all the forms of calix[n]arenes.

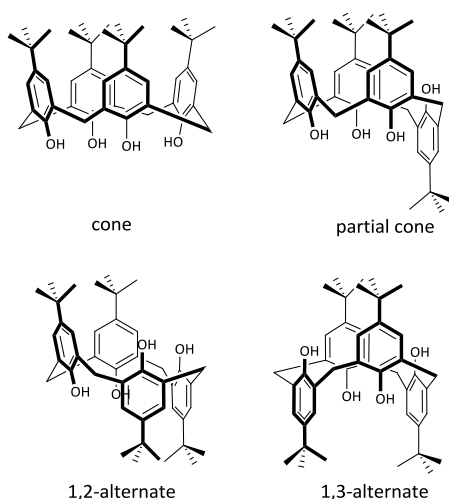


Figure 12. Calix[4]arene conformations.

This section will focus on Langmuir monolayers of calixarenes as self-assembled supramolecular structures with a particular focus on the use of the Langmuir monolayer technique to study interaction related to biological processes such as ionic interactions, metal ions binding, interaction with pharmaceutical molecules and biological molecules as proteins or DNA.

Interaction with Ions

Calixarenes forming host-guest complexes.³² In 1989, Ishikawa et al. studied the effect of Li^+ , Na^+ , K^+ and Rb^+ cations on ester calixarene derivatives monolayers. They described, for the first time, a selective complexation of metal ions by calixarenes at the air-water interface.⁵⁰ The potential of calixarenes as a selective membranes was investigated by Yagi et al.,⁵¹ in 1996. They studied the influence of alkali metal chlorides on *tert*-butylcalix[4]arene ester and *tert*-butylcalix[6]arenes ester monolayers at the air-water interface.

Yagi et al.,⁵¹ observed a selectivity of the calix[6]arenes monolayer that is consistent with the selectivity obtained in a solvent $\text{Cs}^+ > \text{Rb}^+ > \text{Na}^+ > \text{Li}^+$. They also evaluated the permeability of the monolayers toward ions by cyclic voltammetry either at the air-water interface or after transfer to an electrode using the Langmuir-Blodgett technique.⁵¹ They showed that calix[4]arene and calix[6]arene ethyl esters on glassy carbon electrodes enhanced the response toward Na^+ and Cs^+ , respectively.

Lo Nostro et al., studied the interaction of *tert*-butyl-calix[6]arene, *tert*-butyl-calix[6]arene hexamide and *tert*-butyl-calix[8]arene with alkali metals (NaCl , KCl , CsCl and $[\text{C}(\text{NH}_2)_3]\text{SCN}$) in order to investigate the formation of interfacial host-guest systems.⁵² They demonstrated that *tert*-butylcalix[6]arenes formed stable films with chloride ions with alkali metals in the order $\text{Cs}^+ > \text{K}^+ > \text{Na}^+$. Following the work of Lo Nostro, Lonetti studied the effect of potassium salts on *tert*-butylcalix[6]arene and *tert*-butylcalix[8]arene and demonstrated a rearrangement of the

monolayer and a reversal of the Hofmeister series ($\text{Cl}^- > \text{NO}_3^- > \text{I}^- > \text{SCN}^-$) as a function of the increase of the surface pressure.⁵³ Lonetti,⁵⁴ also studied the effect of strontium and barium ions on diethylamidecalix[8]arene monolayers and demonstrated a selectivity for barium cations.

Lonetti correlated the ability to complex cations with the functionalization of the rims, showing the possibility to modulate the stability of the complex. Capuzzi et al.,⁵⁵ studied the interaction of 1,3-alternate calix[4]arene-crown with cesium and potassium ions and demonstrated the selectivity of the calix[4]arene for cesium ions at the air-water interface.

Interaction with Transition Metal Ions

Copper ions play an important role in Human metabolism, they enable the proper functionality of many enzymes.⁵⁶ For example, copper ions contribute to the production of collagen and elastin proteins, and to the production of oxygen and peroxide hydrogen for the skin and muscles. Korchowiet al.,⁵⁷ demonstrated a selectivity at the air-water interface of *p-tert-butylcalix[4]arene* mono- or bis-propylalidixate for copper and zinc compared to alkali metals. They also showed that *p-tert-butylcalix[4]arene*-bis-propylalidixate formed stable complexes with divalent metal cations two to seven times stronger than monovalent cations. Shahgaldian et al. designed amphiphilic calix[4]resorcinarene bearing four L-prolyl moieties and studied the effect of cations on the stability of Langmuir monolayers. Calixarene-Cu²⁺ complex showed enantioselective recognition properties for phenylalanine.⁵⁸

Zinc is the second most abundant metal in living organisms after iron.⁵⁹ Zhang reported on calix[4]arene porphyrin able to complex Pd^{2+} and Zn^{2+} at the air-water interface and formed stable Langmuir films with the porphyrin tilted to the surface of water.⁶⁰ Zhang and co-workers, transferred the calix[4]arene porphyrin Langmuir monolayers with or without the transition metal ions in the subphase on a solid surface using the Langmuir-Blodgett films technique. They demonstrated by UV-Visible absorption and FTIR spectra that the porphyrin also adopt a tilted position after deposition on a solid surface as LB films and the LB film of the calix[4]arene porphyrin in the presence of Pd^{2+} and Zn^{2+} display higher molecular ordering than the calix[4]arene porphyrin on water surface. He et al. designed a calixarene with two methionine moieties able to complex palladium and form intermolecular metal complexes.⁶¹ The monolayer exhibited high cohesiveness and stability. The intermolecular metal complexes could be used to produce robust film at the air-water interface.

Interaction with Pharmaceutical Molecules

Langmuir monolayers of amphiphilic calixarenes have been used to efficiently build self-assembled structures that act as crystallization templates at the air-solution interface. Such assemblies have revealed specific recognition properties of ions, amino acids, supramolecular nanostructures based on calixarenes, nucleic acids, and proteins and also act as crystallization templates.

With regard to a calixarene-drug template for crystallization, Elend et al. investigated interaction properties of the amphiphilic 5,11,17,23-tetra(carboxy)-25,26,27,28-tetra(dodecyloxy)-calix[4]arene with salicylic acid, acetylsalicylic acid and acetaminophen at the air-water interface by means of the Langmuir balance technique.⁶² Moridi et al. produced three aminophenol-modified calix[4]arenes by the reaction of the 5,11,17,23-tetra(carboxy)-25,26,27,28-tetra(dodecyloxy)-calix[4]arene with ortho-, meta-, and para-aminophenol and demonstrated that the amphiphiles produced interact with acetaminophen with a relevant preference for the *para*-derivative that possesses substituents in its structure that are analogous to the target.⁶³ Further, using the same carboxy-calix[4]arene, Moridi et al. studied the formation of Langmuir-Blodgett bilayers with acetaminophen and investigated the crystallization of the acetaminophen on the surface.⁶⁴ Recently, Tulli et al. reported on calixarene-based Langmuir monolayers to control the polymorphism of gabapentin.⁶⁵

Calixarene Langmuir Films: Protein Interactions

In 2004, Schrader's group introduced a new concept of protein sensing at the air-water interface based on amphiphilic receptor molecules self-assembled as Langmuir monolayer. In Schrader's group, Zadmard et al. studied the interaction of tetraphosphonate calix[4]arene (**1**) and tetraammonium calix[4]arene (**2** and **3**) with large peptides and proteins and showed optimal binding of the tetraphosphonate calix[4]arene (**1**) monolayer with protein with a large flat surface covered with arginines and lysines (Figure 13).⁶⁶

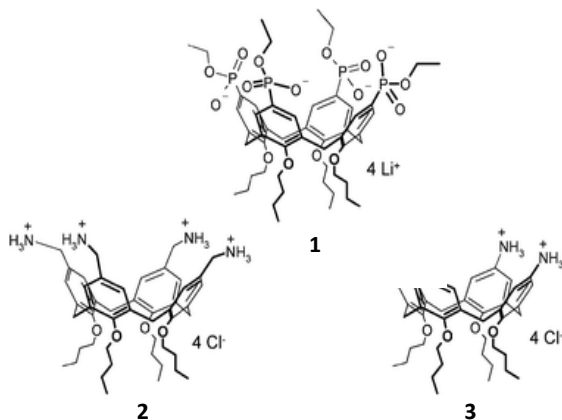


Figure 13. Structures of the charged calix[4]arene derivatives. [Reprinted with permission from ref. 66 Copyright (2010) Royal Society of Chemistry].

In 2005, Zadmard et al. studied the effect of the addition of amphiphilic calixarene derivatives **1**, **2** and **3** (Figure 13) into a stearic acid Langmuir monolayers formed in the presence of peptide or protein in the aqueous subphase at a surface pressure of 15 mN m⁻¹. The tetraphosphate calixarene **1** demonstrated affinity for basic amino acid, peptides and proteins, calixarene **2** is selective for acidic proteins and calixarene **3** recognized all polar proteins. This system allows, depending on the calixarene structure, to form selective monolayers for basic or acidic proteins.⁶⁷ Following the work of Zadmard, Kolusheva et al. achieved color detection of proteins by calixarene receptors within phospholipids and the chromatic polymer polydiacetylene vesicles.⁶⁸ These studies showed that calixarene derivative might be used as a biological tool for protein–protein interaction, protein–DNA interaction and an enzyme activity assay.

Calixarene Langmuir Films: DNA Binding

In 2002 Liu et al. studied the formation of a monolayer of *tert*-butylcalix[4]arene bearing, at the lower rim, two amine or cyclic guanidinium groups in the presence of 5'-AMP⁻ or 5'-GMP²⁻.⁶⁹ The isotherms of the monolayer in contact with the 5'-AMP⁻ in the subphase possessed a larger molecular area than the monolayer in the presence of 5'-GMP²⁻. The monolayer isotherm containing 5'-AMP⁻ in the subphase possessed a larger molecular area and a higher collapse pressure in the presence of 5'-GMP²⁻. The authors proposed two possible interactions (Figure 14): for both nucleotides, two ammonium moieties interact with the phosphate group of the nucleotides. In the case of 5'-GMP²⁻ the carbonyl function can also form two hydrogen bonds with the ammonium moieties, a 1:2 complex is formed. For 5'-AMP⁻, a 1:1 complex is expected as the nucleotide's ammonium can only form one hydrogen bond.

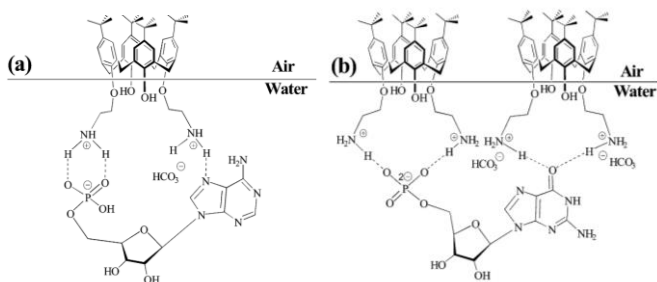


Figure 14. Interaction of 5,11,17,23-tetra-*tert*-butyl-25,27-bis(2-aminoethoxy)-26,28-dihydroxy-calix[4]arene amino calixarene monolayer at the air-water interface with the nucleotides a) 5'-AMP⁻ and b) 5'-GMP²⁻. [Reprinted with permission from ref. 76. Copyright (2002) Royal Society of Chemistry].

In 2004, the same group designed calixarene derivatives bearing one or two bicyclic guanidinium moieties at the lower rim and showed enantioselective recognition for D-/L- phenylalanine in solution and at the air-water interface.⁷⁰ The calixarene bearing one bicyclic guanidinium exhibited a poor enantioselectivity for L-phenylalanine compared to the calixarene bearing two bicyclic guanidinium units (Figure 15). Therefore, there is an enantioselectivity for L-phenylalanine dependent of the molecular structure.

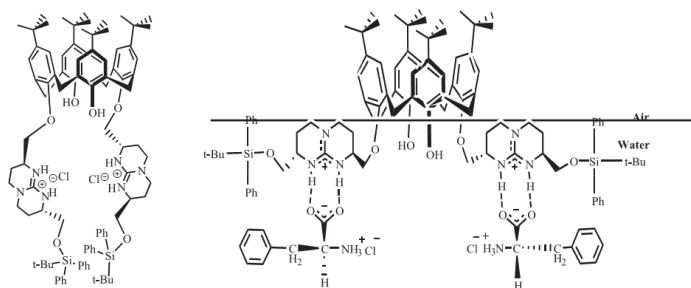


Figure 15. Interaction mechanism of a bicyclic guanidinium calixarene monolayer at the air-water interface with phenylalanine. [Reprinted with permission from ref. 77. Copyright (2004) Elsevier].

Guo et al. studied the properties of a Langmuir monolayer of calixarene derivatives bearing adenine functional groups, in the presence of complementary nucleosides (uridine and thymine).⁷¹ They demonstrated that the complementary nucleotides are efficiently bound to the monolayer and the monolayer can be transferred onto a solid substrate using the Langmuir-Blodgett technique due to strong hydrogen bonding.

In general, Langmuir monolayer studies allow analysis of the effect of natural or synthetic substances dissolved in the subphase on the properties of the Langmuir film and might also help to understand the binding mechanism between Langmuir films and the molecules in the subphase.

1.3 Gene Therapy

In the development of new healthcare strategies, the study of amphiphilic molecules has gained much attention. The investigation of the interaction between biomolecules and amphiphilic compounds are motivated amongst others, by the design of nanomaterials that could lead to progress in the field of gene therapy.

Gene therapy is a promising therapeutic strategy to treat or prevent diseases by the direct transfer of genetic material, such as DNA, RNA or oligonucleotides, into cells or tissues.⁷² The delivery of DNA into the nucleus of the targeted cells, might induce the incorporation of the nucleic acids into the cells genetic material and lead to the production of specific proteins. The introduction of small interfering RNA (siRNA), on the opposite, can selectively turn off the production of specific proteins. Gene therapy using injection of naked plasmid DNA have been carried out but showed low transfection efficiency, due to the negative nature of cellular membrane and negative charge of DNA molecules thus a carrier system is necessary to cross the cell membrane.⁷³⁻⁷⁴ The carrier systems for gene delivery are named vectors.

The ideal vector for gene therapy must fulfil several criteria: the carrier system must be able to condense DNA, cross the cell membrane, protect DNA from nucleases attacks and reach the nucleus of the targeted cells to deliver the genetic information. Viral and non-viral vectors are the two main type of vectors used in gene therapy.

Viral Vectors

Viruses transport their genetic material from one cell to another and introduce their genetic material into the host cell as part of their replication cycle. A viral vector is made when harmful genetic material is removed from a virus and replaced with desirable genetic material. In gene therapy clinical trials, the commonly studied viral vectors rely on retrovirus,⁷⁵ lentivirus,⁷⁶⁻⁷⁷ adenovirus,⁷⁸ adeno-associated virus (AAV) and herpes simplex virus (HSV)⁷⁹ to deliver the genetic information. Viral vectors are more efficient than non-viral vectors for DNA delivery but may present significant side effects such as excessive immune response (adeno-virus) and insertion mutagenesis (retroviruses).

Non-Viral Vectors

The use of non-viral vectors can be an alternative and overcome the side-effect mentioned in Section 1.2.1. Non-viral carriers are expected to be less immunogenic, with simple preparation and a possible versatile surface modification but typically exhibit lower transfection efficiencies.

Non-viral delivery vectors can be categorized as organic (for example, lipid complexes, conjugated polymers, cationic polymers, and dendrimers) and inorganic (for example, magnetic nanoparticles, quantum dots, carbon nanotubes, gold nanoparticles) systems. The delivery carriers need to be small (around 100 nm) to be internalized into the cells and enter the nucleus. To achieve suitable carrier systems, nanoparticles can be considered as good candidates for therapeutic applications. Nanoparticles are solid and spherical structures ranging from 1 nm to 1 μm in size and prepared from natural or synthetic molecules. Nanoparticles have several advantages: their size can be controlled, their surface can be functionalized, they have a large surface area and they possess controllable absorption and release properties. The use of self-assembled nanoparticles in gene therapy can provide a suitable vehicle to protect DNA against nuclease degradation and to deliver the genetic information into the target cell.

1.4 Self-Assembly of Calixarenes in Aqueous Solution

Amphiphilic Calixarenes and Self-Assembly as Nanoparticles

There are a number of nano-systems that have been investigated as carrier systems for therapeutic purposes including dendrimers, micelles, liposomes, carbon nanotubes, polymers, nanoparticles, liquid crystals and nanocapsules (as host-guest complexes), some of these are illustrated in Figure 16.

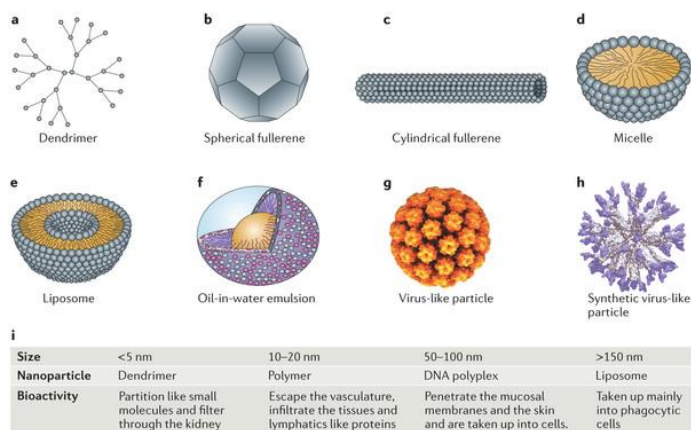


Figure 16. Examples of nanostructure. [Reprinted with permission from ref. 78. Copyright (2013) Nature Publishing Group].

Solid lipid nanoparticles (SLNs) are colloids ranging from 50 nm to 1 μm . SLNs consist of a spherical, solid, lipid core, stabilized by surfactants. The spherical shape of the nanoparticle contributes to its general stability.

SLNs are an alternative to other carrier systems and offer advantages such as the ability to control drug release and long-term storage.

Historically, D'Arcy Hart and Conforth in 1955 described the first calixarene that showed biological activities "a polyethylene glycol ether of *p*-*tert*-octylphenol formaldehyde cyclic tetramer" named Macrocyclon as shown in Figure 17.⁸⁰

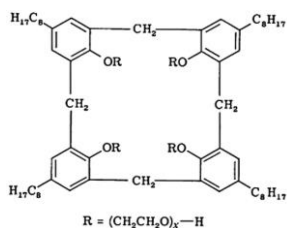


Figure 17. Structure of the Macrocyclon.

Considerable effort has been focused on approaches to increase the water solubility of calixarenes via the introduction of polar functional groups or moieties such as sulfonates, phosphonates, amines and amino acids, different lower rim modifications, guanidinium, peptides and saccharides. Shinkai et al. demonstrated that the conformation of the calixarene is a crucial parameter that affects the aggregation properties of the amphiphiles.⁸¹⁻⁸² Shinkai et al. established that tetraammonium-propoxycalix[4]arene derivatives in the cone conformation form micelles and the cylindrical shape of the 1,3-alternate conformation calixarene favors lamellar structure. Not only conformation plays a role in self-assembly behavior but functionalization does as well.

Strobel et al. showed that the nature of the ionic head group is a key parameter in controlling the aggregation behavior of calixarene amphiphiles.⁸³ They studied the self-assembly of carboxylic or trimethylammonium calixarene in water with different alkyl chains and demonstrated that carboxylate calixarenes form vesicles, while calixarenes bearing trimethyl-ammonium head groups provide high solubility and most likely form micelles.

Interaction with Proteins

Anionic calixarenes have been investigated over the years for their capacity to complex biomolecules, including a wide range of proteins. Tauran et al. studied the binding of several serum albumins from different mammalian species (bovine, human, porcine and sheep) with silver nanoparticles covered by *p*-sulphonatocalix[4]arene or 1,3-di-*O*-phosphonato-calix[4]arene.⁸⁴ Tauran et al., demonstrated that the use of only two types of nanoparticles allows the discrimination of serum albumins from different mammalian species. In addition to providing valuable information on protein recognition, the data also indicated that calixarene is a mediator of protein–protein interactions, with potential applications in generating assemblies and promoting crystallization. Crowley and co-workers⁸⁵ used NMR and X-ray crystallography to study how *p*-sulfonato-calix[4]arene binds to lysine-rich cytochrome *c*.

The NMR and X-ray data were in agreement and suggested that calixarene binds to three or more lysine side chains. Masking lysines is an established trick for coaxing protein crystallization, another potential calixarene application.

Interaction with DNA Molecules

The water-soluble amphiphilic tetra(alkylammonium)-tetra(alkyloxy)-calix[4]arene has been intensively investigated for its self-assembly properties.⁸⁶ This calixarene forms small nanoparticles and interacts with DNA via electrostatic interaction. Rodik et al. reported on the influence of the hydrophobic moieties on the ability of the tetra(alkylammonium)-tetra(alkyloxy)-calix[4]arene to bind DNA (Figure 18).⁸⁷

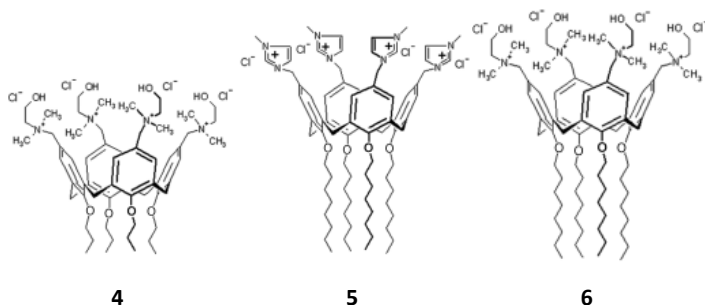


Figure 18. Calixarene structure studied by Rodik. [Reprinted with permission from ref. 88. Copyright (2011) John Wiley and Sons].

Rodik et al. demonstrated that ammonium calixarene **5** and **6** bearing octyl chains form micelles of 6 nm, which condense DNA and form small particles of 50 nm in the presence of DNA. While calix[4]arene with shorter alkyl chains **4** cannot self-assemble as micelles and loses its ability to interact with DNA, in 2006 Schrader and co-workers designed a series of dimeric aniline-calixarenes as major groove binders (Figure 19).⁸⁸ The anilino-calixarene dimers **7** and **8** interact with 12 base pairs DNA via the major groove. Due to the binding, the DNA undergoes a B- to A- transition.

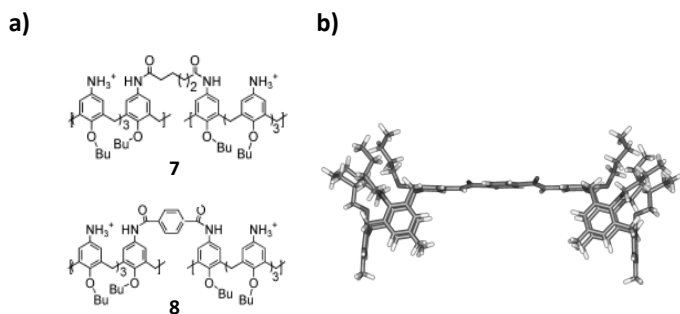


Figure 19. a) Anilino-calix[4]arene dimers **7** and **8** and b) Molecular mechanics calculation for the rigid hexaanilinium calixarene dimer **8**. [Adapted with permission from ref. 89. Copyright (2006) John Wiley and Sons].

Molecular mechanics calculations of the interaction between the DNA (12 bp) and the calixarene **7** showed a minimum energy when the ammonium groups are in the major groove (Figure 20).

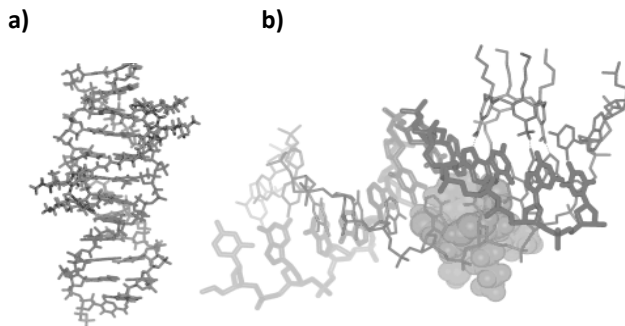


Figure 20. **a)** B-DNA (12 bp, green and blue) with tightly bound anilino-calixarene dimer **7** (red). **b)** View along the major groove, revealing three hydrogen bond contacts between the ligand $\text{NH}_2/\text{NH}_3^+$ groups and various nucleic bases at the groove floor (MacroModel 7.0, MMFFs, water, 1000 steps). [Adapted with permission from ref. 89. Copyright (2006) John Wiley and Sons].

Depending on the DNA sequence, the molecular calculation showed up to six hydrogen bonds between the carbonyl oxygen and nitrogen of the DNA and the amine function of the calixarene dimer. In 2012 Hu et al.⁸⁹ synthesized new dimeric anilino-calixarene with extended spacers and new dimeric guanidinium-calix[4]arene (Figure 21) and demonstrated the ability of the amino and guanidinium dimer to interact with the major groove of 20 mer DNA molecule.

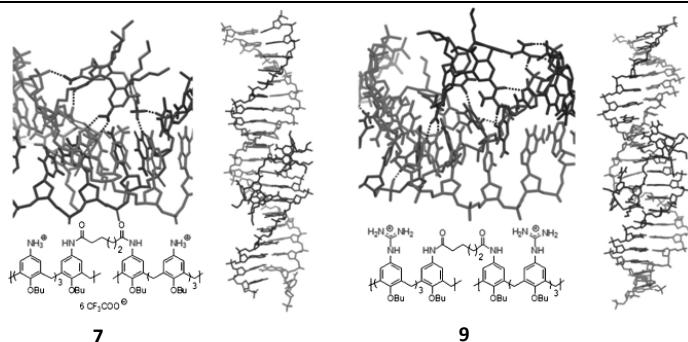


Figure 21. Calculated structure of the dimer with 20 bp DNA. [Reprinted with permission from ref. 90. Copyright (2012) John Wiley and Sons].

Figure 21 depicts the Monte-Carlo simulations of the anilino-dimers calixarene **7** and guanidino-dimers calixarene **9**. Dimeric calixarenes **7** and **9** formed hydrogen bonds with the acceptors at the triple helix formation sites of the DNA base pairs with the butoxy tails pointing outward off the DNA molecule. Hu et al. studied the interaction by fluorescence displacement assay and the binding mechanism by NMR spectroscopy and molecular modeling. They demonstrated that the binding with DNA is stronger with the guanidino-calixarene dimers than the aniline calixarene dimers. The aniline calixarene dimers **7** formed hydrogen bonds with six base pairs, and the guanidinium dimers with nine base pairs. In 2004, Dudik et al. designed a new series of water soluble calixarene functionalized at the upper rim with guanidinium moieties and at the lower rim with different alkyl chains (Figure 22).⁹⁰

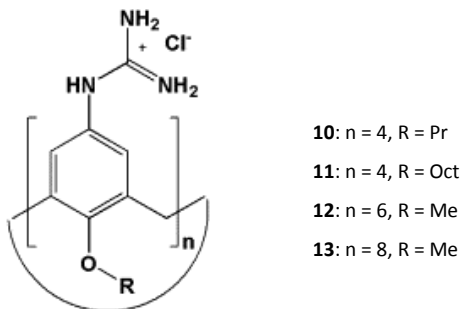


Figure 22. *Para*-guanidinium-calix[n]arene. [Adapted with permission from ref. 91. Copyright (2004) Elsevier].

Dudik et al. studied the influence of the length the carbon chains at the lower rim, the size of the calixarene macrocycle (4, 6 or 8 phenolic units), and bearing propyl or methyl carbon alkyl chains at the lower rim. They demonstrated that increasing the length of the alkyl chains decreases the solubility in water. All the calixarene with the exception of calixarene **11** show solubility in water.

In 2006, Sansone et al., following the work of Dudik, studied the influence of the size, conformation and number of guanidinium functions on the ability of the calixarene to condense DNA and transfect cells.⁹¹ Sansone et al. demonstrated that the calixarenes were able to compact DNA by imaging the interaction using atomic force microscopy (AFM). Calix[4]arenes bearing hexyl and octyl chains at the lower rim confer cell transfection ability due to intramolecular DNA condensates, while larger and mobile calixarene with 6 or 8 phenolic units fail to transfect cells due to electrostatic interactions.

Bagnacani et al. introduced guanidinium groups at the lower rim of calix[4]arenes in cone conformation (Figure 22).⁹²⁻⁹³ The lower rim guanidinium-calixarenes (Figure 23) showed higher transfection efficiency and lower toxicity than the upper rim guanidinium-calixarenes (Figure 22).

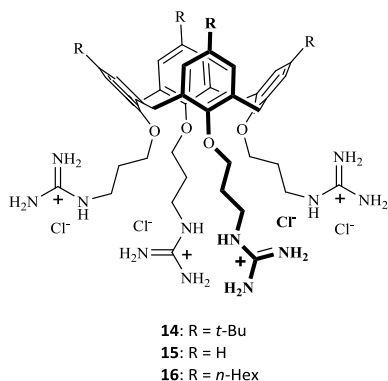


Figure 23. Lower rim guanidinium-calixarenes. [Adapted with permission from ref. 94. Copyright (2008) American Chemical Society].

Furthermore, when dioleoylphosphatidylethanolamine (DOPE) is added to the calixarene **15** solution to form lipoplexes, the transfection rate is even higher than commercial Lipofectamine. The interaction is driven by a combination of hydrophobic interaction and electrostatic interaction between the guanidinium and the phosphate esters of the backbone. In 2013, Bagnacani et al. described the synthesis of calix[4]arenes in cone conformation functionalized at the upper or lower rim with four L-arginine or L-lysine units (Figure 24).⁹⁴

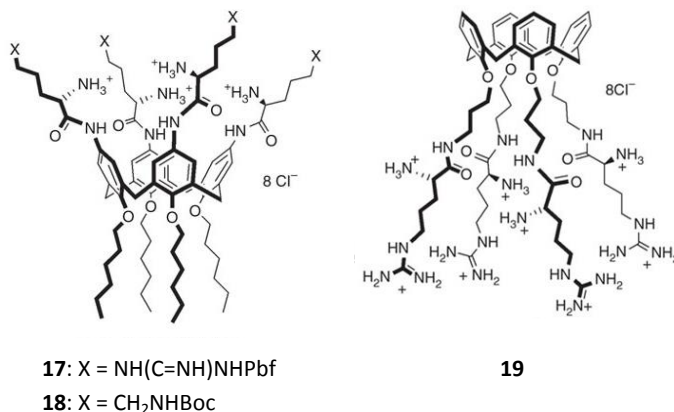


Figure 24. Peptidocalix[4]arene synthesis. [Adapted with permission from ref. 95. Copyright (2013) Nature Publishing Group].

Bagnacani et al. studied the DNA-binding properties and transfection efficiency of those calixarenes, the calixarene **17** bearing L-arginine units is more efficient than one functionalized with four L-lysine units **18** to transfect cells. The addition of DOPE to form lipoplexes decreases the transfection rate in the presence of tetraarginino-calixarene **17** and increases in the presence of tetraarginino-calixarene **18**. Calixarene **19**⁹⁴ on the opposite of calixarene **15**⁹²⁻⁹³ showed a low transfection even in the presence of DOPE as it formed a large aggregate with DNA. They assumed it could be due to a lack of hydrophobic function to balance the high polarity of the arginine function.

In 2010, Nault et al demonstrated the ability of tetraamino-dodecyloxy-calix[4]arene (**4NH₂4C₁₂**) to self-assemble as solid lipid nanoparticles (SLNs) in water and to interact with DNA (Figure 25).

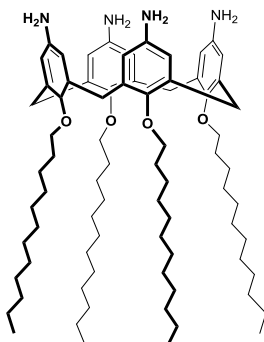


Figure 25. 5,11,17,23-Tetra(amino)-25,26,27,28-tetra(dodecyloxy)-calix[4]arene (**4NH₂4C₁₂**).

Nault et al. demonstrated that DNA molecules form a layer around calixarene **4NH₂4C₁₂** SLNs. Then wrapped with a polycationic biopolymer called chitosan, those SLNs were able to deliver the genetic information into mammalian cells.⁹⁵

Calixarenes derivatives have demonstrated interesting properties toward interaction with biomolecules. Their functionalization and conformation is a key parameter in their ability to self-assemble and to bind to DNA molecules. In addition, it also plays a major role in the ability to transport the genetic information into the cells. It is evident from the literature that phospholipids such as DOPE, or polymers such as chitosan might improve the ability of the calixarene-DNA complexes to cross the cell membrane and transfect cells.

1.5 Layer-by-Layer Self-Assembly

The potential for non-viral gene therapy to treat diseases has been limited by the difficulty in delivering the nucleic acids into the target cells due to many biological barriers. First of all, the genetic information should cross the cellular membrane, and then enter the nucleus. The design of non-viral systems for gene delivery using layer-by-layer (LbL) self-assembly allows the adsorption of an opposite charge layer around the nanoparticles via electrostatic interaction (Figure 26).⁹⁶

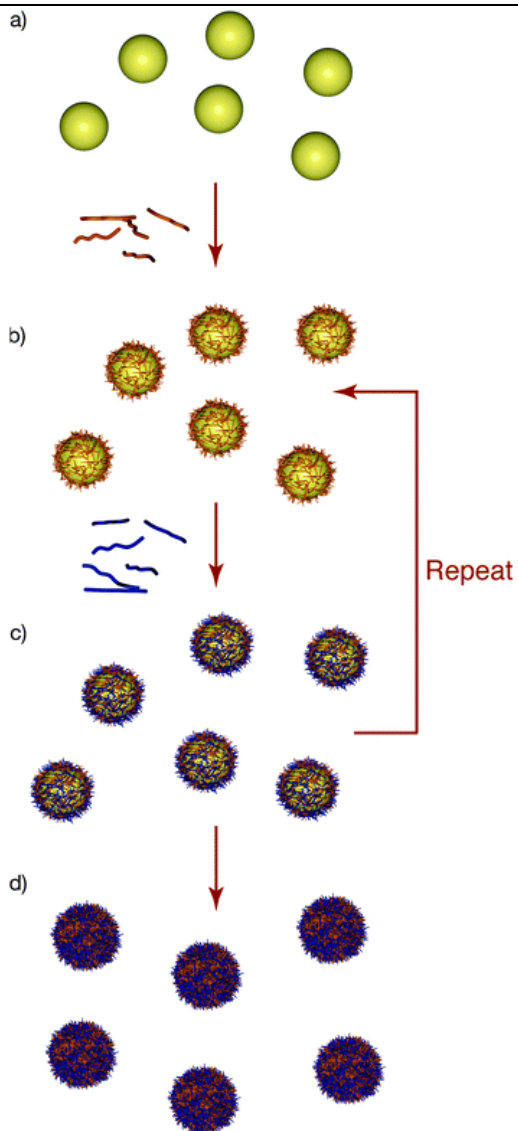


Figure 26. Schematic illustration of layer-by-layer assembly of polyelectrolytes on particles. [Reprinted with permission from ref. 97. Copyright (2010) Royal Society of Chemistry].

The LbL technique, which involves consecutive depositions of oppositely charged materials, provides a simple way to develop multifunctional particles with a precise control of their physicochemical properties. In addition to the original LbL assembly by electrostatic interaction,⁹⁷⁻⁹⁹ hydrogen bonding,¹⁰⁰ covalent bonding,¹⁰¹⁻¹⁰² and base pair interactions,¹⁰³⁻¹⁰⁴ have been used to design particles. Particles are used as a template for LbL adsorption, the particles might be a part of the multilayer (core-shell particles) or might be sacrificial and dissolved after the LbL assembly to form a capsule (Figure 27).¹⁰⁵⁻¹⁰⁶

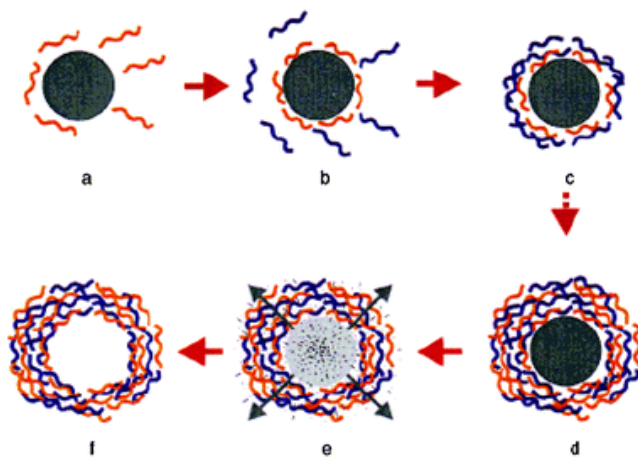


Figure 27. Schematic illustration of the layer-by-layer assembly and the subsequent dissolution of the template particle to form a capsule. [Reprinted with permission from ref. 107. Copyright (2012) Royal Society of Chemistry].

There are several disadvantages to using sacrificial template materials: the diffusion out of the capsules may apply pressure on the layers, the capsule can be deformed due to the removal of the template, or the diffusion can lead to complete rupture of the shells.¹⁰⁷⁻¹⁰⁹ Furthermore, the dissolution in organic solvents can also affect the property and stability of the polyelectrolyte layers.¹⁰⁹ Other disadvantages could be the presence of residual polymers trapped in the shell.¹⁰⁵

Core-Shell Nanoparticles as DNA Vectors

The LbL technique was first introduced by Gero Decher in 1990s and was used to assemble multilayered films with an alternate deposition of polycations and polyanions.¹¹⁰ As DNA is negatively charged, it can be incorporated into multilayered nanoparticles via the LbL technique to be used as non-viral gene delivery system. In addition, the layer self-assembly in aqueous media is favorable for preserving the DNA molecules¹¹¹ and the amount of DNA load on the particle can be controlled. Moreover, the addition of different functional polyelectrolytes might control the release of DNA, enhance the membrane penetration, or be used for intracellular targeting.¹¹² Caruso's group was the first to use DNA molecules to build LbL hollow capsules by assembling DNA onto silica particles.¹⁰³

The encapsulation of DNA in microparticles such as biodegradable poly(lactic-*co*-glycolic acid) is often inefficient and can lead to damage of the DNA.¹¹³ Many of the problems can be avoided by surface functionalization of the particles with polycation/DNA complexes instead of encapsulating DNA inside the particles.¹¹⁴⁻¹¹⁵

Li et al. designed a nanovector via the LbL technique.¹¹⁶ Cationic liposomes coated with DNA-protamine-DNA layers and protected by a layer of o-carboxymethyl-chitosan have shown high transfection efficiency. LbL assembly offers higher DNA loading and better control of the loading. The deposition of polyanions and polycations using the LbL technique might allow to achieve highly sophisticated programmable particles able to control the gene delivery and overcome biological barriers in gene delivery.

References

1. Cram, D. J., The design of molecular hosts, guests, and their complexes (Nobel lecture). *Angew. Chem. Int. Ed.* **1988**, 27 (8), 1009-1020.
2. Lehn, J. M., Supramolecular chemistry—scope and perspectives molecules, supermolecules, and molecular devices (Nobel Lecture). *Angew. Chem. Int. Ed.* **1988**, 27 (1), 89-112.
3. Pedersen, C. J., The discovery of crown ethers (Noble Lecture). *Angew. Chem. Int. Ed.* **1988**, 27 (8), 1021-1027.
4. Whitesides, G. M.; Grzybowski, B., Self-Assembly at All Scales. *Science* **2002**, 295 (5564), 2418-2421.
5. Whitesides, G. M.; Boncheva, M., Beyond molecules: Self-assembly of mesoscopic and macroscopic components. *Proc. Natl. Acad. Sci. U.S.A.* **2002**, 99 (8), 4769-4774.
6. Herb, B. R.; Wolschin, F.; Hansen, K. D.; Aryee, M. J.; Langmead, B.; Irizarry, R.; Amdam, G. V.; Feinberg, A. P., Reversible switching between epigenetic states in honeybee behavioral subcastes. *Nat. Neurosci.* **2012**, 15 (10), 1371-1373.
7. Chiti, F.; Dobson, C. M., Protein misfolding, functional amyloid, and human disease. *Annu. Rev. Biochem.* **2006**, 75, 333-366.
8. Cooper, G. M.; Hausman, R. E., *The cell*. Sinauer Associates Sunderland: 2000.

9. Dean, B.; Bhushan, B., Shark-skin surfaces for fluid-drag reduction in turbulent flow: a review. *Phil. Trans. R. Soc. A* **2010**, *368* (1929), 4775-4806.
10. Lee, S.-J.; Lim, H.-C.; Han, M.; Lee, S. S., Flow control of circular cylinder with a V-grooved micro-riblet film. *Fluid Dyn. Res.* **2005**, *37* (4), 246-266.
11. Viswanath, P., Aircraft viscous drag reduction using riblets. *Prog. Aerosp. Sci.* **2002**, *38* (6), 571-600.
12. Magin, C. M.; Finlay, J. A.; Clay, G.; Callow, M. E.; Callow, J. A.; Brennan, A. B., Antifouling performance of cross-linked hydrogels: refinement of an attachment model. *Biomacromolecules* **2011**, *12* (4), 915-922.
13. Long, C. J.; Schumacher, J. F.; Brennan, A. B., Potential for tunable static and dynamic contact angle anisotropy on gradient microscale patterned topographies. *Langmuir* **2009**, *25* (22), 12982-12989.
14. Bartlett, M. D.; Croll, A. B.; King, D. R.; Paret, B. M.; Irschick, D. J.; Crosby, A. J., Looking Beyond Fibrillar Features to Scale Gecko-Like Adhesion. *Adv. Mater.* **2012**, *24* (8), 1078-1083.
15. King, D. R.; Bartlett, M. D.; Gilman, C. A.; Irschick, D. J.; Crosby, A. J., Creating Gecko-Like Adhesives for “Real World” Surfaces. *Adv. Mater.* **2014**, *26* (25), 4345-4351.

16. Weaver, J. C.; Milliron, G. W.; Miserez, A.; Evans-Lutterodt, K.; Herrera, S.; Gallana, I.; Mershon, W. J.; Swanson, B.; Zavattieri, P.; DiMasi, E.; Kisailus, D., The Stomatopod Dactyl Club: A Formidable Damage-Tolerant Biological Hammer. *Science* **2012**, *336* (6086), 1275-1280.
17. Kang, S. O.; Llinares, J. M.; Day, V. W.; Bowman-James, K., Cryptand-like anion receptors. *Chem. Soc. Rev.* **2010**, *39* (10), 3980-4003.
18. Chen, Y.; Liu, Y., Cyclodextrin-based bioactive supramolecular assemblies. *Chem. Soc. Rev.* **2010**, *39* (2), 495-505.
19. Brotin, T.; Dutasta, J.-P., Cryptophanes and Their Complexes Present and Future. *Chem. Rev.* **2008**, *109* (1), 88-130.
20. Pedersen, C. J., Cyclic polyethers and their complexes with metal salts. *J. Am. Chem. Soc.* **1967**, *89* (26), 7017-7036.
21. Gokel, G. W.; Leevy, W. M.; Weber, M. E., Crown ethers: sensors for ions and molecular scaffolds for materials and biological models. *Chem. Rev.* **2004**, *104* (5), 2723-2750.
22. Fyles, T. M., Synthetic ion channels in bilayer membranes. *Chem. Soc. Rev.* **2007**, *36* (2), 335-347.
23. Clark, P. G.; Day, M. W.; Grubbs, R. H., Switching and Extension of a [c2]Daisy-Chain Dimer Polymer. *J. Am. Chem. Soc.* **2009**, *131* (38), 13631-13633.
24. Davis, F.; Higson, S., *Macrocycles: Construction, Chemistry and Nanotechnology Applications*. Wiley: 2011.

-
25. Lehn, J. M.; Sauvage, J. P., Cryptates. XVI. [2]-Cryptates. Stability and selectivity of alkali and alkaline-earth macrobicyclic complexes. *J. Am. Chem. Soc.* **1975**, *97* (23), 6700-6707.
 26. Kayaci, F.; Umu, O. C.; Tekinay, T.; Uyar, T., Antibacterial electrospun poly (lactic acid)(PLA) nanofibrous webs incorporating triclosan/cyclodextrin inclusion complexes. *J. Agric. Food Chem.* **2013**, *61* (16), 3901-3908.
 27. Del Valle, E. M., Cyclodextrins and their uses: a review. *Process Biochem.* **2004**, *39* (9), 1033-1046.
 28. Hedges, A. R., Industrial applications of cyclodextrins. *Chem. Rev.* **1998**, *98* (5), 2035-2044.
 29. Buschmann, H.-J.; Schollmeyer, E., Applications of cyclodextrins in cosmetic products: a review. *J. Cosmetic Sci.* **2002**, *53* (3), 185-192.
 30. Bilensoy, E., *Cyclodextrins in Pharmaceuticals, Cosmetics, and Biomedicine: Current and Future Industrial Applications*. Wiley: 2011.
 31. Loftsson, T.; Brewster, M. E., Pharmaceutical applications of cyclodextrins. 1. Drug solubilization and stabilization. *J. Pharm. Sci.* **1996**, *85* (10), 1017-1025.
 32. Gutsche, C. D., *Calixarenes Revisited*. Royal Society of Chemistry: 1998.
 33. Gutsche, C. D.; Chemistry, R. S. o., *Calixarenes: An Introduction*. RSC Publishing: 2008.
 34. Shinkai, S., Calixarenes - the third generation of supramolecules. *Tetrahedron* **1993**, *49* (40), 8933-8968.

35. Rebek Jr, J., Host-guest chemistry of calixarene capsules. *Chem. Commun.* **2000**, (8), 637-643.
36. Casnati, A.; Pochini, A.; Ungaro, R.; Ugozzoli, F.; Arnaud, F.; Fanni, S.; Schwing, M.-J.; Egberink, R. J.; de Jong, F.; Reinhoudt, D. N., Synthesis, complexation, and membrane transport studies of 1, 3-alternate calix [4] arene-crown-6 conformers: a new class of cesium selective ionophores. *J. Am. Chem. Soc.* **1995**, *117* (10), 2767-2777.
37. Tieke, B.; Toutianoush, A.; Jin, W., Selective transport of ions and molecules across layer-by-layer assembled membranes of polyelectrolytes, *p*-sulfonato-calix[n]arenes and Prussian Blue-type complex salts. *Adv. Colloid Interface Sci.* **2005**, *116* (1), 121-131.
38. Lehn, J. M.; Pousse, A., *La chimie supramoléculaire: Concepts et perspectives*. De Boeck Supérieur: 1997.
39. Vicens, J.; Harrowfield, J.; Baklouti, L., *Calixarenes in the Nanoworld*. Springer: 2006.
40. Weis, R. M.; McConnell, H. M., Two-dimensional chiral crystals of phospholipid. *Nature* **1984**, *310* (5972), 47-49.
41. Hénon, S.; Meunier, J., Microscope at the Brewster angle: Direct observation of first-order phase transitions in monolayers. *Rev. Sci. Instrum.* **1991**, *62* (4), 936-939.
42. Helm, C. A.; Möhwald, H.; Kjaer, K.; Als-Nielsen, J., Phospholipid monolayers between fluid and solid states. *Biophys. J.* **1987**, *52* (3), 381-390.

-
43. Blaudez, D.; Buffeteau, T.; Cornut, J.; Desbat, B.; Escafre, N.; Pezolet, M.; Turlet, J., Polarization-modulated FT-IR spectroscopy of a spread monolayer at the air/water interface. *Applied spectroscopy* **1993**, *47* (7), 869-874.
 44. Blaudez, D.; Buffeteau, T.; Cornut, J.; Desbat, B.; Escafre, N.; Pezolet, M.; Turlet, J., Polarization modulation FTIR spectroscopy at the air-water interface. *Thin Solid Films* **1994**, *242* (1), 146-150.
 45. Mendelsohn, R.; Mao, G.; Flach, C. R., Infrared reflection-absorption spectroscopy: principles and applications to lipid-protein interaction in Langmuir films. *Biochimica et Biophysica Acta (BBA)-Biomembranes* **2010**, *1798* (4), 788-800.
 46. Kawaguchi, M.; Tohyama, M.; Mutoh, Y.; Takahashi, A., Ellipsometric study of polymer monolayers spread at the air-water interface. 1. Thickness of monolayers. *Langmuir* **1988**, *4* (2), 407-410.
 47. Somasundaran, P., *Encyclopedia of Surface and Colloid Science*. Taylor & Francis: 2006.
 48. Sliwa, W.; Kozlowski, C., *Calixarenes and Resorcinarenes*. Wiley: 2009.
 49. Stewart, D. R.; Gutsche, C. D., Isolation, Characterization, and Conformational Characteristics of *p*-*tert*-Butylcalix[9-20]arenes. *J. Am. Chem. Soc.* **1999**, *121* (17), 4136-4146.
 50. Ishikawa, Y.; Kunitake, T.; Matsuda, T.; Otsuka, T.; Shinkai, S., Formation of calixarene monolayers which selectively respond to metal ions. *J. Chem. Soc., Chem. Commun.* **1989**, (11), 736-738.

51. Yagi, K.; Khoo, S. B.; Sugawara, M.; Sakaki, T.; Shinkai, S.; Odashima, K.; Umezawa, Y., Channel mimetic sensing membranes for alkali metal cations based on oriented monolayers of calixarene esters. *J. Electroanal. Chem.* **1996**, *401* (1–2), 65-79.
52. Nostro, P. L.; Casnati, A.; Bossoletti, L.; Dei, L.; Baglioni, P., Complexation properties of calixarenes in Langmuir films at the water-air interface. *Colloids Surf., A* **1996**, *116* (1), 203-209.
53. Lonetti, B.; Lo Nostro, P.; Ninham, B. W.; Baglioni, P., Anion Effects on Calixarene Monolayers: A Hofmeister Series Study. *Langmuir* **2005**, *21* (6), 2242-2249.
54. Lonetti, B.; Fratini, E.; Casnati, A.; Baglioni, P., Langmuir monolayers of calix[8]arene derivatives: complexation of alkaline earth ions at the air/water interface. *Colloids Surf., A* **2004**, *248* (1–3), 135-143.
55. Capuzzi, G.; Fratini, E.; Dei, L.; LoNostro, P.; Casnati, A.; Gilles, R.; Baglioni, P., Counterion complexation of calixarene ligands in monolayers and micellar solutions. *Colloids Surf., A* **2000**, *167* (1–2), 105-113.
56. Harris, E. D., Copper Homeostasis: The Role of Cellular Transporters. *Nutrition Rev.* **2001**, *59* (9), 281-285.
57. Korchowiec, B.; Orlof, M.; Sautrey, G.; Ben Salem, A.; Korchowiec, J.; Regnouf-de-Vains, J.-B.; Rogalska, E., The mechanism of metal cation binding in two nalidixate calixarene conjugates. A Langmuir film and molecular modeling study. *J. Phys. Chem. B* **2010**, *114* (32), 10427-10435.

-
58. Shahgaldian, P.; Pieleś, U.; Hegner, M., Enantioselective Recognition of Phenylalanine by a Chiral Amphiphilic Macrocyclic at the Air–Water Interface: A Copper-Mediated Mechanism. *Langmuir* **2005**, *21* (14), 6503-6507.
 59. Wapnir, R. A., *Protein Nutrition and Mineral Absorption*. Taylor & Francis: 1990.
 60. Zhang, L.; Zhang, Y.; Tao, H.; Sun, X.; Guo, Z.; Zhu, L., Investigation of calix[4]arene–porphyrin and its Palladium(II) and Zinc(II) complexes at air/water interface and in Langmuir–Blodgett film. *Thin Solid Films* **2002**, *413* (1–2), 224-230.
 61. He, W.; Liu, F.; Ye, Z.; Zhang, Y.; Guo, Z.; Zhu, L.; Zhai, X.; Li, J., Monolayers of Novel Calix[4]arene Derivative and Its Palladium(II) Complexes Formed at the Air–Water Interface. *Langmuir* **2001**, *17* (4), 1143-1149.
 62. Elend, D.; Pieleś, U.; Shahgaldian, P., Para-Carboxy Modified Amphiphilic Calixarene, Self-Assembly and Interactions with Pharmaceutically-Relevant Molecules. *Chimia* **2010**, *64* (1), 45-48.
 63. Moridi, N.; Elend, D.; Danylyuk, O.; Suwinska, K.; Shahgaldian, P., Amidophenol-Modified Amphiphilic Calixarenes: Synthesis, Interfacial Self-Assembly, and Acetaminophen Crystal Nucleation Properties. *Langmuir* **2011**, *27* (15), 9116-9121.
 64. Moridi, N.; Danylyuk, O.; Suwinska, K.; Shahgaldian, P., Monolayers of an amphiphilic para-carboxy-calix[4]arene act as templates for the crystallization of acetaminophen. *J. Colloid Interface Sci.* **2012**, *377* (1), 450-455.

65. Tulli, L. G.; Moridi, N.; Wang, W.; Helttunen, K.; Neuburger, M.; Vaknin, D.; Meier, W.; Shahgaldian, P., Polymorphism control of an active pharmaceutical ingredient beneath calixarene-based Langmuir monolayers. *Chem. Commun.* **2014**, 50 (30), 3938-3940.
66. Zadnard, R.; Arendt, M.; Schrader, T., Multipoint Recognition of Basic Proteins at a Membrane Model. *J. Am. Chem. Soc.* **2004**, 126 (25), 7752-7753.
67. Zadnard, R.; Schrader, T., Nanomolar Protein Sensing with Embedded Receptor Molecules. *J. Am. Chem. Soc.* **2005**, 127 (3), 904-915.
68. Kolusheva, S.; Zadnard, R.; Schrader, T.; Jelinek, R., Color Fingerprinting of Proteins by Calixarenes Embedded in Lipid/Polydiacetylene Vesicles. *J. Am. Chem. Soc.* **2006**, 128 (41), 13592-13598.
69. Liu, F.; Lu, G.-Y.; He, W.-J.; Liu, M.-H.; Zhu, L.-G.; Wu, H.-M., Molecular recognition of nucleotides by a calix[4]arene derivative with two alkyl guanidinium groups at the air-water interface. *New J. Chem.* **2002**, 26 (5), 601-606.
70. Liu, F.; Lu, G.-Y.; He, W.-J.; Liu, M.-H.; Zhu, L.-G., Enantioselective recognition of calix[4]arene derivatives bearing chiral bicyclic guanidinium for d/l-phenylalanine zwitterions at the air-water interface. *Thin Solid Films* **2004**, 468 (1-2), 244-249.
71. Guo, X.; Lu, G.-Y.; Li, Y., Interaction between calix[4]arene derivative bearing adenino units and complementary nucleosides at the air-water interface. *Thin Solid Films* **2004**, 460 (1-2), 264-268.

-
72. Kresina, T. F., *An Introduction to Molecular Medicine and Gene Therapy*. Wiley: 2004.
 73. Mansouri, S.; Lavigne, P.; Corsi, K.; Benderdour, M.; Beaumont, E.; Fernandes, J. C., Chitosan-DNA nanoparticles as non-viral vectors in gene therapy: strategies to improve transfection efficacy. *European Journal of Pharmaceutics and Biopharmaceutics* **2004**, *57* (1), 1-8.
 74. Vijayanathan, V.; Thomas, T.; Thomas, T., DNA nanoparticles and development of DNA delivery vehicles for gene therapy. *Biochemistry* **2002**, *41* (48), 14085-14094.
 75. Biasco, L.; Baricordi, C.; Aiuti, A., Retroviral integrations in gene therapy trials. *Mol. Ther.* **2012**, *20* (4), 709-716.
 76. Tomás, H. A.; Rodrigues, A. F.; Alves, P. M.; Coroadinha, A. S., *Lentiviral Gene Therapy Vectors: Challenges and Future Directions, Gene Therapy - Tools and Potential Applications*, Dr. Francisco Martin (Ed.), **2013**.
 77. Liechtenstein, T.; Perez-Janices, N.; Escors, D., Lentiviral vectors for cancer immunotherapy and clinical applications. *Cancers* **2013**, *5* (3), 815-837.
 78. Breyer, B.; Jiang, W.; Cheng, H.; Zhou, L.; Paul, R.; Feng, T.; He, T.-C., Adenoviral vector-mediated gene transfer for human gene therapy. *Curr. Gene Ther.* **2001**, *1* (2), 149-162.
 79. Brenner, M.; Hung, M. C., *Cancer Gene Therapy by Viral and Non-viral Vectors*. Wiley: 2014.

80. Cornforth, J. W.; Hart, P. D. A.; Nicholls, G. A.; Rees, R. J. W.; Stock, J. A., Antituberculous effects of certain surface-active polyoxyethylene ethers. *Br. J. Pharmacol.* **1955**, *10* (1), 73-86.
81. Arimori, S.; Nagasaki, T.; Shinkai, S., Tailor-making of desired assemblies from well-designed monomers: use of calix[4]arene conformers as building blocks. *J. Chem. Soc., Perkin Trans. 1* **1993**, (8), 887-889.
82. Arimori, S.; Nagasaki, T.; Shinkai, S., Self-assembly of tetracationic amphiphiles bearing a calix[4]arene core. Correlation between the core structure and the aggregation properties. *J. Chem. Soc., Perkin Trans. 2* **1995**, (4), 679-683.
83. Strobel, M.; Kita-Tokarczyk, K.; Taubert, A.; Vebert, C.; Heiney, P. A.; Chami, M.; Meier, W., Self-Assembly of Amphiphilic Calix[4]arenes in Aqueous Solution. *Adv. Funct. Mater.* **2006**, *16* (2), 252-259.
84. Tauran, Y.; Brioude, A.; Kim, B.; Perret, F.; Coleman, A., Anionic Calixarene-Capped Silver Nanoparticles Show Species-Dependent Binding to Serum Albumins. *Molecules* **2013**, *18* (5), 5993-6007.
85. McGovern, R. E.; Fernandes, H.; Khan, A. R.; Power, N. P.; Crowley, P. B., Protein camouflage in cytochrome c-calixarene complexes. *Nat. Chem.* **2012**, *4* (7), 527-533.
86. Mchedlov-Petrossyan, N.; Vilkovala, L.; Vodolazkaya, N.; Yakubovskaya, A.; Rodik, R.; Boyko, V.; Kalchenko, V., The Nature of Aqueous Solutions of a Cationic Calix[4]arene: A Comparative Study of Dye-Calixarene and Dye-Surfactant Interactions. *Sensors* **2006**, *6* (8), 962-977.

-
87. Rodik, R. V.; Klymchenko, A. S.; Jain, N.; Miroschnichenko, S. I.; Richert, L.; Kalchenko, V. I.; Mély, Y., Virus-Sized DNA Nanoparticles for Gene Delivery Based on Micelles of Cationic Calixarenes. *Chem. Eur. J.* **2011**, *17* (20), 5526-5538.
 88. Zadnarm, R.; Schrader, T., DNA Recognition with Large Calixarene Dimers. *Angew. Chem. Int. Ed.* **2006**, *45* (17), 2703-2706.
 89. Yuan, Z.; Andrew, S.; Leaf, H., In Vivo Gene Delivery by Nonviral Vectors: Overcoming Hurdles? *Molecular Therapy* **2012**, *20* (7), 1298-1304.
 90. Dudic, M.; Colombo, A.; Sansone, F.; Casnati, A.; Donofrio, G.; Ungaro, R., A general synthesis of water soluble upper rim calix[n]arene guanidinium derivatives which bind to plasmid DNA. *Tetrahedron* **2004**, *60* (50), 11613-11618.
 91. Sansone, F.; Dudič, M.; Donofrio, G.; Rivetti, C.; Baldini, L.; Casnati, A.; Cellai, S.; Ungaro, R., DNA Condensation and Cell Transfection Properties of Guanidinium Calixarenes: Dependence on Macrocyclic Lipophilicity, Size, and Conformation. *J. Am. Chem. Soc.* **2006**, *128* (45), 14528-14536.
 92. Bagnacani, V.; Franceschi, V.; Fantuzzi, L.; Casnati, A.; Donofrio, G.; Sansone, F.; Ungaro, R., Lower Rim Guanidinocalix[4]arenes: Macrocyclic Nonviral Vectors for Cell Transfection. *Bioconjugate Chem.* **2012**, *23* (5), 993-1002.

93. Bagnacani, V.; Sansone, F.; Donofrio, G.; Baldini, L.; Casnati, A.; Ungaro, R., Macrocyclic nonviral vectors: high cell transfection efficiency and low toxicity in a lower rim guanidinium calix [4] arene. *Org. Lett.* **2008**, *10* (18), 3953-3956.
94. Bagnacani, V.; Franceschi, V.; Bassi, M.; Lomazzi, M.; Donofrio, G.; Sansone, F.; Casnati, A.; Ungaro, R., Arginine clustering on calix[4]arene macrocycles for improved cell penetration and DNA delivery. *Nat. Commun.* **2013**, *4*, 1721.
95. Nault, L.; Cumbo, A.; Pretot, R. F.; Sciotti, M. A.; Shahgaldian, P., Cell transfection using layer-by-layer (LbL) coated calixarene-based solid lipid nanoparticles (SLNs). *Chem. Commun.* **2010**, *46* (30), 5581-5583.
96. Such, G. K.; Johnston, A. P.; Caruso, F., Engineered hydrogen-bonded polymer multilayers: from assembly to biomedical applications. *Chemical Society Reviews* **2011**, *40* (1), 19-29.
97. Caruso, F.; Caruso, R. A.; Möhwald, H., Nanoengineering of inorganic and hybrid hollow spheres by colloidal templating. *Science* **1998**, *282* (5391), 1111-1114.
98. Donath, E.; Sukhorukov, G. B.; Caruso, F.; Davis, S. A.; Möhwald, H., Novel hollow polymer shells by colloid-templated assembly of polyelectrolytes. *Angew. Chem. Int. Ed.* **1998**, *37* (16), 2201-2205.
99. Donath, E.; Sukhorukov, G. B.; Caruso, F.; Davis, S. A.; Möhwald, H., Novel Hollow Polymer Shells by Colloid-Templated Assembly of Polyelectrolytes. *Angew. Chem. Int. Ed.* **1998**, *37* (16), 2201-2205.

-
100. Such, G. K.; Johnston, A. P.; Caruso, F., Engineered hydrogen-bonded polymer multilayers: from assembly to biomedical applications. *Chem. Soc. Rev.* **2011**, *40* (1), 19-29.
 101. Zhang, Y.; Yang, S.; Guan, Y.; Cao, W.; Xu, J., Fabrication of stable hollow capsules by covalent layer-by-layer self-assembly. *Macromolecules* **2003**, *36* (11), 4238-4240.
 102. Tong, W.; Gao, C.; Möhwald, H., Single Polyelectrolyte Microcapsules Fabricated By Glutaraldehyde-Mediated Covalent Layer-By-Layer Assembly. *Macromol. Rapid Commun.* **2006**, *27* (24), 2078-2083.
 103. Johnston, A. P.; Read, E. S.; Caruso, F., DNA multilayer films on planar and colloidal supports: sequential assembly of like-charged polyelectrolytes. *Nano Lett.* **2005**, *5* (5), 953-956.
 104. Johnston, A. P.; Mitomo, H.; Read, E. S.; Caruso, F., Compositional and structural engineering of DNA multilayer films. *Langmuir* **2006**, *22* (7), 3251-3258.
 105. Peyratout, C. S.; Dähne, L., Tailor-Made Polyelectrolyte Microcapsules: From Multilayers to Smart Containers. *Angew. Chem. Int. Ed.* **2004**, *43* (29), 3762-3783.
 106. Tong, W.; Song, X.; Gao, C., Layer-by-layer assembly of microcapsules and their biomedical applications. *Chem. Soc. Rev.* **2012**, *41* (18), 6103-6124.
 107. Gao, G.; Moya, S.; Lichtenfeld, H.; Casoli, A.; Fiedler, H.; Donath, E.; Mohwald, H., The decomposition process of melamine formaldehyde cores: the key step in the fabrication of ultrathin polyelectrolyte multilayer capsules. *Macromol. Mater. Eng.* **2001**, *286* (6), 355-361.

108. Gao, C.; Moya, S.; Donath, E.; Mohwald, H., Melamine formaldehyde core decomposition as the key step controlling capsule integrity: optimizing the polyelectrolyte capsule fabrication. *Macromol. Chem. Phys.* **2002**, *203* (7), 953-960.
109. Déjugnat, C.; Sukhorukov, G. B., pH-responsive properties of hollow polyelectrolyte microcapsules templated on various cores. *Langmuir* **2004**, *20* (17), 7265-7269.
110. Decher, G., Fuzzy Nanoassemblies: Toward Layered Polymeric Multicomposites. *Science* **1997**, *277* (5330), 1232-1237.
111. Saurer, E. M.; Jewell, C. M.; Kuchenreuther, J. M.; Lynn, D. M., Assembly of erodible, DNA-containing thin films on the surfaces of polymer microparticles: toward a layer-by-layer approach to the delivery of DNA to antigen-presenting cells. *Acta Biomater.* **2009**, *5* (3), 913-924.
112. Avram, L.; Cohen, Y.; Rebek Jr, J., Recent advances in hydrogen-bonded hexameric encapsulation complexes. *Chem. Commun.* **2011**, *47* (19), 5368-5375.
113. Wang, C.; Ge, Q.; Ting, D.; Nguyen, D.; Shen, H.-R.; Chen, J.; Eisen, H. N.; Heller, J.; Langer, R.; Putnam, D., Molecularly engineered poly (ortho ester) microspheres for enhanced delivery of DNA vaccines. *Nat. Mater.* **2004**, *3* (3), 190-196.
114. Kasturi, S. P.; Sachaphibulkij, K.; Roy, K., Covalent conjugation of polyethyleneimine on biodegradable microparticles for delivery of plasmid DNA vaccines. *Biomaterials* **2005**, *26* (32), 6375-6385.

115. Trimaille, T.; Pichot, C.; Delair, T., Surface functionalization of poly (D, L-lactic acid) nanoparticles with poly (ethylenimine) and plasmid DNA by the layer-by-layer approach. *Colloids Surf., A* **2003**, *221* (1), 39-48.
116. Li, P.; Liu, D.; Miao, L.; Liu, C.; Sun, X.; Liu, Y.; Zhang, N., A pH-sensitive multifunctional gene carrier assembled via layer-by-layer technique for efficient gene delivery. *Int. J. Nanomed* **2012**, *7*, 925-939.

2 Synthesis and Characterization of Calixarene Derivatives

As outlined in the general introduction, extensive research involving cationic calixarenes for their interaction with DNA has been undertaken. Beside the lack of demonstrated toxicity, calixarene macrocycles – particularly the 4-membered ring derivatives – possess a rigid structure compared to larger calixarene-based amphiphiles.¹ The rigidity allows better control over the position of the “decorative” chemical functions added: the ability of calixarenes’ aromatic units to establish

π - π interactions represents an additional driving force for their self-assembly in water.² There is also an increasing interest in using calixarenes for biomolecular applications and calixarene derivatives demonstrated to interact with biomolecules such as amino acids,³ proteins,⁴⁻⁵ and nucleic acids.^{6-8,9-11}

This chapter discusses the synthesis of cationic calix[4]arenes in the cone conformation: a calix[4]arene functionalized with four guanidino functions at the upper rim and four dodecyloxy chains at the lower rim, a series of amino calix[4]arenes bearing four dodecyloxy chains at the lower rim and with one, two or three amine functions to produce the mono, di and trisubstituted calixarene derivatives at the upper rim.

2.1 Upper Rim Functionalization

Synthesis of 5,11,17,23-tetra(guanidinium)-25,26,27,28-tetra(dodecyloxy)-calix[4]arene (GC12)

The 5,11,17,23-tetra(guanidinium)-25,26,27,28-tetra(dodecyloxy)-calix[4]arene (**GC12**) was synthesized in the cone conformation¹² using a procedure described by Ungaro et al. for shorter alkyl chains.^{8, 13} The calix[4]arene **GC12** can be produced in a five steps synthesis as depicted in Figure 28.

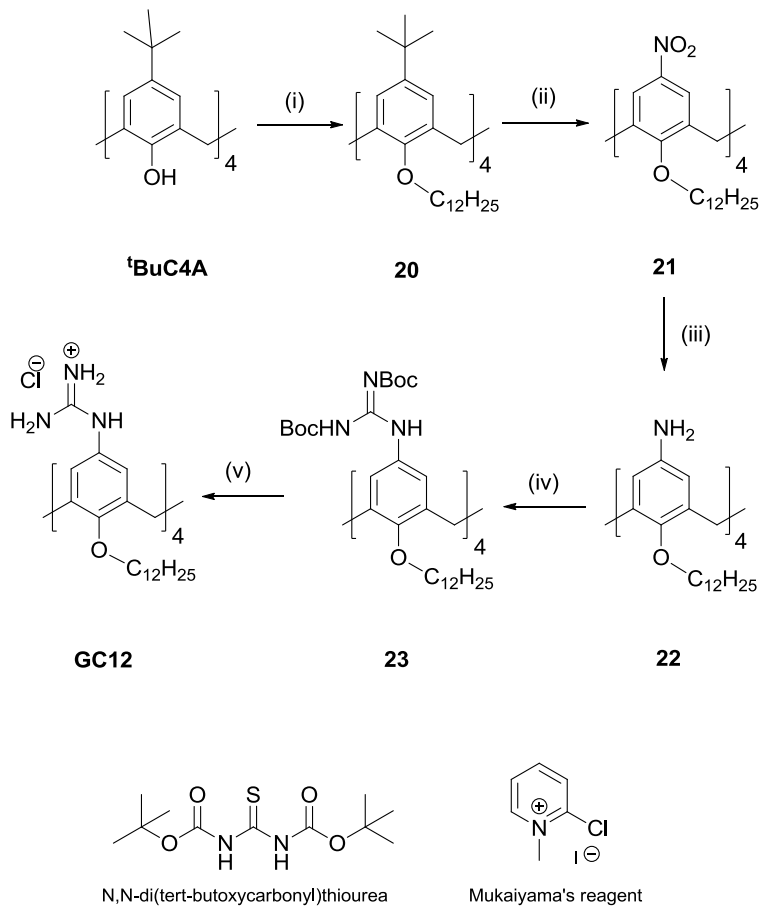


Figure 28. Synthesis route to **GC12**; reagents and conditions: (i) $\text{BrC}_{12}\text{H}_{25}$, NaH in DMF, (ii) HNO_3 (100 %), CH_3COOH CH_2Cl_2 , rt; (iii) $\text{NH}_2\text{NH}_2 \cdot \text{H}_2\text{O}$, Pd/C (10%) in EtOH under reflux; (iv) Boc-NH-C(S)-NH-Boc, Mukaiyama's reagent in CH_2Cl_2 , rt; (v) HCl/1,4-dioxane, rt.

A based catalyzed reaction of *p*-*tert*-butylphenol with formaldehyde provided the starting *p*-*tert*-butyl-calix[4]arene (**^tBuC4A**).¹⁴⁻¹⁵ Alkylation of **^tBuC4A** using an alkylating agent (bromododecane) in the presence of sodium hydride as a base in DMF, allowed to fix the calix[4]arene **20** in the cone conformation as the dodecyloxy chains are too large to allow rotation along the methylene bridges.¹³ *Para*-nitration of the calixarene **20** with nitric acid (100 %) and glacial acetic acid in dry ethanol gives 5,11,17,23-tetra(nitro)-25,26,27,28-tetra(dodecyloxy)-calix[4]arene **21**. Subsequent reduction of the nitro functions to amine is achieved using hydrazine monohydrate and palladium in ethanol under reflux. The 5,11,17,23-tetra(amino)-25,26,27,28-tetra(dodecyloxy)-calix[4]arene **22** is obtained in a yield of 80 %.¹¹ Calixarene **22** was mixed with *N,N'*-di-(*tert*-butoxycarbonyl)thiourea in the presence of 1-methyl-2-chloropyridinium iodide (Mukaiyama's reagent) and triethylamine in dry dichloromethane to provide 5,11,17,23-tetrakis[(bis-*N*-Boc)guanidine]-25,26,27,28-tetra(dodecyloxy)-calix[4]arene **23** after purification by column chromatography in a yield of 44 %. The final step involved the cleavage of the Boc protecting groups using hydrochloridric acid to produce the 5,11,17,23-tetra(guanidinium)-25,26,27,28-tetra(dodecyloxy)-calix[4]arene named **GC12** in a yield of 69 % and a general yield for the five steps synthesis of 13%.

Synthesis of *p*-amino-25,26,27,28-tetra(dodecyloxy)-calix[4]arene derivatives

In order to assess the role played by the number and position of the recognition moieties on the upper rim of the calixarene, a strategy similar to the synthesis of **GC12** was developed to produce a series of *para* amino calix[4]arenes as depicted in Figure 29.

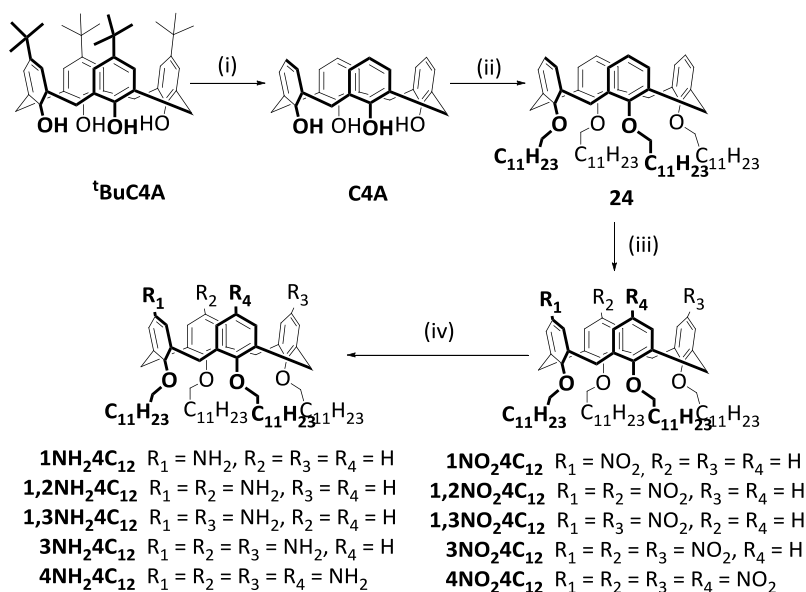


Figure 29. Synthesis route to the amino-dodecyloxy-calix[4]arene derivatives, reagents and conditions: (i) AlCl₃, phenol in toluene, rt; (ii) BrC₁₂H₂₅, NaH in DMF, rt; (iii) HNO₃ (65%), CH₃COOH in CH₂Cl₂, rt; (iv) NH₂NH₂·H₂O, Pd/C (10%) in EtOH under reflux. To facilitate identification of the calixarene structure, the calixarenes were denominated as follows: **nNO₂4C₁₂** or **nNH₂4C₁₂** where **n** indicates the number and position of the functional group, **NO₂**, **NH₂** and **NH₃⁺** the functional group at the upper rim and **4C₁₂** the tetrasubstitution of the lower rim with four dodecyloxy chains.

The amino calix[4]arene derivatives can be produced in a four-step synthesis. To functionalize the upper rim of the calix[4]arene, the *tert*-butyl functions are removed by retro Friedel-Craft alkylation in the presence of a Lewis acid (anhydrous aluminium trichloride) and phenol in toluene, to provide the 25,26,27,28-tetra(hydroxyl)-calix[4]arene **C4A** in a yield of 72 %. Calix[4]arene **24** is obtained in cone conformation after functionalization of **C4A** at the lower rim with four dodecyloxy chains.¹⁴ *Para*-nitration of **24**¹⁶ was achieved in CH₂Cl₂ with nitric acid (65 %) and glacial acetic acid, and monitored by thin layer chromatography (TLC). After 90 minutes of reaction, the TLC plate revealed two spots: the starting material calix[4]arene **24** and a new material. The two compounds were separated by flash column chromatography. After characterization by proton NMR and mass spectroscopy the new spot on the TLC was attributed to the 5-mono(nitro)-25,26,27,28-tetra(dodecyloxy)-calix[4]arene, **1NO₂4C₁₂** (yield of 16 %). With an additional 30 minutes reaction time, the TLC analysis showed two new spots and the disappearance of calixarenes **24** and **1NO₂4C₁₂** from the reaction mixture. After column chromatography, two different dinitro derivatives were obtained, with two nitro functions on either proximal rings (5,11-di(nitro)-25,26,27,28-tetra(dodecyloxy)-calix[4]arene, **1,2NO₂4C₁₂**) or opposite rings (5,17-di(nitro)-25,26,27,28-tetra(dodecyloxy)-calix[4]arene, **1,3NO₂4C₁₂**). Calixarenes **1,2NO₂4C₁₂** and **1,3NO₂4C₁₂** were produced in a yield of 4 % and 12 % respectively. The symmetric calix[4]arene **1,3NO₂4C₁₂** seems to be favored toward the asymmetric **1,2NO₂4C₁₂**, most likely as a result of steric arrangement of the nitro groups.

After 180 minutes of reaction, two new calixarenes were obtained and isolated by flash column chromatography: the 5,17-di(nitro)-25,26,27,28-tetra(dodecyloxy)-calix[4]arene **1,3NO₂4C₁₂** and the 11,17-di(nitro)-25,26,27,28-tetra(dodecyloxy)-calix[4]arene **3NO₂4C₁₂** produced in yields of 30 % and 33 % respectively. In addition, the calix[4]arene **1,2NO₂4C₁₂** could be observed on the TLC after 180 minutes of reaction. It can be assumed that present in smaller amounts than **1,3NO₂4C₁₂**, the calixarene **1,2NO₂4C₁₂** was consumed faster than **1,3NO₂4C₁₂** to form the calix[4]arene **3NO₂4C₁₂**.

The proton NMR of **1,3NO₂4C₁₂** exhibits two doublets for the protons of the four methylene bridges characteristic of a symmetrical cone calix[4]arene.¹⁷ Two multiplet signals were observed on the proton NMR spectra of **1NO₂4C₁₂**, **1,2NO₂4C₁₂** and **3NO₂4C₁₂**, indicating asymmetric calixarenes. The presence of the nitro groups in *para* position was confirmed by the shift downfield from 6.5 ppm to 7.11, 7.49, 7.43 and 7.79 ppm of the aromatic *meta* protons in the nitrated phenolic ring for **1NO₂4C₁₂**, **1,2NO₂4C₁₂**, **1,3NO₂4C₁₂** and **3NO₂4C₁₂** respectively. The subsequent reduction of the nitro groups in the corresponding amine with hydrazine and palladium on charcoal provided the calixarenes **1NH₂4C₁₂**, **1,2NH₂4C₁₂**, **1,3NH₂4C₁₂** and **3NH₂4C₁₂**, in good yields of 84 %, 87 %, 75 % and 54 % respectively. The NMR signal of the aromatic protons in *meta* position on the phenolic ring of **1NH₂4C₁₂**, **1,2NH₂4C₁₂**, **1,3NH₂4C₁₂** and **3NH₂4C₁₂** shifted upfield to 6 ppm as a result of the reduction of the nitro in amine functions.

The 5,11,17,23-tetra(amino)-25,26,27,28-tetra(dodecyloxy)-calix[4]arene **4NH₂4C₁₂** was synthesized according to the literature procedure.¹¹ All the amino calixarenes were obtained in the non-protonated amine form.

To investigate the influence of the protonation of the amine functions on the self-assembly as nanoparticles and on the interaction with DNA, the amino calixarene derivatives were protonated in the presence of hydrochloridric acid. Briefly, the solution of calixarenes in dichloromethane was washed once with an HCl solution at 0.1 N. The organic phase was dried over Na₂SO₄ and the solvent evaporated under reduced pressure. The protonation of the tertiary amines of the calixarene derivatives was confirmed by NMR. Strong chemical shifts were observed for the aromatic protons on the proton NMR. The appearance of a broad peak at 10.20 ppm, 9.37 ppm, 9.41 ppm, 6.03 ppm and 3.92 ppm that integrated respectively for 3, 6, 5, 9, and 12 protons was observed for the NH protons of **1NH₃⁺4C₁₂**, **1,2NH₃⁺4C₁₂**, **1,3NH₃⁺4C₁₂**, **3NH₃⁺4C₁₂** and **4NH₃⁺4C₁₂** respectively.

2.2 Lower Rim Functionalization

Tetrasubstitution of *p*-acyl-calix[4]arene

Lower rim modifications at the phenolic hydroxyl groups with guanidine moieties while acyl functions are present in *para* position are more challenging than the functionalization of the upper rim.

To fix the calixarenes in the cone conformation, Friedel-Craft acylation was performed with lauryl chloride and aluminium chloride as the catalyst in nitrobenzene (Figure 30).¹⁸

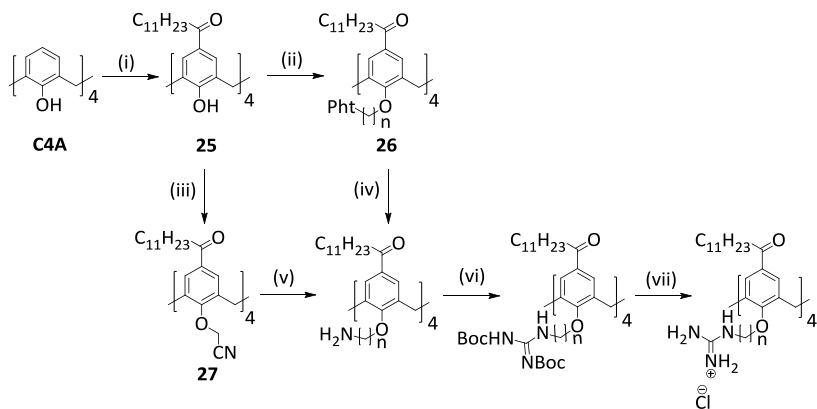


Figure 30. Synthesis route planned to the tetraacyl-tetraguanidino-calix[4]arene, reagents and conditions: (i) $C_{11}H_{23}C(O)Cl$, $AlCl_3$, in nitrobenzene, rt; (ii) $Br(CH_2)_nPh$, base (NaH or K_2CO_3) in CH_3CN under reflux; (iii) XCH_2CN ($X = Cl, Br$ or I), base (NaH or K_2CO_3) in different solvents (DMF and acetone), rt; (iv) $NH_2NH_2 \cdot H_2O$, Pd/C (10%) in EtOH under reflux; (v) $LiAlH_4$ or BH_3 in THF under reflux; (vi) $Boc-NH-C(S)-NH-Boc$, Mukaiyama's reagent in CH_2Cl_2 , rt; (vii) $HCl/1,4$ -dioxane, rt.

Friedel-Crafts acylation involves electrophilic substitution catalyzed by aluminium trichloride, a Lewis acid. The aluminium trichloride assists in the formation of an acyl cation that serves as an electrophile for aromatic substitution. Electrophilic aromatic substitution begins with the addition of the electrophile into the aromatic π system of the ring. A conjugated, carbocation intermediate is formed, a resonance combination of three forms, concentrating positive charge at three locations: the two ortho and one para positions. Finally, the proton departs and substitution at the carbon is complete with aromaticity restored.

As shown in Figure 30, two synthetic routes were considered to produce the lower rim guanidino-calixarene derivatives. The electrophilic substitution using bromoethyl or bromopropyl phthalimide in dry DMF in the presence of a base (e.g. sodium hydride or potassium carbonate) leads to the production of a mixture, even after a few days of reaction, in which the different compounds were impossible to isolate. For the second synthetic route, chloro-, bromo- or iodo-acetonitrile were tested as alkylating agents. Independently of the condition tested (e.g. base, solvent, temperature), only a mixture or the starting materials could be recovered. The steric hindrance of the phthalimide or cyanide functions does not favor the *O*-substitution of the calixarene due to the small cavity of the calix[4]arene and the presence of the acyl function in *para* position. Indeed, the acyl group due to the electronegativity of the oxygen atom, which draws electron density toward itself and leaves the carbon electron-poor is an electron withdrawing group.

Nevertheless, Jebors et al., reported on *para* acylcalix[8]arenes fully functionalized with four butyronitrile at the lower rim. However, in the same publication they also reported on *para* acylcalix[6]arenes bearing octanoyl and hexadecanoyl chains at the upper rim. Their attempts to functionalize the lower rim with different alkylating agents (e.g. bromoacetonitrile, bromopropionitrile) were unsuccessful and an intractable mixture or decomposition was observed.^{1, 19} To functionalize the lower rim in the presence of acyl function at the upper rim, an alkylating agent with a longer alkyl spacer between the halogen and the phthalimide or cyanide function could be investigated.

Selective Disubstitution of *p*-diacyl-calix[4]arene

Synthesis of the di(guanidino)-calixarene at the lower rim was also attempted. The synthesis involved six reaction steps as shown in Figure 31.

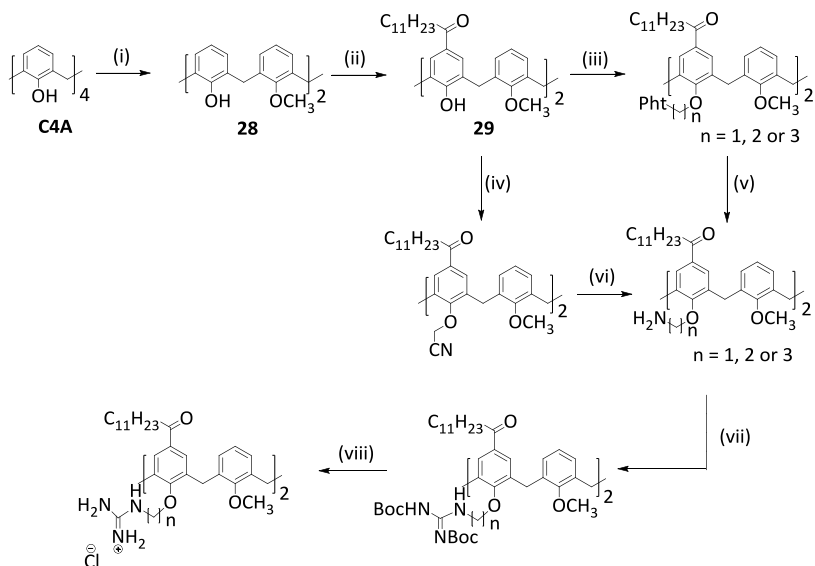


Figure 31. Synthesis route planned to the 5,11,17,23-diaacyl-25,26,27,28-tetra(guanidino)-calix[4]arene, reagents and conditions: (i) MeI, K₂CO₃ in CH₃CN under reflux; (ii) C₁₁H₂₃C(O)Cl, AlCl₃, in nitrobenzene, rt; (iii) Br(CH₂)_nPht, base in CH₃CN under reflux; (iv) XCH₂CN (X = Cl, Br or I), K₂CO₃ in different solvents (DMF and acetone), under reflux; (v) NH₂NH₂·H₂O, Pd/C (10%) in EtOH under reflux; (vi) LiAlH₄ or BH₃ in THF under reflux; (vii) Boc-NH-C(S)-NH-Boc, Mukaiyama's reagent in CH₂Cl₂, rt; (viii) HCl/1,4-dioxane, rt.

Partial alkylation of the lower rim of the calixarene **4A** was performed using iodomethane and potassium carbonate as a base in acetonitrile; it provided calixarene **28** in a good yield of 63 %. Partial alkylation allows to selectively acylate the *para* position of the calixarene.

The selective acylation was performed in nitrobenzene, with two equivalents of lauroyl chloride and aluminium trichloride as described in Section 2.1.1. The calixarene **29** was synthesized in a yield of 66 %. All attempts to alkylate the remaining hydroxyl groups with an alkylating agent (halogeno-phthalimide or halogeno-cyanide) and a base (potassium carbonate or sodium hydride) were unsuccessful. As with the tetraacyl calixarene, inseparable mixtures were obtained.

Conclusions

A series of calix[4]arenes bearing four dodecyloxy chains as hydrophilic functions at the lower rim and four guanidinium functions (**GC12**) or one, two and three amine functions (**1NH₂4C₁₂**, **1,2NH₂4C₁₂**, **1,3NH₂4C₁₂** and **3NH₂4C₁₂**) as recognition moieties at the upper rim have been synthesized and fully characterized.

On the other hand, lower rim modification of *p*-acyl calixarenes is much more challenging and all attempts to alkylate the lower rim with an alkylating agent such as halogeno-phthalimide or halogeno-cyanide were unsuccessful.

References

1. Jebors, S.; Fache, F.; Balme, S.; Devoge, F.; Monachino, M.; Cecillon, S.; Coleman, A. W., Designer amphiphiles based on para-acyl-calix[8]arenes. *Org. Biomol. Chem.* **2008**, *6* (2), 319-329.
2. Helttunen, K.; Shahgaldian, P., Self-assembly of amphiphilic calixarenes and resorcinarenes in water. *New J. Chem.* **2010**, *34* (12), 2704-2714.
3. Shahgaldian, P.; Pieles, U.; Hegner, M., Enantioselective Recognition of Phenylalanine by a Chiral Amphiphilic Macrocyclic at the Air–Water Interface: A Copper-Mediated Mechanism. *Langmuir* **2005**, *21* (14), 6503-6507.
4. Perret, F.; Coleman, A. W., Biochemistry of anionic calix[n]arenes. *Chem. Commun.* **2011**, *47* (26), 7303-7319.
5. McGovern, R. E.; Fernandes, H.; Khan, A. R.; Power, N. P.; Crowley, P. B., Protein camouflage in cytochrome c-calixarene complexes. *Nat. Chem.* **2012**, *4* (7), 527-533.
6. Bagnacani, V.; Franceschi, V.; Bassi, M.; Lomazzi, M.; Donofrio, G.; Sansone, F.; Casnati, A.; Ungaro, R., Arginine clustering on calix[4]arene macrocycles for improved cell penetration and DNA delivery. *Nat. Commun.* **2013**, *4*, 1721.
7. Rullaud, V.; Siragusa, M.; Cumbo, A.; Gygax, D.; Shahgaldian, P., DNA surface coating of calixarene-based nanoparticles: a sequence-dependent binding mechanism. *Chem. Comm.* **2012**, *48* (100), 12186-12188.

8. Sansone, F.; Dudič, M.; Donofrio, G.; Rivetti, C.; Baldini, L.; Casnati, A.; Cellai, S.; Ungaro, R., DNA Condensation and Cell Transfection Properties of Guanidinium Calixarenes: Dependence on Macrocycle Lipophilicity, Size, and Conformation. *J. Am. Chem. Soc.* **2006**, *128* (45), 14528-14536.
9. Yuan, Z.; Andrew, S.; Leaf, H., In Vivo Gene Delivery by Nonviral Vectors: Overcoming Hurdles? *Molecular Therapy* **2012**, *20* (7), 1298-1304.
10. Liu, F.; Lu, G.-Y.; He, W.-J.; Liu, M.-H.; Zhu, L.-G.; Wu, H.-M., Molecular recognition of nucleotides by a calix[4]arene derivative with two alkyl guanidinium groups at the air-water interface. *New J. Chem.* **2002**, *26* (5), 601-606.
11. Shahgaldian, P.; Sciotti, M. A.; Pielas, U., Amino-Substituted Amphiphilic Calixarenes: Self-Assembly and Interactions with DNA. *Langmuir* **2008**, *24* (16), 8522-8526.
12. Moridi, N.; Wäckerlin, C.; Rullaud, V.; Schelldorfer, R.; Jung, T. A.; Shahgaldian, P., Langmuir–Blodgett monolayer stabilization using supramolecular clips. *Chem. Commun.* **2013**, *49* (4), 367-369.
13. Dudic, M.; Colombo, A.; Sansone, F.; Casnati, A.; Donofrio, G.; Ungaro, R., A general synthesis of water soluble upper rim calix[n]arene guanidinium derivatives which bind to plasmid DNA. *Tetrahedron* **2004**, *60* (50), 11613-11618.
14. Arduini, A.; Casnati, A., *Macrocycle Synthesis: A Practical Approach*. Oxford University Press: 1996.

15. Gutsche, C. D.; Chemistry, R. S. o., *Calixarenes: An Introduction*. RSC Publishing: 2008.
16. Kelderman, E.; Verboom, W.; Engbersen, J. F. J.; Reinhoudt, D. N.; Heesink, G. J. T.; van Hulst, N. F.; Derhaeg, L.; Persoons, A., Nitrocalix [4]arenes as Molecules for Second-Order Nonlinear Optics. *Angew. Chem. Int. Ed.* **1992**, *31* (8), 1075-1077.
17. Vreekamp, R. H.; Verboom, W.; Reinhoudt, D. N., Aggregates of calix[4]arenes based on the 2,6-diaminotriazine · imide system. *Recl. Trav. Chim. Pays-Bas* **1996**, *115* (7-8), 363-370.
18. Shahgaldian, P.; Coleman, A. W.; Kalchenko, V. I., Synthesis and properties of novel amphiphilic calix-[4]-arene derivatives. *Tetrahedron Lett.* **2001**, *42* (4), 577-579.
19. Jebors, S.; Leśniewska, B.; Shkurenko, O.; Suwińska, K.; Coleman, A. W., Para-acylcalix [6] arenes: their synthesis, per-O-functionalisation, solid-state structures and interfacial assembly properties. *J. Incl. Phenom. Macrocycl. Chem.* **2010**, *68* (1-2), 207-217.

3 Calixarene Langmuir Films: Self-Assembly and DNA Interaction Study

Part of the work described in this dissertation was performed using the Langmuir balance technique to study calix[4]arene monolayer films' properties at the water-air interface. In addition, the influence of DNA molecules on calixarene Langmuir monolayers was investigated.

The study of the interactions of three model double-stranded DNA sequences with the produced calix[4]arene (Chapter 2) as Langmuir films is reported in this chapter.

3.1 GC12 Self-Assembly as Langmuir Monolayer and DNA Interaction

To study the interactions of **GC12** (Figure 32), self-assembled at the air-water interface as Langmuir monolayers, compression isotherm experiments were carried out using four different sub-phases: pure water and three different 30-mer duplexes, **AT**, **GC** and **ATGC** at four different concentrations of 10^{-6} (54 pM), 10^{-5} (540 pM), 10^{-4} g L⁻¹ (5.4 nM) and 5.10^{-4} g L⁻¹ (27 nM).

The measured isotherms at a concentration of 5.10^{-4} g L⁻¹ (27 nM) are shown in Figure 33, and the isotherm measured at DNA concentrations of 10^{-6} (54 pM), 10^{-5} (540 pM), 10^{-4} g L⁻¹ (5.4 nM) are reported in Figure S1 in the supporting information in Chapter 7. From the compression isotherms, collapse pressure and apparent limiting molecular area values were extracted. Collapse pressure is defined as the maximum surface pressure before the collapse of the film. The apparent molecular area is the area per molecule under maximum packing conditions extrapolated to zero surface pressure.¹

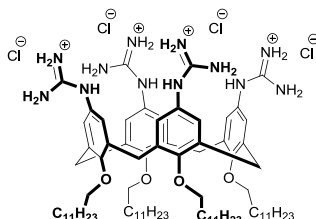


Figure 32. Structure of **GC12** molecule.

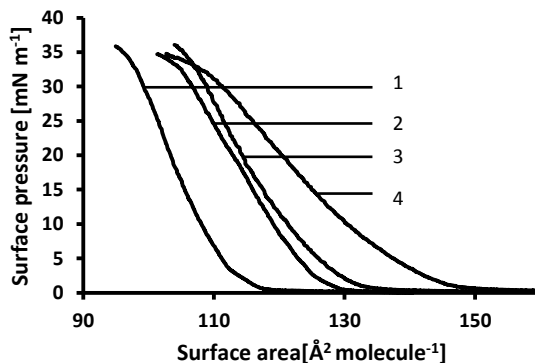


Figure 33. Π -A isotherms of **GC12** monolayers on pure water (1) and on aqueous subphases of **ATGC** (2), **GC** (3) and **AT** (4) at a concentration of $5 \cdot 10^{-4} \text{ g L}^{-1}$ (27 nM).

Figure 33, shows that the compression isotherm of **GC12**, measured on pure water, has a collapse pressure of 37 mN m^{-1} and a limiting area of 111 \AA^2 . The compression isotherm reveals a phase transition at a pressure of 4 mN m^{-1} and a surface area of $103 \text{ \AA}^2 \text{ molecule}^{-1}$, attributed to a liquid-expanded/liquid-condensed phase transition.

In Figure 34 are presented the variation of collapse pressures and apparent molecular areas as function of DNA concentrations.

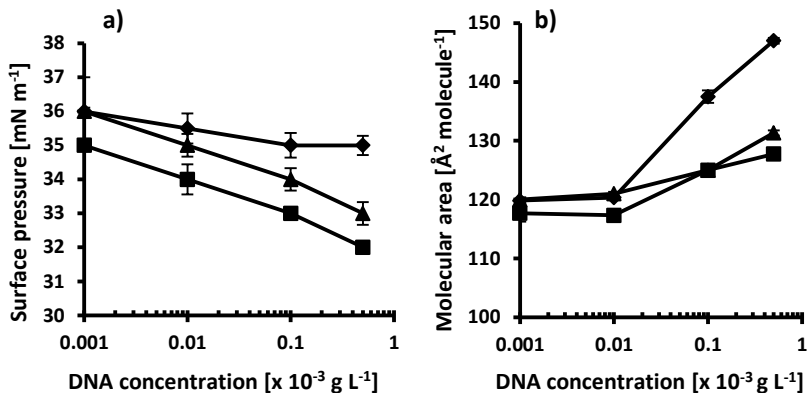


Figure 34. Evolution of collapse pressure **a)** and apparent molecular area **b)** in function of DNA concentration [**AT** (\blacklozenge), **GC** (\blacktriangle) and **ATGC** (\blacksquare)].

From Figure 33 and Figure 34, it can be noticed that the presence of increasing concentrations of **GC** of 10^{-6} , 10^{-5} , 10^{-4} and $5.10^{-4} \text{ g L}^{-1}$ in the subphase causes a decrease of the collapse pressure with values of 36, 35, 34, 33 mN m^{-1} respectively compared to the value of 37 mN m^{-1} obtained on pure water. The decrease in collapse pressure values was attributed to an interaction between the DNA duplex and **GC12** monolayer. In the presence of **ATGC**, a decrease of the collapse pressure values was also observed with values of 35, 34, 33, 32 mN m^{-1} for **ATGC** concentrations of 10^{-6} , 10^{-5} , 10^{-4} and $5.10^{-4} \text{ g L}^{-1}$, respectively. The compression isotherms in the presence of **AT** at concentrations of 10^{-6} , 10^{-5} , 10^{-4} and $5.10^{-4} \text{ g L}^{-1}$ in the subphase showed collapse pressure values of 36, 34, 35 and 35 mN m^{-1} respectively. Those values of collapse pressure are slightly higher than they are with **GC** or **ATGC**. On pure water, the apparent molecular area of $111 \text{ \AA}^2 \text{ molecules}^{-1}$ was measured for **GC12** monolayer.

This value is consistent with the cone conformation of the calixarene macrocycle with the pseudo- C_4 symmetry axis of the macrocycle orthogonal to the air-water interface.² An expansion of **GC12** monolayer is observed in the presence of DNA in the subphase for all sequences and concentrations of DNA tested. In the presence of **ATGC** in the subphase, apparent molecular area values of 118, 125 and 128 Å² molecule⁻¹ were measured for **ATGC** concentrations of 10⁻⁵, 10⁻⁴ and 5.10⁻⁴ g L⁻¹, respectively. In the case of **GC**, the increase of the apparent molecular area values observed at concentrations of 10⁻⁵, 10⁻⁴ and 5.10⁻⁴ g L⁻¹ were slightly higher than with **ATGC** in the subphase. Values of 121, 125 and 131 Å² molecule⁻¹ were measured. Interestingly, **GC12** monolayer expansion was significantly more pronounced when **AT** was present in the subphase. The molecular area values were measured to be 120, 138 and 147 Å² molecule⁻¹ at concentrations of 10⁻⁵, 10⁻⁴ and 5.10⁻⁴ g L⁻¹, respectively. These results suggested a change in the packing of the monolayer due to electrostatic interactions between **GC12** and DNA molecules at the air-water interface as previously observed for amphiphilic amino-calixarene derivatives.³

Overall, the differences observed for both collapse pressure and molecular area values rule out the possibility that the interactions of DNA with **GC12**-based monolayers are of a purely non-specific electrostatic nature, and demonstrate that the interactions with the monolayer are influenced by the composition, and therefore by the structure, of the DNA duplex. It is known that **AT**-DNA preferentially adopts an unusual B-form so-called B'-conformation in which the minor groove is more narrow than in the B-form DNA and has reluctance to conformational changes.⁴⁻⁶

Indeed, the base stacking of B'-DNA is due to purine-purine stacking that is maximized by a high propeller twist (up to 25°) that allows interactions between the neighboring base pairs, producing a zigzag system of hydrogen bonds in the major groove. **GC** and a random DNA sequence such as **ATGC** might adopt a different conformation (e.g. B-, A-, or Z-form). These different DNA conformations have different structural characteristics that can have an effect on the monolayer self-assembly. For example, the change in conformation from B- to A-form induces a change in groove sizes. It is known that the width of the major groove of A-DNA is 2.7 Å while the minor groove width is 11 Å.

In the case of B-DNA, the major and minor grooves have widths of 11.7 and 5.7 Å respectively. The differences observed in the behavior of **GC12**-based monolayer might be explained by the differences in the double helix structure. Indeed, in the presence of **ATGC** or **GC** the packing of the monolayer was tighter compared to that in the presence of **AT**. To further investigate the films' properties, the stability of the **GC12** monolayers on nanopure water, **AT**, **GC** and **ATGC** subphases were studied. The compressions of the monolayers were stopped when the surface pressure reached 35 mN m⁻¹. The evolution of the films' surface tension was monitored as a function of time. The results are shown in Figure 35.

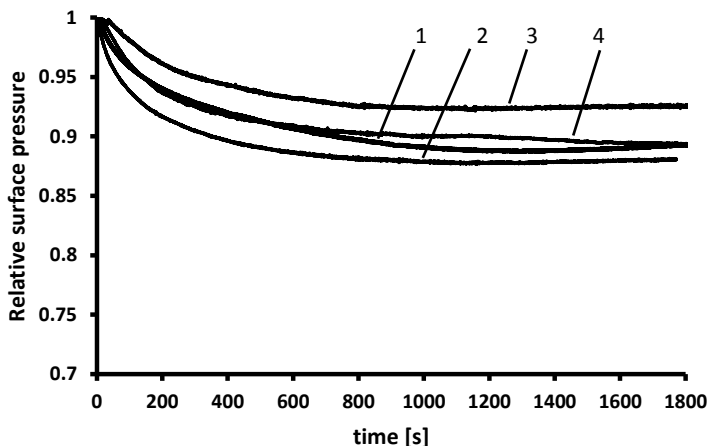


Figure 35. Stability test of **GC12** monolayers in the presence of nanopure water (1), **AT** (2), **GC** (3) and **ATGC** (4) at a concentration of 0.1 mg L^{-1} as a function of time. The relative surface pressure corresponded to the difference between the surface pressure measured after the barriers were stopped and the surface pressure at the moment the barrier were stopped.

Figure 35 shows that the surface pressure decreased by 5 % on **GC** subphase and 10 % on water, **AT** and **ATGC** subphases over 30 minutes of monitoring. Nevertheless, after 10 minutes of relaxation, the surface pressure of **GC12** monolayers are stabilized and no further decrease in surface pressure could be observed for all the surface tested. The decreases in surface pressure could be due to a relaxation of the molecule, but might also be attributed to partial dissolution of the film material into the subphase.

To confirm the interaction with DNA at the air-water interface, the morphologies of **GC12** monolayers were analyzed using a Brewster angle microscope (BAM).⁷⁻⁹ The most relevant images were recorded at a surface pressure of 0.5 mN m^{-1} after 30 minutes of relaxation, as shown in Figure 36.

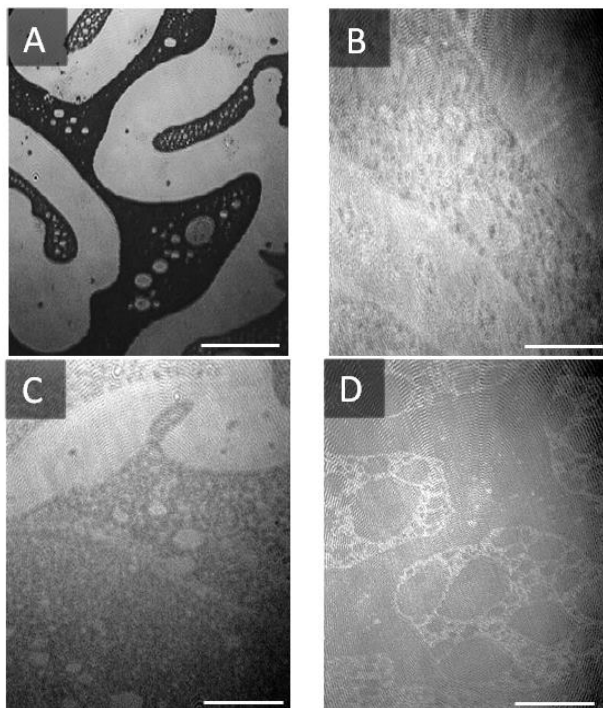


Figure 36. BAM images of **GC12** monolayer at the air-water interface at $\pi = 0.5 \text{ mN m}^{-1}$ (A) on pure water, (B) on **GC-DNA**, (C) on **AT-DNA** and (D) on **ATGC-DNA** subphase at a concentration of 10^{-4} g L^{-1} . Scale bar = $100 \mu\text{m}$.

BAM micrographs of **GC12** monolayer, measured on pure water, revealed the presence of liquid domains (brighter regions) within a gas-phase (dark background). No gas-phase domains, even at a surface pressure as low as 0.5 mN m^{-1} , were observed for **GC12** monolayers acquired on subphases containing **GC** and **AT** (10^{-4} g L^{-1}). The monolayers are composed of phases with different contrasts, suggesting the co-existence of liquid phases with different densities. On **ATGC** subphase, the BAM images of **GC12** monolayer revealed a foam-like texture, most likely composed of a liquid-condensed phase within a lower packing density phase (darker). These results suggest an interaction between **GC12** self-assembled as monolayer and DNA molecules present in the subphase. Upon further compression, and for all the subphases tested, only bright homogeneous domains, attributed to homogenous condensed phases, covered the entire surface of the trough.

To further characterize the interaction between **GC12** monolayers and the different DNA sequences, the thickness of the monolayer at the air-water interface was measured using surface ellipsometry. The thickness of **GC12** monolayers at the air-water interface was estimated using the BAM software calibration procedure, which determined the linear function between the reflectance and the gray level. The gray level of the BAM images, corresponding to optically saturated and totally dark states of the camera and the thickness of the monolayers, was estimated using a refractive index between 1.44 and 1.46.¹⁰⁻¹¹

In Figure 37 the estimated thickness values of the **GC12** monolayers at increasing surface pressure values (10, 20 and 35 mN m^{-1}) are shown.

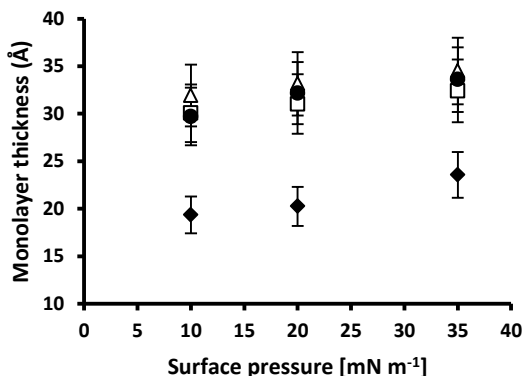


Figure 37. Thickness of **GC12** monolayer as function of the surface pressure on pure water (●), **AT** (□), **GC** (△) and **ATGC** (◆) subphases at a concentration of 10^{-4} g L^{-1} .

The thickness of monolayer **GC12** spread on pure water is measured to be 20 \AA at a surface pressure of 10 mN m^{-1} and increases up to $23 \pm 2 \text{ \AA}$ at a surface pressure of 35 mN m^{-1} . The value of $23 \pm 2 \text{ \AA}$ at high packing density is consistent with the molecular structure of **GC12**, with the alkyl chains oriented in an all-parallel fashion. The thickness of the monolayers increased linearly upon compression as a result of the increasing packing density of **GC12** monolayers. In the presence of DNA in the subphase, the measured thickness was greater in all cases than that measured on pure water. At a surface pressure of 35 mN m^{-1} , thicknesses of $35 \pm 3 \text{ \AA}$, $34 \pm 3 \text{ \AA}$, and $32 \pm 3 \text{ \AA}$ were measured in the presence of **GC**, **AT** and **ATGC** respectively at a concentration of 10^{-4} g L^{-1} in the subphase.

An increase of 12 Å, 11 Å and 9 Å was observed in the presence of **GC**, **AT** and **ATGC** respectively. As the DNA double helix has a diameter of approximately 20 Å, a measured thickness of approximately 43 Å can be expected in the case of a fully compact layer of DNA beneath the calixarene monolayer. Castano et al., have studied the thickness of a lipid monolayer at the air-water interface beneath an incomplete DNA layer. They measured an increase of 7 Å of the monolayer in the presence of DNA.¹² The discrepancy between the measured thicknesses could be explained by the non-homogeneous density of the DNA monolayer under the closed packed monolayer calixarene.

3.2 Amino-Calix[4]arene Derivatives Self-Assembly as Langmuir Monolayers and DNA Interaction

The self-assembly of the amino calix[4]arene derivatives **1NH₂4C₁₂**, **1,2NH₂4C₁₂**, **1,3NH₂4C₁₂**, **3NH₂4C₁₂** and **4NH₂4C₁₂** (Figure 38) as Langmuir monolayers was also investigated; Langmuir monolayer experiments were performed on nanopure water and on DNA subphases.

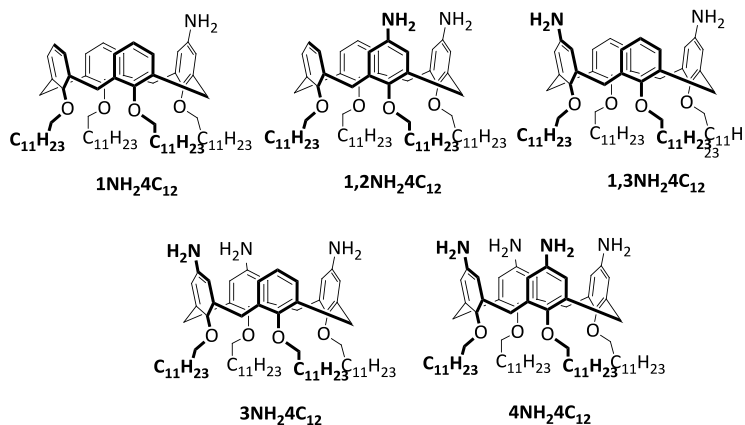


Figure 38. Structures of the amino-calixarene derivatives.

Compression isotherm experiments were carried out using the 30-mer duplex **ATGC** at a concentration of 10^{-4} g L⁻¹. The measured isotherms are shown in Figure 39 and the characteristic values extracted from the compression isotherms are shown in Table 1. The amino-calixarenes derivatives **1,2NH₂4C₁₂**, **1,3NH₂4C₁₂**, **3NH₂4C₁₂** and **4NH₂4C₁₂** formed stable Langmuir monolayers on pure water with a collapse pressure of 40, 45, 52 and 46 mN m⁻¹ respectively. The lowest collapse pressure value was obtained for **1NH₂4C₁₂** monolayer, with a collapse pressure value of 20 mN m⁻¹. **1NH₂4C₁₂** formed a less stable monolayer at the air-water interface than the di-, tri- and tetraamino-calixarene derivatives. This difference of stability can be explained by the presence of only one amine function at the upper rim of the calixarene.

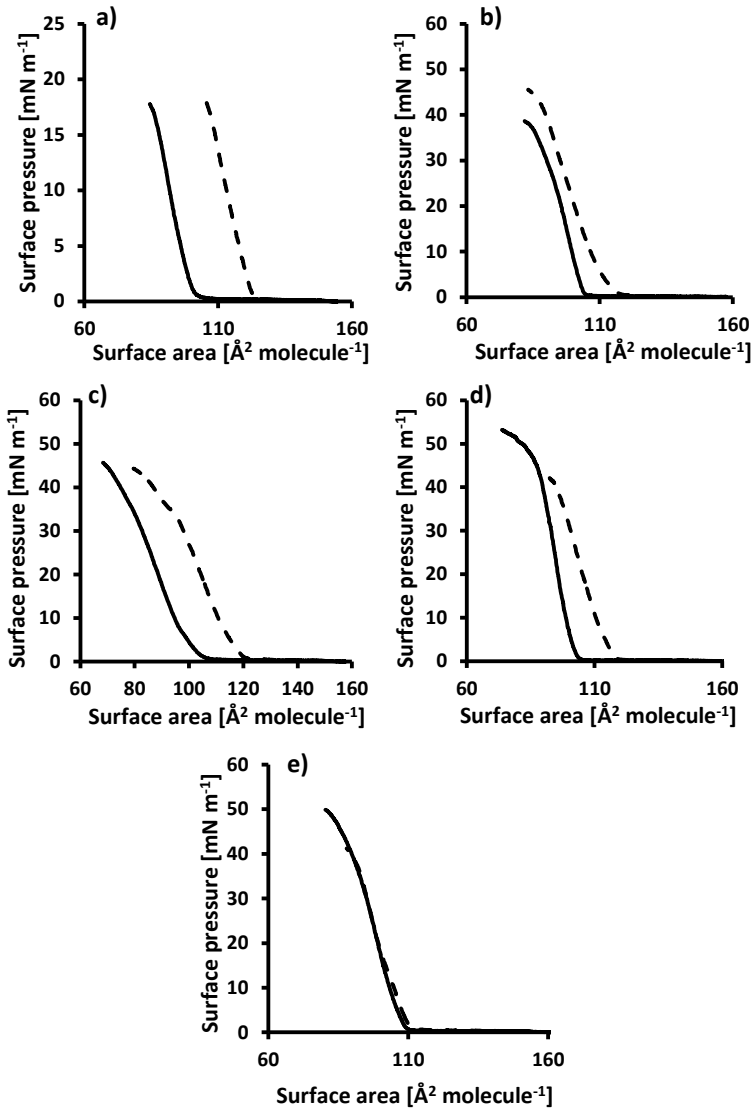


Figure 39. Langmuir isotherms of a) 1NH₂4C₁₂, b) 1,2NH₂4C₁₂, c) 1,3NH₂4C₁₂, d) 3NH₂4C₁₂ and e) 4NH₂4C₁₂ on water (—) and on ATGC (---) subphase.

Table 1. Characteristic values extracted from Langmuir compression isotherms of **1NH₂4C₁₂**, **1,2NH₂4C₁₂**, **1,3NH₂4C₁₂**, **3NH₂4C₁₂** and **4NH₂4C₁₂** on a water subphase or on a subphase containing **ATGC** at a concentration of 10⁻⁴ g L⁻¹.^a

	Nanopure water		ATGC	
	Collapse pressure [mN m ⁻¹]	Limiting molecular area [Å ² molecule ⁻¹]	Collapse pressure [mN m ⁻¹]	Limiting molecular area [Å ² molecule ⁻¹]
1NH₂4C₁₂	20	99	18	123
1,2NH₂4C₁₂	40	105	45	112
1,3NH₂4C₁₂	45	101	45	118
3NH₂4C₁₂	52	98	42	118
4NH₂4C₁₂	46	106	40	108

^a The limiting molecular area was obtained by extrapolation of the linear part of the isotherm on the x-axis.

From the compression isotherms (Figure 39), molecular area values of 99, 105, 101, 98 and 106 Å² molecule⁻¹ were extracted for calixarenes **1NH₂4C₁₂**, **1,2NH₂4C₁₂**, **1,3NH₂4C₁₂**, **3NH₂4C₁₂** and **4NH₂4C₁₂** respectively. As Figure 39 shows, no phase transition on the compression isotherms of all the amino-calixarene derivatives for the liquid-expanded/liquid-condensed phase on pure water could be observed. As shown in Table 1, the collapse pressure values of **1NH₂4C₁₂**, **3NH₂4C₁₂** and **4NH₂4C₁₂** monolayers decreased from to 20, 52 and 46 mN m⁻¹ on pure water to 18, 42 and 40 mN m⁻¹ respectively in the presence of **ATGC** in the subphase. Interestingly, an increase of the collapse pressure was observed for the calixarene **1,2NH₂4C₁₂** with a collapse pressure value of 40 mN m⁻¹ on pure water to 45 mN m⁻¹ on **ATGC**-DNA subphase.

No changes were observed for the collapse pressure of **1,3NH₂4C₁₂** monolayer with a value of 45 mN m⁻¹ both on water and on **ATGC**-DNA subphase. A clear expansion of the limiting molecular areas was observed in the presence of **ATGC** for all the amino-calixarene derivatives tested, with values of 123, 112, 118, 118 and 108 Å² molecule⁻¹ for **1NH₂4C₁₂**, **1,2NH₂4C₁₂**, **1,3NH₂4C₁₂**, **3NH₂4C₁₂** and **4NH₂4C₁₂** respectively. The limiting molecular area values obtained on **ATGC** subphase with respect to the limiting molecular areas measured on pure water subphase increased by 7 Å² molecule⁻¹, 17 Å² molecule⁻¹, 20 Å² molecule⁻¹ and 32 Å² molecule⁻¹ for **1,2NH₂4C₁₂**, **3NH₂4C₁₂**, **4NH₂4C₁₂** and **1NH₂4C₁₂** respectively. The decrease of the collapse pressure values and the increase of the limiting molecular areas in the presence of **ATGC** suggest a change in the packing of the monolayer owing to interactions with **ATGC**-DNA. Moreover, the differences observed between all the amino-calixarene derivatives monolayers show that the interaction with DNA is dependent on the number of recognition moieties on the *para* position of the calixarenes.

The effect of the DNA sequence on **4NH₂4C₁₂** Langmuir monolayers have been investigated using **AT** and **GC** in the subphase. From Figure 40 and Table 2, it can be noticed that while the collapse pressure values of **4NH₂4C₁₂** monolayers are 46 mN m⁻¹ and 40 mN m⁻¹ on pure water and on **ATGC** respectively, collapse pressures of 44 and 34 mN m⁻¹ were obtained in the presence of **AT** and **GC** in the subphase.

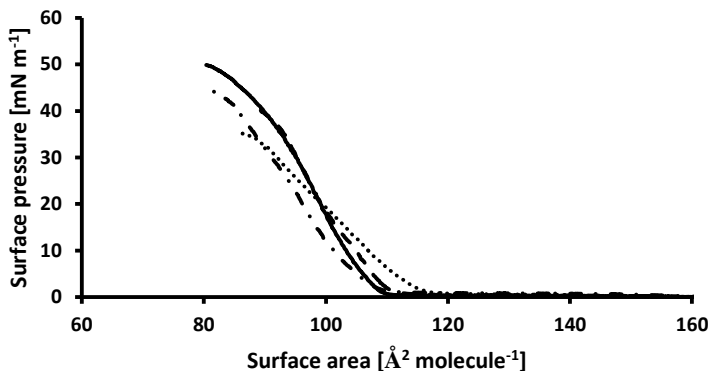


Figure 40. Π -A isotherms of $4\text{NH}_24\text{C}_{12}$ monolayer measured on a pure water (—) subphase, and on, **GC** (.....), **ATGC** (- - -) or **AT** (- . - .) DNA subphase at a concentration of 10^{-4} g L^{-1} .

Table 2. Characteristic values extracted from Langmuir compression isotherms of $4\text{NH}_24\text{C}_{12}$ and **GC12**: on pure water subphase and on subphase containing **ATGC**, **AT** or **GC** at a concentration of 10^{-4} g L^{-1} .

	4NH₂4C₁₂		GC12	
	Collapse pressure [mN m⁻¹]	Limiting molecular area [Å² molecule⁻¹]	Collapse pressure [mN m⁻¹]	Limiting molecular area [Å² molecule⁻¹]
Nanopure water	46	106	37	111
ATGC	40	108	33	125
AT	44	106	35	138
GC	34	116	34	125

The decrease of the collapse pressure observed for all the DNA subphases tested with respect to the values obtained on pure water with **GC12** monolayers was also observed for $4\text{NH}_24\text{C}_{12}$ monolayers. The molecular area of $4\text{NH}_24\text{C}_{12}$ was measured to be $106 \text{ Å}^2 \text{ molecule}^{-1}$ on pure water and $108 \text{ Å}^2 \text{ molecule}^{-1}$ on **ATGC** subphase.

The presence of **GC** in the subphase caused a clear expansion of the monolayer, with a molecular area value of $115 \text{ \AA}^2 \text{ molecule}^{-1}$. In the presence of **AT** in the subphase, an apparent molecular area of $106 \text{ \AA}^2 \text{ molecule}^{-1}$ was measured. Interestingly, the presence of **AT** in the subphase did not affect the monolayer packing of **4NH₂4C₁₂**, while the expansion of **GC12** monolayer was highly pronounced on **AT** subphase. The collapse pressure and limiting molecular area values suggest a difference in the interaction of **4NH₂4C₁₂** monolayer dependent of the DNA sequence. **4NH₂4C₁₂** Langmuir monolayers on DNA subphases at a concentration of 10^{-4} g L^{-1} , were less expanded than **GC12** monolayer in the same conditions. These results suggest a difference in the packing of the monolayers. Indeed, the guanidinium moieties of **GC12** act as a chelate and can form two hydrogen bonds while the amine function of **4NH₂4C₁₂** can only form one hydrogen bond with the molecules in the subphase.

Conclusions

The self-assembly at the air-water interface as Langmuir monolayers of the cationic amphiphilic calixarenes **GC12** was investigated in the presence of three model DNA sequence (30-mer) at different DNA concentrations. The effect of the DNA sequence on **GC12** monolayers was studied. All the characteristic values of the monolayer isotherms increased with increased DNA concentration. An expansion of the monolayer isotherm at the air-water interface in the presence of DNA was observed.

This expansion of the monolayer was larger in the presence of **AT** than it was in the presence of **GC** in the subphase, which, in turn was larger than **ATGC** for all the concentrations tested. This suggests an interaction dependent on the DNA sequence. The BAM images of the monolayers at the air-water interface confirm the interaction between **GC12** and double-stranded DNA. Ellipsometric measurements at the air-water interface in the presence of DNA showed an increase of the thickness compared to a pure water subphase.

The monolayer films of amino calixarene derivatives **1NH₂4C₁₂**, **1,2NH₂4C₁₂**, **1,3NH₂4C₁₂**, **3NH₂4C₁₂** and **4NH₂4C₁₂** were investigated in the presence of **ATGC** at a concentration of 10^{-4} g L⁻¹. Expansion of the monolayers in the presence of DNA was observed. The numbers of polar moieties on the upper rim of the calixarenes had an effect on the expansion of the monolayers, suggesting a mechanism of interaction dependent on the calixarene functionalization. To compare **GC12** monolayers and **4NH₂4C₁₂** monolayers behavior, the **4NH₂4C₁₂** monolayers formation was also investigated on **AT** and **GC** subphases.

In summary, the monolayer formation was dependent on different parameters: the number of functionalization on the calixarene, the type of recognition moieties and the DNA sequence.

References

1. Nostro, P.; Capuzzi, G.; Fratini, E.; Dei, L.; Baglioni, P. Modulation of interfacial properties of functionalized calixarenes. In *Trends in Colloid and Interface Science XV*, Koutsoukos, P., Ed.; Springer Berlin Heidelberg, **2001**; *118*, 238-242.
2. Zadnand, R.; Schrader, T., DNA Recognition with Large Calixarene Dimers. *Angew. Chem. Int. Ed.* **2006**, *45* (17), 2703-2706.
3. Shahgaldian, P.; Sciotti, M. A.; Pielec, U., Amino-Substituted Amphiphilic Calixarenes: Self-Assembly and Interactions with DNA. *Langmuir* **2008**, *24* (16), 8522-8526.
4. Nelson, H. C.; Finch, J. T.; Luisi, B. F.; Klug, A., The structure of an oligo(dA).oligo(dT) tract and its biological implications. *Nature* **1987**, *330*, 221-226.
5. Yoon, C.; Privé, G. G.; Goodsell, D. S.; Dickerson, R. E., Structure of an alternating-B DNA helix and its relationship to A-tract DNA. *Proc. Natl. Acad. Sci. U.S.A.* **1988**, *85* (17), 6332-6336.
6. Hud, N. V.; Plavec, J., A unified model for the origin of DNA sequence-directed curvature. *Biopolymers* **2003**, *69* (1), 144-158.
7. Stine, K. J., Brewster angle microscopy. In *Supramolecular Chemistry: From Molecules to Nanomaterials*, Gale, P. A.; Steed, J. W., Eds. John Wiley and Sons: Chichester, 2012.
8. Vollhardt, D., Morphology of monolayers at air/water interfaces. In *Encyclopedia of surface and colloid science*, Hubbard, A., Ed. Dekker: New York, 2002; pp 3585-3601.

9. Kaganer, V. M.; Möhwald, H.; Dutta, P., Structure and phase transitions in Langmuir monolayers. *Rev. Mod. Phys.* **1999**, *71* (3), 779-819.
10. Kresina, T. F., *An Introduction to Molecular Medicine and Gene Therapy*. Wiley: 2004.
11. Nabok, A.; Richardson, T.; McCartney, C.; Cowlam, N.; Davis, F.; Stirling, C.; Ray, A.; Gacem, V.; Gibaud, A., Size-quantization in extremely small CdS clusters formed in calixarene LB films. *Thin Solid Films* **1998**, *327*, 510-514.
12. Castano, S.; Delord, B.; Février, A.; Lehn, J.-M.; Lehn, P.; Desbat, B., Brewster Angle Microscopy and PMIRRAS Study of DNA Interactions with BGTC, a Cationic Lipid Used for Gene Transfer. *Langmuir* **2008**, *24* (17), 9598-9606.

4 Calixarene-Based Nanoparticles: DNA-Binding Study

The aim of my PhD work was to design new cationic calix[4]arenes locked in the cone conformation as a building block for the formation of self-assembled calixarene-based nanoparticles and to evaluate the DNA-binding ability of the self-assembled structure in order to use the calixarene-based nanoparticles as a non-viral vector for transfection. In this chapter, the self-assembly of calixarene molecules as nanoparticles and the ability of the calixarene-based nanoparticles to interact with DNA are discussed.

4.1 Calixarene-Based Nanoparticles: Preparation and Characterization

5,11,17,23-Tetra(guanidinium)-25,26,27,28-Tetra(dodecyloxy)-Calix[4]arene (GC12)

Nanoparticles of **GC12** were produced by following the nanoprecipitation method previously developed for *para*-acyl-calix[4]arenes.¹ Briefly, 15 mg of the **GC12** is dissolved in 3 mL of THF and kept under stirring while a volume of 50 mL of water is added. After one minute of stirring, the organic solvent is evaporated under reduced pressure at 40°C. The produced colloidal suspension was analyzed using dynamic light scattering (DLS) and electrophoretic mobility measurements (ζ -potential).

The results revealed a mean hydrodynamic diameter of 145 ± 5 nm and a ζ -potential of $+35 \pm 3$ mV. The positive potential suggested that the guanidine functions of **GC12** are protonated at neutral pH, and some of the guanidino functions point outward the SLNs. A sample of the suspension was spread on a mica surface, dried and analyzed using non-contact mode atomic force microscopy (AFM).

A representative micrograph is shown in Figure 41.

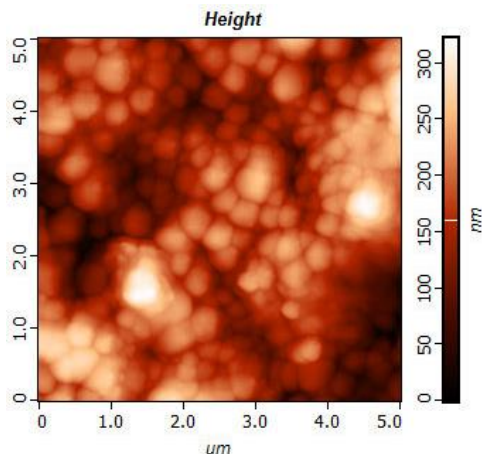


Figure 41. Atomic force micrograph of **GC12**-SLNs spread on a mica surface and imaged in non-contact mode at a scan range of 5 μm .

The AFM image is in good agreement with the DLS results and revealed a suspension composed of spherical objects of approximately 160 nm in diameter and 80 nm in height. Guanidinium-calixarenes bearing four octyl chains at the lower rim could self-assemble in water to form micelles with a critical micellar concentration of $2.0 \times 10^{-4} \text{ M}$.² To rule out possible **GC12** micellar behavior, the surface tension of the SLNs' suspension was measured at different concentrations. No change in the surface tension was observed (Figure 42).

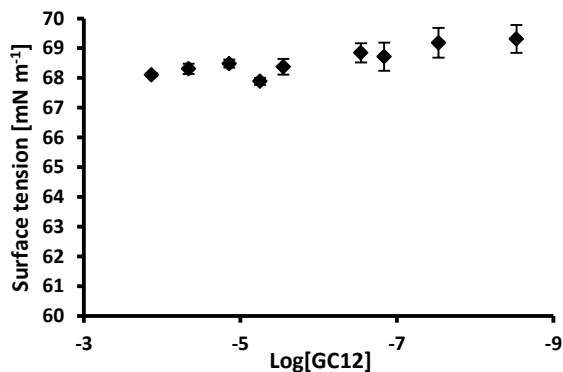


Figure 42. Critical micellar concentration measurement of **GC12-SLNs**.

This result confirmed that the solubility of calixarene reduced while increasing the alkyl chain's length and gives the molecule the ability to self-assemble as SLNs rather than micelles.

Amino-Calix[4]arene Derivatives

The ability of the amino-calixarene derivatives to self-assemble in water as SLNs using the solvent evaporation method was studied. Calixarenes **1NH₂4C₁₂**, **1,2NH₂4C₁₂** and **1,3NH₂4C₁₂** in the amine form were not able to form stable nanoparticles in pure water: the suspensions were destabilized during the evaporation process. The electrons of a lone pair of the aromatic amine were conjugated with a phenol ring. Thus, their tendency to engage in hydrogen bonding was diminished. The solubility of the amino-calixarene derivatives in water reflected their ability to form hydrogen bonds with water molecules or intermolecular hydrogen bonds between primary amines.

A milky suspension was obtained for the calix[4]arene **3NH₂4C₁₂** in the amine form in pure water. This difference of stability can be explained by the number of amine groups available to interact with water molecules and form intermolecular bonding to stabilize the suspension.

The self-assembly of the protonated calixarenes **1NH₂4C₁₂**, **1,2NH₂4C₁₂**, **1,3NH₂4C₁₂**, **3NH₂4C₁₂** and **4NH₂4C₁₂** in water were investigated to overcome the stability issues of **1NH₂4C₁₂**, **1,2NH₂4C₁₂** and **1,3NH₂4C₁₂** to form nanoparticles in the amine form. The protonated calixarenes **1NH₃⁺4C₁₂**, **1,2NH₃⁺4C₁₂** and **1,3NH₃⁺4C₁₂** were able to form stable suspensions in nanopure water. The suspensions were characterized by DLS and ζ -potential. The results of the measurements are presented in Table 3.

Table 3. Calixarene-based nanoparticles size, polydispersity and ζ -potential.

	1NH₃⁺4C₁₂	1,2NH₃⁺4C₁₂	1,3NH₃⁺4C₁₂	3NH₃⁺4C₁₂	4NH₃⁺4C₁₂	3NH₂4C₁₂	4NH₂4C₁₂
Z-average (nm)^a	123	83	117	-	-	177	123
ζ-potential (mV)	50 ± 8	39 ± 8	28 ± 9	-	-	52 ± 6	37 ± 8
Pdl^b	0.148	0.164	0.143	-	-	0.189	0.177

^a Z-average: average hydrodynamic diameter

^b Pdl: Polydispersity index

The nanoparticles were monodisperse in size with hydrodynamic diameters of 123 nm, 82 nm, 117 nm and 177 nm for **1NH₃⁺4C₁₂**, **1,2NH₃⁺4C₁₂**, **1,3NH₃⁺4C₁₂** and **3NH₂4C₁₂** respectively. The protonation of the calixarenes **3NH₂4C₁₂** and **4NH₂4C₁₂** led to the formation of polydispersed suspensions and were not used in this study. The calixarene-based nanoparticles exhibited positive ζ -potentials of $+ 50 \pm 8$ mV, $+ 39 \pm 8$ mV, $+ 28 \pm 9$ mV and $+ 52 \pm 6$ mV for **1NH₃⁺4C₁₂**, **1,2NH₃⁺4C₁₂**, **1,3NH₃⁺4C₁₂** and **3NH₂4C₁₂** respectively. The positively charged surface of the nanoparticles confirmed the presence of amine functions at the surface of the nanoparticles. The difference of ζ -potential is attributed to greater repulsion forces. Depending on the system, steric repulsion and other types of intermolecular forces can also contribute to the interaction potential. The nanoparticles were imaged using AFM in air, in non-contact mode. Solid shape nanoparticles can be observed on the AFM micrographs (Figure 43). The average height and average diameter of the nanoparticles are summarized in Table 4.

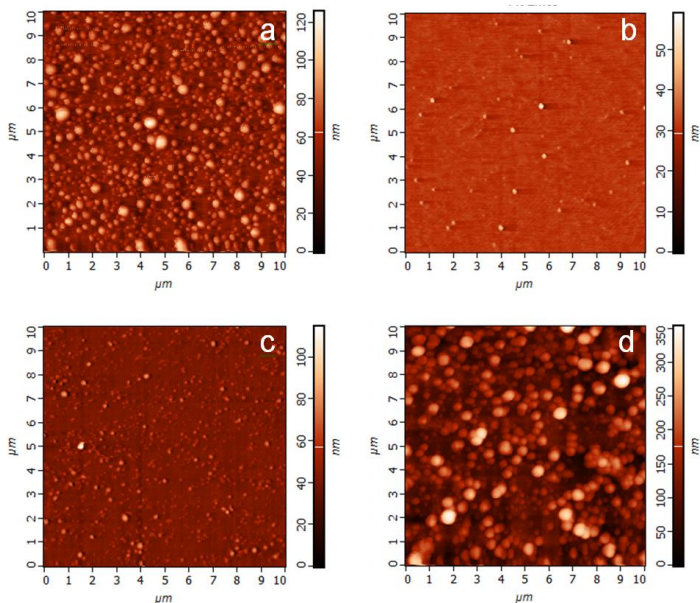


Figure 43. Atomic force microscopy images of a) $1\text{NH}_3^+4\text{C}_{12}$ -SLNs, b) $1,2\text{NH}_3^+4\text{C}_{12}$ -SLNs c) $1,3\text{NH}_3^+4\text{C}_{12}$ -SLNs and d) $3\text{NH}_24\text{C}_{12}$ -SLNs prepared on mica and imaged in non-contact mode.

Table 4. AFM characteristic values obtained for the calixarene-based nanoparticles.

	$1\text{NH}_3^+4\text{C}_{12}$	$1,2\text{NH}_3^+4\text{C}_{12}$	$1,3\text{NH}_3^+4\text{C}_{12}$	$3\text{NH}_24\text{C}_{12}$	$4\text{NH}_24\text{C}_{12}$
Diameter (nm)	253 ± 5	112 ± 5	128 ± 3	447 ± 15	190 ± 5
Height (nm)	32 ± 1	20 ± 1	23 ± 2	139 ± 4	78 ± 4
d/h	7.9	5.6	5.6	3.2	2.44

From the analysis of line profiles, much greater values were obtained for the diameter of the nanoparticles than the values obtained for the height. The analysis of AFM images indicated that the diameter-to-height ratio (d/h) of the nanoparticles decreased with the increase of amine functions on the calixarenes starting from $d/h = 7.9$ for $1\text{NH}_3^+4\text{C}_{12}$, $d/h = 5.6$ for $1,2\text{NH}_3^+4\text{C}_{12}$ and $1,3\text{NH}_3^+4\text{C}_{12}$, $d/h = 3.2$ for $3\text{NH}_24\text{C}_{12}$ and $d/h = 2.44$ for $4\text{NH}_24\text{C}_{12}$ (Table 5 and Figure 44). A flattening of nanoparticles that may result from the collapse of nanoparticles upon drying has been reported for polyamide nanoparticles based on the AFM analysis.³ Montassier et al. postulated that nanoparticles could be considered as solid nanostructures if d/h ratio is ≤ 4 .³

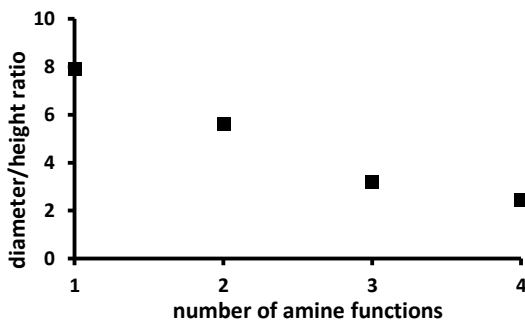


Figure 44. Ratio of the diameter/height of the nanoparticles as function of the number of amine groups on *para* position of the calix[4]arene.

The diameter-to-height ratio decreased with the increase of amine functions present on *para* position of the calixarene. It is likely that the number of hydrophilic functions per calixarene has an influence on the stability of the nanoparticles when deposited on a surface.

The calixarenes $1\text{NH}_3^+\text{4C}_{12}$, $1,2\text{NH}_3^+\text{4C}_{12}$ and $1,3\text{NH}_3^+\text{4C}_{12}$ most likely formed stable nanoparticles in solution that were destabilized when dried on a mica surface. Relatively flat nanoparticles were observed.

The newly produced amino calix[4]arene derivatives were able to self-assemble as nanoparticles in pure water. Their positively charged surfaces pointed out the presence of amine or protonated amine functions at the surface of the nanoparticles that allowed interaction with the negatively charged DNA phosphate backbone.

4.2 Calixarene-Based Nanoparticles: Interaction with DNA

Ethidium Bromide Displacement Assay

5,11,17,23-Tetra(guanidinium)-25,26,27,28-Tetra(dodecyloxy)-Calix[4]arene (GC12)

To investigate the DNA-binding properties of **GC12**-based SLNs, a fluorescence displacement assay was carried out using ethidium bromide (EtBr). EtBr is known to intercalate between double-stranded DNA base pairs, resulting in an enhanced fluorescence of the dye.

In this assay, the displacement of EtBr from the double helix caused a decrease in fluorescence as a result of the ability of DNA-binding molecules to modify the conformation of the DNA and to cause a decrease of its affinity for the dye, thus causing it to release in solution.

The fluorescence displacement assay was carried out with three different DNA duplexes: **AT**, **GC**, and **ATGC** (used in Chapter 2). The plot of normalized fluorescence intensity against the concentration of **GC12**-based SLNs measured at a NaCl concentration of 10 mM, shown in Figure 45, revealed an exponential decay in fluorescence intensity for the three DNA systems tested.

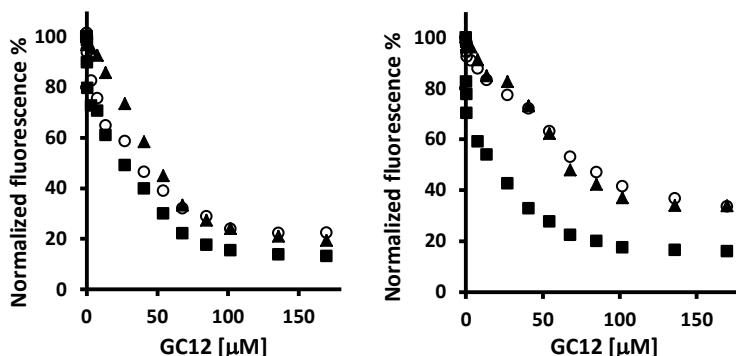


Figure 45. Ethidium bromide displacement assay by fluorescence spectroscopy (measured at 595 nm with excitation at 510 nm) with **AT** (■), **GC** (○), **ATGC** (△) in the presence of increasing concentration of **GC12** SLNs in buffer solution (20 mM HEPES, 10 mM NaCl, pH 7.1) (left), in buffer solution (20 mM HEPES, 100 mM NaCl, pH 7.1) (right). The values are presented normalized with the value of fluorescence measured for the different duplex-EtBr complexes in the absence of **GC12**-based SLNs.

The AC_{50} values reported in Table 5, are the **GC12**-based SLNs concentration at which the fluorescence intensity reaches 50 % of maximal fluorescence. The AC_{50} values provide an indirect method to measure the binding affinity constant.

Table 5. AC₅₀ values of the SLNs with polyoligonucleotides in mM.

Polynucleotide	GC12 [μ M]	
	NaCl 10 mM ^a	NaCl 100 mM ^b
AT	33 \pm 6	14 \pm 4
GC	50 \pm 15	75 \pm 11
ATGC	60 \pm 12	108 \pm 35

^a Interaction condition in a buffer solution 20 mM HEPES, 10 mM NaCl, pH 7.1.

^b Interaction condition in a buffer solution 20 mM HEPES, NaCl 100 mM NaCl, pH 7.1.

All the values reported in Table 5 were calculated as a function of the absolute concentration of calixarenes and part of the calixarene molecules are hidden within the SLNs. AC₅₀ with a value of 33, 50 and 60 mM were obtained in the presence of **AT**, **GC** and **ATGC** respectively in a buffer solution (20 mM HEPES, 10 mM NaCl, pH 7.1). The AC₅₀ value of **AT** was significantly lower compared to the values for **GC** and **ATGC**. To rule out the possibility that the interactions between the DNA molecules and the SLNs surface were only due to electrostatic interactions, the same set of experiments was carried out using a higher salt concentration (100 mM NaCl, Figure 45). For both **GC** and **ATGC**, there was only a slight decrease in the affinity, with AC₅₀ values of 75 and 108 mM respectively. In the case of **AT**, there is even a slight increase of the affinity with an AC₅₀ value of 14 mM. These results clearly demonstrated that the interactions between the **GC12**-based SLNs are not purely due to electrostatic interactions.

Amino-Calix[4]arene Derivatives

In Figure 46 the results from the ethidium bromide displacement assay performed with the amino calixarene derivatives (**1NH₃⁺4C₁₂**, **1,2NH₃⁺4C₁₂**, **1,3NH₃⁺4C₁₂**, **3NH₂4C₁₂** and **4NH₂4C₁₂**) and **ATGC**-DNA duplex are depicted.

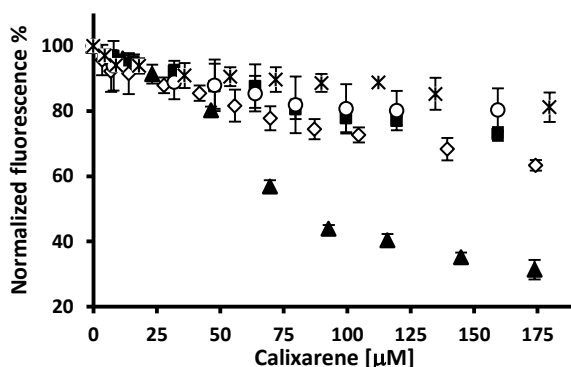


Figure 46. Ethidium bromide displacement assay by fluorescence spectroscopy (measured at 595 nm with excitation at 510 nm) with **ATGC**, in the presence of increasing concentration of increasing concentration of SLNs, (*) **1NH₃⁺4C₁₂**-SLNs, (○) **1,2NH₃⁺4C₁₂**-SLNs, (■) **1,3NH₃⁺4C₁₂**-SLNs, (◇) **3NH₂4C₁₂**-SLNs and (▲) **4NH₂4C₁₂**-SLNs, in buffer solution (20 mN HEPES, 10 mM NaCl, pH 7.1). The values are presented normalized with the value of fluorescence measured for the different duplex-EtBr complexes in the absence of calixarene nanoparticles.

In the presence of **1NH₃⁺4C₁₂**, **1,2NH₃⁺4C₁₂**, **1,3NH₃⁺4C₁₂** and **3NH₂4C₁₂** nanoparticles, a slight decrease of the fluorescence was observed. The decrease in fluorescence is slightly more pronounced for **3NH₂4C₁₂**-based SLNs, with a loss of 30 % of fluorescence, than for **1NH₃⁺4C₁₂**, **1,2NH₃⁺4C₁₂** and **1,3NH₃⁺4C₁₂** nanoparticles with a decrease of

20 % at a concentration of 250 mg L⁻¹. In the case of **4NH₂4C₁₂**-SLNs, the fluorescence decreased up to 80 %. No fluorescence was observed for the nanoparticles in buffer solution (HEPES 20 mM, NaCl 10 mM, pH 7.1) and no change in the fluorescence of EtBr was detected in the presence of increasing nanoparticle concentrations (see Chapter 7, Figure S2). Only a slight decrease in the fluorescence of **ATGC**-EtBr complex was observed. It can be assumed that the interactions between the **1NH₃⁺4C₁₂**, **1,2NH₃⁺4C₁₂**, **1,3NH₃⁺4C₁₂** and **3NH₂4C₁₂** nanoparticles and DNA most probably occur via electrostatic interactions resulting in almost no release of the dye in solution. The amine functions at the surface of the nanoparticles interact with the phosphate backbone of DNA but cannot unwind the double helix, and the EtBr molecules remain trapped inside the double-strand of the DNA.

To further study the interaction with the calixarene **4NH₂4C₁₂**, a fluorescence displacement assay was carried out using **AT** and **GC** 30-mer oligonucleotides. The result of the displacement assay in the presence of **AT** and **GC** is depicted in Figure 47. From Figure 47, a decrease in fluorescence up to 80 % for the three DNA tested can be observed.

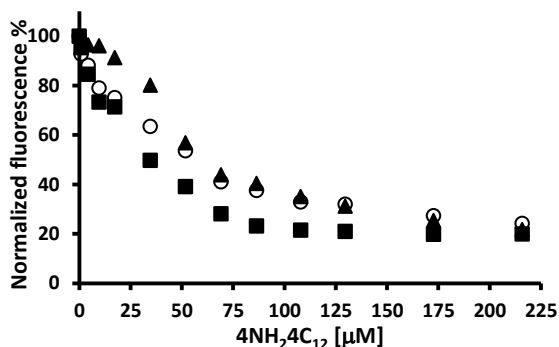


Figure 47. Ethidium bromide displacement assay by fluorescence spectroscopy (measured at 595 nm with excitation at 510 nm) with **AT** (■), **GC** (○), **ATGC** (▲), in the presence of increasing concentration of **4NH₂4C₁₂**-SLNs in buffer solution (20 mM HEPES, 10 mM NaCl, pH 7.1) (left), in buffer solution (20 mM HEPES, 100 mM NaCl, pH 7.1) (right). The values are presented normalized with the value of fluorescence measured for the different duplex-EtBr complexes in the absence of **4NH₂4C₁₂**-based SLNs.

In Table 6 are reported the AC_{50} values for **GC12**-SLNs and **4NH₂4C₁₂**-SLNs in 20 mM HEPES, 10 mM NaCl, pH 7.1 buffer solution, **4NH₂4C₁₂**-SLNs seem to show a slight preference for **AT** sequence as **GC12** with AC_{50} values of 48, 70 and 70 μ M for **AT**, **GC** and **ATGC** respectively.

Table 6. AC_{50} values of the **GC12**-SLNs and **4NH₂4C₁₂**-SLNs with polyoligonucleotides

Polynucleotide	GC12 [μ M]	4NH ₂ 4C ₁₂ [μ M]
	NaCl 10 mM ^a	NaCl 10 mM ^a
AT	33	48
GC	50	70
ATGC	60	70

^a Interaction condition in a buffer solution 20 mM HEPES, 10 mM NaCl, pH 7.1

Circular Dichroism Spectroscopy (CD)

To further study the interaction mechanism, circular dichroism (CD) experiments were carried out. CD spectra obtained with the three DNA duplexes upon addition of increasing amounts of **GC12** or **4NH₂4C₁₂** are shown in Figure 48 and Figure 49 respectively.

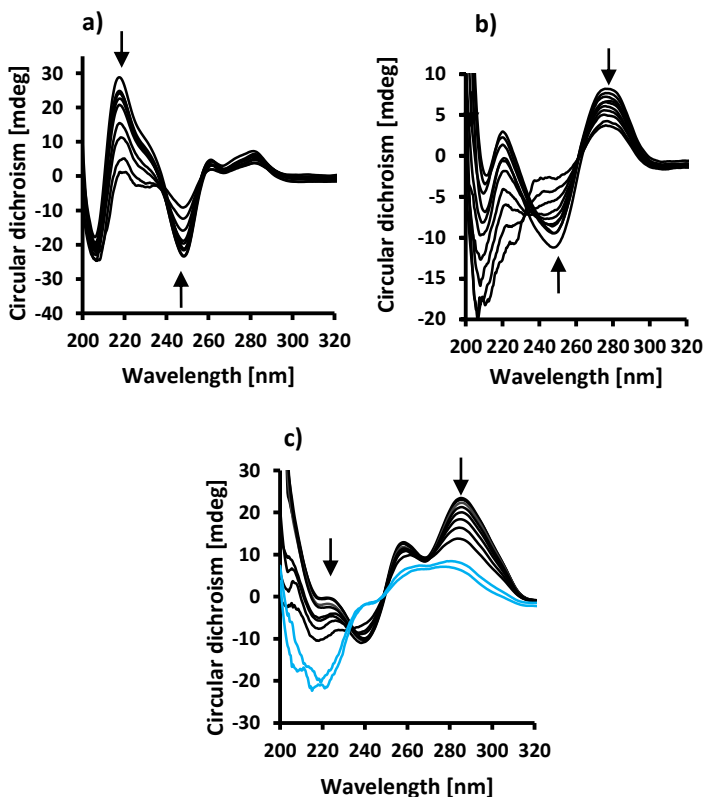


Figure 48. CD spectra of the titration by **GC12** SLNs in buffered solution of **a) AT, b) GC; c) ATGC**. The arrows indicate changes in optical rotation with increasing amount of **GC12** SLNs.

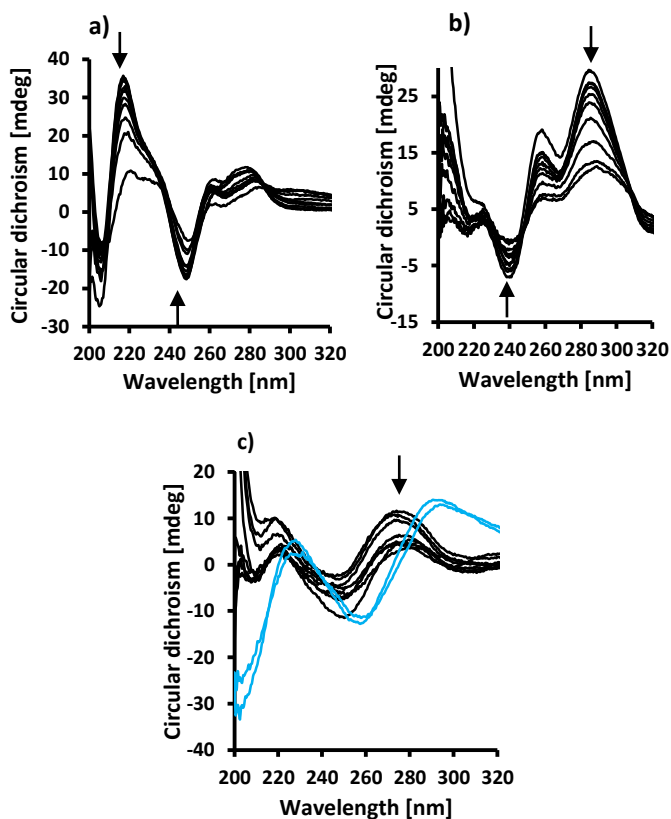


Figure 49. CD spectra of the titration by 4NH₂C₁₂-SLNs in buffered solution of a) AT, b) GC; c) ATGC. The arrows indicate changes in optical rotation with increasing amount of 4NH₂C₁₂-SLNs.

The CD spectra of AT, in the absence of SLNs (GC12 or 4NH₂C₁₂), revealed two characteristic peaks, one positive at 220 nm and one negative at 245 nm, characteristic of the expected B'-DNA conformation for this duplex.⁴⁻⁵

In the presence of increasing concentrations of calixarene-based SLNs, the same behavior could be observed upon addition of either **GC12**-SLNs or **4NH₂4C₁₂**-SLNs. A decrease in the spectral intensity was measured and confirmed the formation of a DNA–SLN complex and the unwinding of the double-stranded DNA. The **ATGC** CD spectrum measured in buffer was characterized by two positive bands at 278 and 220 nm and a negative band at 248 nm, all characteristic of B-DNA.³

Upon addition of **GC12**-SLNs or **4NH₂4C₁₂**-SLNs in **ATGC** solution, the same trend could be observed on the CD spectra. The disappearance of the peak at 248 nm and the amplification of the peak at 210 nm suggested a phase transition of the DNA duplex conformation from a B-DNA to an A-like form. Surprisingly, the positive peak observed at 278 nm decreased, which is not typical for this transition, suggesting a more complex mechanism. Upon further addition of **4NH₂4C₁₂**-SLNs, a clear change in conformation was observed, which was not observed for **GC12**-SLNs at the same concentration: the appearance of two negative peaks at 208 nm and 258 nm and two positive peaks at 220 and 295 nm. This spectrum is not typical of duplex DNA and suggests the formation of triplex DNA. In the case of **GC**, the CD spectrum in buffer, a negative peak at 240 nm and a positive peak at 20 nm suggest a B-conformation. In the presence of **4NH₂4C₁₂**-SLNs a decrease was observed, but no change in conformation. Interestingly, more complex spectra were obtained for **GC**-DNA upon addition of **GC12**-SLNs. However, the trend observed is similar to the CD spectra measured with **ATGC** and suggests a B-to-A-like transition.

Isothermal Titration Calorimetry (ITC)

The ITC measurements of the binding of calixarene-based SLNs and DNA provide thermodynamic information on the binding. It is known that the enthalpy differences are essentially balanced by entropic factors, major and minor groove-binding phenomena present comparable Gibbs free energies. But major groove-binding is primarily enthalpy-driven while binding to the minor groove is characterized by an unfavorable enthalpy that is compensated by favorable entropic contributions.⁶

Nevertheless, the ITC measurements of the binding between the calixarene-based SLNs (**GC12**-SLNs or **4NH₂4C₁₂**-SLNs) and the three oligonucleotides (**AT**, **GC**, and **ATGC**) are presented in Table 7 and Figure S8 and Figure S9 (Chapter 7).

Table 7. ITC thermodynamic profile for the binding of **GC12** SLNs and **4NH₂4C₁₂**-SLNs with oligonucleotides

SLNs	Polynucleotide	ΔH [kJ mol ⁻¹]		ΔS [J (mol K) ⁻¹]	ΔG [kJ mol ⁻¹]
GC12	AT	160.5	± 2.87	665	-34.3
	GC	-231.1	± 19.1	-680	-31.9
	ATGC	-	-	-	-
4NH₂4C₁₂	AT	48.85	± 37.65	259	-27.0
	GC	-94.46	± 2.355	-215	-31.5
	ATGC	-	-	-	-

Enthalpy values of 160.5 kJ mol⁻¹ and 48.85 kJ mol⁻¹ were measured for **GC12**-SLNs and **4NH₂4C₁₂**-SLNs respectively with **AT**-DNA.

These results reveal a positive enthalpy characteristic of a minor groove-binding phenomenon for both SLNs studied. Interestingly, for **GC**, negative entropy was measured, suggesting a major groove-binding phenomenon with entropic values of $-680 \text{ J (mol K)}^{-1}$ for **GC12**-SLNs and $-215 \text{ J (mol K)}^{-1}$ for **4NH₂4C₁₂**-SLNs. No enthalpy could be determined for **ATGC** for the two SLNs systems but it is clear from the CD measurements that **GC12**-based SLNs and **4NH₂4C₁₂**-SLNs have caused a conformational B-to-A-like transition for **GC** and **ATGC** sequences. It is known that the width of the major groove of A-DNA is 2.7 \AA while the minor groove width is 11 \AA .

In the case of B-DNA, the major and minor grooves have widths of 11.7 and 5.7 \AA , respectively. The results suggest that, for **GC** the binding was done preferentially to the wide major groove of the B-DNA duplex, which underwent a conformational change that tended to diminish the width of the DNA groove. In the case of the **AT** sequence, as no B-to-A conformational transition could occur, the SLNs had a preference for the minor groove that is narrower than the major groove. As it is likely that calixarene molecules have a certain degree of freedom when self-assembled as SLNs, our results suggested that the DNA-binding mechanism was rather due to a synergistic effect of the guanidinium functions within the calixarene macrocycle, as observed for dimeric calixarenes,⁷ rather than different **GC12** or **4NH₂4C₁₂** molecules within the outer layer of the SLNs.

4.3 Calixarene-Based Nanoparticles: Layer-by-Layer Coating

As noted above, my PhD work aimed to build a layer-by-layer (LbL) assembly at the surface of calixarene-based SLNs. To protect the DNA in the cell against attacks and to help the SLN-DNA complex to cross the cell membrane, chitosan, a polycationic biocompatible polymer, also known for its ability to enhance cellular uptake, was used. Nault et al., reported on the LbL assembly of **4NH₂4C₁₂**-based SLNs with the successive addition of plasmid DNA and chitosan. They monitored the additions of DNA and chitosan by ζ -potential measurement. An increase was observed in the ζ -potential values upon addition of DNA and a decrease in the ζ -potential confirmed the addition of chitosan and the formation of a LbL coating at the surface of the **4NH₂4C₁₂**-SLNs. The SLNs were titrated with increasing amounts of DNA as shown in Figure 50. The ζ -potential decreased, confirming the addition of DNA around the calixarene-based nanoparticle. The opposite behavior was observed in the presence of increasing amounts of chitosan. Independently of the DNA, the **GC12**-based nanoparticles were fully coated with DNA 4 mg L⁻¹ of DNA and 2 mg L⁻¹ of chitosan.

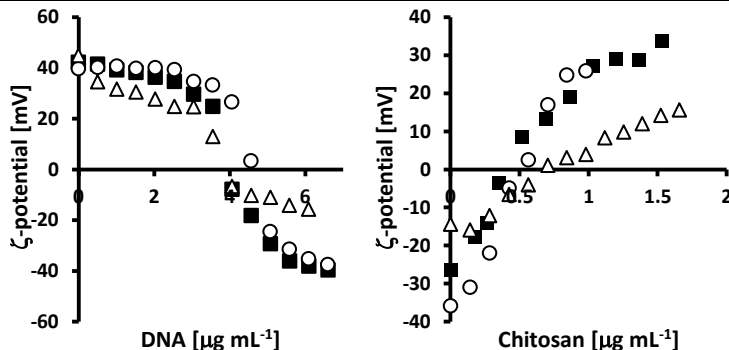


Figure 50. ζ -potential titration of AT (■), GC (○), ATGC (△) in the presence of increasing amounts of **GC12**-based SLNs, in buffer solution (20 mM HEPES, 10 mM NaCl, pH 7.1) (left), and **GC12**-DNA complex with AT (■), GC (○), ATGC (△) in the presence of increasing amounts of chitosan in buffer solution (20 mM HEPES, 100 mM NaCl, pH 7.1) (right).

The formation of a LbL assembly at the surface of **GC12**-SLNs was followed by ζ -potential measurements. The positively charged **GC12**-SLNs in the presence of increasing amounts of DNA become negatively charged. Upon addition of chitosan to a solution of **GC12**-SLNs loaded with DNA, the objects in suspension become positively charged. The ζ -potential increases after the addition of chitosan confirms the adsorption of the polymer at the surface of the SLNs. **GC12**-SLNs were successfully loaded using the LbL assembly technique (Figure 51).

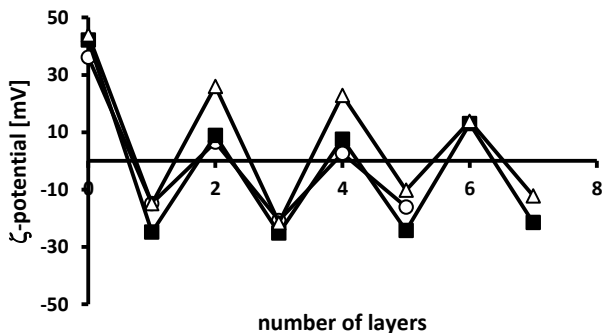


Figure S11. ζ -potential of **GC12**-SLNs in the presence of **AT** (■), **GC** (○), **ATGC** (△) in buffer solution LbL coating of **GC12**-SLNs with DNA and chitosan layers.

The suspension were destabilized after addition of seven layers around the SLNs for **AT** and **ATGC** and five layers for **GC**. These differences are likely due to the specific DNA sequence used in the experiments. Further polyelectrolyte layer additions have been shown to cause a decrease in the stability of the suspensions, certainly due to particle aggregation. DLS measurements were carried out after the addition of DNA and chitosan layers but high polydispersity index values were obtained, most likely due to the formation of larger aggregates. The addition of plasmid DNA into a suspension of nanoparticles was monitored by ζ -potential. The titration curves of the amino calixarene derivatives and **GC12** are shown in Figures S11-S16 (Chapter 7). The addition of the first layer of DNA to a **1NH₂4C₁₂**-SLNs lead to a destabilization of the system.

To fully coat the calixarene-based nanoparticles, DNA at a concentration of 3 mg L^{-1} , 4 mg L^{-1} , 4 mg L^{-1} , 5 mg L^{-1} and 4 mg L^{-1} was required for **1,2NH₂4C₁₂**, **1,3NH₂4C₁₂**, **3NH₂4C₁₂**, **4NH₂4C₁₂** and **GC12** nanoparticles respectively. The subsequent titration of the nanoparticles' DNA complex with chitosan reveals that the **1,2NH₂4C₁₂**, **1,3NH₂4C₁₂**, **3NH₂4C₁₂**, **4NH₂4C₁₂** and **GC12** nanoparticles need to be incubated with 3 mg L^{-1} , 3 mg L^{-1} , 5 mg L^{-1} , 5 mg L^{-1} and 6 mg L^{-1} of chitosan respectively.

4.4 Calixarene-DNA Complexes: Self-Assembled Lipoplexes

Due to electrostatic interactions, cationic lipids spontaneously interact with DNA molecules in aqueous solution, resulting in the formation of so-called lipoplexes. Lipoplexes are bilayer structures prepared by mixing preformed cationic liposomes with DNA in aqueous solution or by mixing cationic amphiphile with DNA without preformation of liposomes. Electrostatic interactions between the phosphate backbone of the DNA and the cationic recognition moieties of the amphiphile are the driving forces of the lipoplex formation. To study the self-assembly for calixarene–DNA complexes as lipoplexes, cationic calixarene liposomes were prepared. Calixarene powders (**GC12** or the amino-calix[4]arene derivatives) were mixed at 40°C for 120 minutes in nanopure water or in buffer solutions. Four buffer solutions were tested: sodium phosphate buffer pH 7.5, HEPES buffer pH 7.05, Cacodylate buffer pH 7.1 and Tris-HCl

buffer pH 8.8. After 120 minutes the insoluble calixarene **GC12** formed a clear solution.

Surprisingly, all the amino derivatives remained insoluble in aqueous solution in those conditions. The nano-suspension formed was characterized by ζ -potential. The results are depicted in Table 8.

Table 8. ζ -potential values of **GC12-DNA** lipoplexes in different conditions.

Buffer	ζ -potential		
	GC12 liposomes	GC12 liposomes mixed with DNA at 20°C	GC12-DNA lipoplex formed in-situ at 40°C
Nanopure water	+ 45 ± 5 mV	+ 52 ± 6 mV	+ 58 ± 23 mV
Phosphate	-14 ± 11 mV	-15 ± 9 mV	-
HEPES	+ 50 ± 12 mV	-	-
Cacodylate	+ 67 ± 21 mV	+ 105 ± 17 mV	+105 ± 9 mV
Tris-HCl	-	-	+ 71 ± 8 mV

In water, HEPES buffer, and cacodylate buffer, ζ -potential values of **GC12** self-assemblies were measured to be + 45 ± 5 mV, + 50 ± 12 mV, + 67 ± 21 mV respectively. Positive ζ -potentials suggest that the guanidino functions are pointing outward the nanoparticle. In phosphate buffer solution, a negative ζ -potential was measured. This was attributed to the interaction of the phosphate ions with the guanidine functions at the surface of nanoparticles. In the Tris-HCl buffer, ζ -potential distribution contained multiple peaks. It is likely that the positively charged **GC12** interacted with the Tris-HCl molecules which led to a loss of organization,

thereby increasing the distance between the calixarene molecules and different species are measured in solution. Those preformed liposomes were mixed with DNA for 30 minutes, 1.6 μg , at room temperature. To investigate the in-situ formation of lipoplexes, **GC12** powder was mixed with DNA in nanopure water or in buffer at 40°C for 30 minutes. Both systems – the preformed **GC12** nanostructure mixed with DNA at 20°C and the in-situ formation of **GC12**-DNA lipoplexes at 40°C – were analyzed by DLS and ζ -potential. High polydispersity indexes were measured with large nanoparticle diameters. This was attributed to the presence of salt that may influence the stern layer around the nanoparticle. Discussion on these values will be highly speculative. In water and cacodylate buffer, as shown in Table 8, positive ζ -potentials were measured for **GC12**-DNA complexes for both systems. **GC12**-DNA complexes prepared using preformed liposomes in water and cacodylate exhibited positive ζ -potential values of $+ 52 \pm 6$ mV and $+ 105 \pm 17$ mV respectively. The **GC12**-DNA complexes formed in-situ at 40°C exhibited similar positive ζ -potential values of $+ 57 \pm 23$ mV and $+ 105 \pm 9$ mV in water and cacodylate buffer respectively. Those ζ -potential values were higher than the ζ -potential values of $+ 45 \pm 5$ mV, $+ 67 \pm 21$ mV obtained for **GC12** liposomes without DNA in nanopure water and cacodylate buffer respectively. Multiple peaks could be measured for lipoplexes prepared with the preformed liposomes at 20°C in Tris-HCl buffer. This was attributed to a different organization of the self-assembly. A positive ζ -potential of $+ 71 \pm 8$ mV was measured for **GC12**-DNA lipoplexes formed in-situ in Tris-HCl buffer. In HEPES and phosphate buffer, the addition of DNA disorganized the system and

negative or no ζ -potential could be measured. It is known that cationic liposomes are destabilized upon addition of increasing amounts of DNA. Indeed, the liposomes might even release the DNA in solution at a certain lipid/DNA ratio.⁸⁻⁹

Conclusions

In this chapter, the ability of **GC12** and of the amino calix[4]arene derivatives to self-assemble in aqueous solution as nanoparticles was demonstrated. DLS and AFM confirmed the presence of round nanoparticles in solution. Positive ζ -potentials were measured, confirming the presence of the recognition functions at the surface of the nanoparticles. Interaction with DNA was studied by fluorescence displacement assay and revealed that **1NH₂4C₁₂**, **1,2NH₂4C₁₂**, **1,3NH₂4C₁₂** and **3NH₂4C₁₂** cannot displace the intercalating dye from the double-stranded DNA, most likely because the interactions are mainly driven by electrostatic interactions. On the other hand, **4NH₂4C₁₂** and **GC12** displaced up to 80 % of the ethidium bromide from the double helix.

Circular dichroism spectra and isothermal titration calorimetry data confirmed that the interaction of both SLNs with DNA is not only driven by electrostatic interactions but also by a groove-binding mechanism. Indeed, the SLNs interact with **AT**-DNA via a minor groove-binding and with **GC** via a major groove mechanism.

The calixarene-based nanoparticles **1,2NH₂4C₁₂**, **1,3NH₂4C₁₂**, **3NH₂4C₁₂**, **4NH₂4C₁₂** and **GC12** were coated with several layers of DNA-chitosan using the layer-by-layer technique. In addition, the ability of **GC12** to form lipoplexes in aqueous solutions was investigated. **GC12** can form lipoplexes in the presence of DNA in pure water or in buffer solution.

References

1. Shahgaldian, P.; Da Silva, E.; Coleman, A. W.; Rather, B.; Zaworotko, M. J., *Para*-acyl-calix-arene based solid lipid nanoparticles (SLNs): a detailed study of preparation and stability parameters. *International journal of pharmaceutics* **2003**, *253* (1), 23-38.
2. Sansone, F.; Dudič, M.; Donofrio, G.; Rivetti, C.; Baldini, L.; Casnati, A.; Cellai, S.; Ungaro, R., DNA Condensation and Cell Transfection Properties of Guanidinium Calixarenes: Dependence on Macrocycle Lipophilicity, Size, and Conformation. *J. Am. Chem. Soc.* **2006**, *128* (45), 14528-14536.
3. Montasser, I.; Fessi H.; Coleman, A. W., Atomic force microscopy imaging of novel type of polymeric colloidal nanostructures. *Eur. J. Pharm. Biopharm.* **2002**, *54*, 281-284.
4. Kypr, J.; Kejnovská, I.; Renčiuk, D.; Vorlíčková, M., Circular dichroism and conformational polymorphism of DNA. *Nucleic acids research* **2009**, *37* (6), 1713-1725.
5. Herrera, J. E.; Chaires, J. B., A premelting conformational transition in poly (dA)-poly (dT) coupled to daunomycin binding. *Biochemistry* **1989**, *28* (5), 1993-2000.
6. Privalov, P. L.; Dragan, A. I.; Crane-Robinson, C.; Breslauer, K. J.; Remeta, D. P.; Minetti, C. A., What drives proteins into the major or minor grooves of DNA? *Journal of molecular biology* **2007**, *365* (1), 1-9.

7. Yuan, Z.; Andrew, S.; Leaf, H., In Vivo Gene Delivery by Nonviral Vectors: Overcoming Hurdles? *Molecular Therapy* **2012**, *20* (7), 1298-1304.
8. El Ouahabi, A.; Thiry, M.; Pector, V.; Fuks, R.; Ruysschaert, J. M.; Vandenbranden, M., The role of endosome destabilizing activity in the gene transfer process mediated by cationic lipids. *FEBS letters* **1997**, *414* (2), 187-192.
9. Elouahabi, A.; Ruysschaert, J.-M., Formation and intracellular trafficking of lipoplexes and polyplexes. *Molecular therapy* **2005**, *11* (3), 336-347.

5 Transfection Tests

The transfection experiments performed with calixarene-based SLNs coated with alternate layers of DNA and chitosan and with **GC12**-DNA lipoplexes are discussed in this chapter.

To assess the possibility of transfecting mammalian cells, calixarene-based SLNs (**1,2NH₂4C₁₂**, **1,3NH₂4C₁₂**, **3NH₂4C₁₂**, **4NH₂4C₁₂** and **GC12**) covered with alternate layers of DNA and chitosan have been investigated for their ability to deliver DNA into Chinese hamster ovary cells (CHO). The transfection was followed by fluorescence of a red fluorescent protein (DsRed2) for which the loaded DNA codes. The commercially available transfection agent Lipofectamine was used as a positive control.

Transfection Tests

Naked plasmid DNA was used as negative controls in the different aqueous solutions. Surprisingly, after 48 hours of transfection, no fluorescence could be detected using the calixarene-based SLNs coated with the LbL technique as a DNA carrying system. As Nault et al., were able to transfect MDCK (Madin-Darby canine kidney) cells using the **4NH₂4C₁₂**-SLNs coated with several layers of DNA-chitosan, these results could be attributed to the use of different cells and different DNA for the transfection experiments.

The ability of the **GC12**-DNA lipoplexes to transfect DNA into the CHO cells was also investigated. The fluorescence microscopy images obtained after 48 hours incubation are presented below in Figure 52.

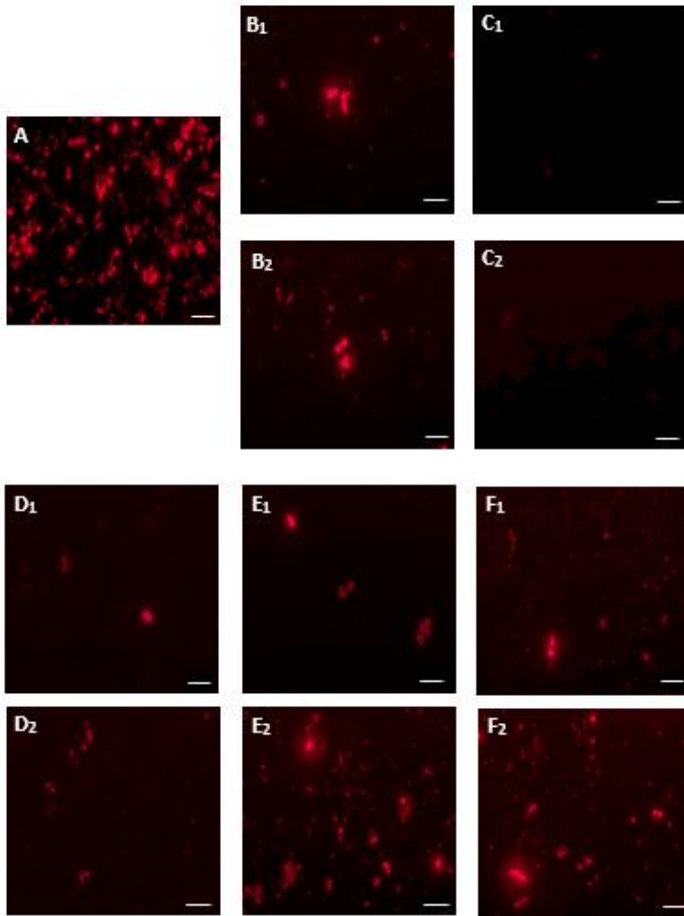


Figure 52. Fluorescence microscope images of CHO cells 48 hours after the incubation with (A) Lipofectamine, (B₁-F₁) GC12-DNA lipoplexes prepared with preformed GC12 liposomes: (B₁) in nanopure water, (C₁) in sodium phosphate buffer (D₁) in Hepes buffer, (E₁) in cacodylate buffer, (F₁) in Tris-HCl buffer; (B₂-F₂) GC12-DNA lipoplexes prepared in-situ: (B₂) in nanopure water, (C₂) in sodium phosphate buffer (D₂) in Hepes buffer, (E₂) in cacodylate buffer, (F₂) in Tris-HCl buffer. Imaged with 10x objective.

Figure 52 shows that **GC12**-DNA complexes in phosphate buffer solution (**C₁** and **C₂**) were not capable of transfection. These results are consistent as **GC12**-DNA lipoplexes are negatively charged in phosphate buffer, therefore the **GC12**-DNA complex could not cross the negatively charged cell membrane. For **GC12**-DNA lipoplexes formed in nanopure water (performed liposomes or formed in-situ), only a few healthy cells could be observed (Figure 52, **B₁** and **B₂**). In HEPES or cacodylate buffer, a few healthy fluorescent cells and fluorescent aggregates could be observed (Figure 52, **D₁** and **E₁**). The fluorescence increased using lipoplexes formed in-situ in HEPES or cacodylate buffer, but the presence of aggregates was more pronounced (Figure 52, **D₂** and **E₂**). It is likely that the system is toxic or the cell self-destructed due to the presence of an unknown system. The lipoplexes in Tris-HCl buffer solution (Figure 52, **F₁** and **F₂**) showed the highest fluorescence intensity, but also the largest amount of aggregates. The aggregates observed might be attributed to the necrosis of the cell or the aggregate observed might be small fractions of the cell that agglomerate. In the conditions tested, **GC12**-DNA lipoplexes seem to be toxic for the cells, but **GC12**-DNA complexes are able carry and protect the DNA to the nucleus and the protein fluorescence is expressed: the lipoplexes could reach the nucleus of the cell and deliver the DNA. The ability of lipoplexes to transfect cells appears to be related to the method of preparation of the lipoplexes.

Several parameters such as the temperature, the buffer solution or method of preparation in one step (in-situ formation of the lipoplexes) or two steps (first the liposomes and then the lipoplexes) seem to be crucial parameters that affect the transfection.

In this chapter, the ability of **GC12**-SLNs coated with several DNA-chitosan layers and **GC12**-DNA lipoplexes to deliver DNA into mammalian cells was investigated. Surprisingly, calixarenes-based SLNs coated with several DNA-chitosan layers were unable to deliver the genetic information into the cells. All the lipoplexes tested, with the exception of **GC12**-DNA lipoplexes prepared in phosphate buffer, were able to deliver the genetic information into the cells and express the protein. In particular the lipoplexes prepared in Tris-HCl buffer showed the highest fluorescence but also the highest amount of dead cells. On the other hand, **GC12** lipoplexes in nanopure water were able to transfect cells with less efficiency, but the system was also cell toxic. The results are promising for the development of **GC12** lipoplexes with high transfection and low toxicity. Several parameters can be tuned, such as the size, the lipid/DNA charge ratio, and the use of lipids (e.g. DOPE, DOTMA) to improve transfection efficiency.

6 Conclusions and Outlook

This thesis investigated the synthesis of new cationic amphiphilic calixarenes, the study of their self-assembly in water as nanoparticles, and the assessment of the calixarene-based nanoparticles to be used as a carrier system for DNA.

The first achievement was the synthesis of amphiphilic calixarenes in the cone conformation, bearing guanidinium or amine recognition moieties at the upper rim and four dodecyloxy chains as hydrophobic functions at the lower rim.

The investigation of the self-assembly of cationic calix[4]arene at the air-water interface showed that all the cationic calixarenes tested were able to form stable Langmuir monolayers on a pure water surface. The interaction of the amino-dodecyloxy-calix[4]arene derivatives (**1NH₂4C₁₂**, **1,2NH₂4C₁₂**, **1,3NH₂4C₁₂**, **3NH₂4C₁₂** and **4NH₂4C₁₂** and **GC12**) with **ATGC** in the subphase revealed different behavior depending on the number of amine functions available to interact with DNA double helix. Indeed, the compression isotherms of **1NH₂4C₁₂**, **1,2NH₂4C₁₂**, **1,3NH₂4C₁₂** and **3NH₂4C₁₂** measured in the presence of **ATGC** in the subphase leads to an expansion of the calixarene monolayers. No clear expansion, but a change in the shape of the isotherm could be observed with **4NH₂4C₁₂**.

To study the influence of the recognition function on the interaction of the calix[4]arene monolayer with DNA duplexes sequence, **GC12** or **4NH₂4C₁₂** monolayer isotherms were performed on three oligonucleotides sequences: **AT**, **GC** and **ATGC**. The interaction of **GC12** and **4NH₂4C₁₂** monolayer at the air-water interface with the oligonucleotides (**AT**, **GC** and **ATGC**) in the subphase showed differences in interaction of the guanidinium and the amino functions with DNA molecules present in the subphase. Indeed, the compression isotherms of **GC12** on a DNA subphase revealed a more important expansion of the monolayer than in the case of **4NH₂4C₁₂** in the same conditions for all DNA tested. This was attributed to the ability of guanidinium functions of **GC12** to form two hydrogen bonds while the amine functions can form one hydrogen bond with the phosphate backbone of the DNA.

Moreover, the interaction with the Langmuir monolayers is dependent on the DNA sequence. Different behaviors could be observed in the presence of **AT**, **GC** or **ATGC**.

The ability of **GC12** and of the amino calix[4]arene derivatives to self-assemble as nanoparticles was investigated in nanopure water. **GC12**, **4NH₂4C₁₂** and **3NH₂4C₁₂** form stable solid lipid nanoparticles in nanopure water. **1NH₂4C₁₂**, **1,2NH₂4C₁₂** and **1,3NH₂4C₁₂** in the non-protonated form cannot form stable nanoparticles, but after protonation of the amine function, **1NH₃⁺4C₁₂**, **1,2NH₃⁺4C₁₂** and **1,3NH₃⁺4C₁₂** formed stable suspensions.

The interaction of the calixarene-based nanoparticles with the oligonucleotides **ATGC** was investigated by fluorescence displacement assay using ethidium bromide as intercalating agent. A slight decrease in the fluorescence intensity could be observed upon addition of **1NH₃⁺4C₁₂**, **1,2NH₃⁺4C₁₂**, **1,3NH₃⁺4C₁₂** and **3NH₂4C₁₂**-based nanoparticles. These results were attributed to the impossibility for the calixarene-based nanoparticles to unwind the double-strand of the DNA and to release the ethidium bromide in solution, most probably because the interaction with DNA double helix is mainly electrostatic. In the case of **GC12**-SLNs and **4NH₂4C₁₂**-SLNs, up to 80 % of the ethidium bromide was displaced for the double-stranded **ATGC**.

To investigate the influence of the DNA sequence in the binding capacity, the fluorescence displacement assay was performed in the presence of the 30-mer DNA **AT** and **GC**. The results suggested that **GC12**-SLNs and **4NH₂4C₁₂**-SLNs displaced the intercalating dye for all DNA tested.

It was shown that the binding was not purely based on electrostatic interactions. In addition, the fluorescence displacement assay revealed a slight preference for **AT**-DNA for both systems.

Circular dichroism experiments for **GC12** and **4NH₂4C₁₂** showed that the SLNs interact with DNA molecules and that those interactions caused a B-to-A-like transition for **GC** and **ATGC** and no transition in **AT**-DNA conformation. After the interaction, DNA duplexes remained in B'-form. The binding mechanism of **GC12** and **4NH₂4C₁₂**-SLNs with DNA was investigated with ITC. The ITC results suggested that the binding with **AT** proceeded via a minor groove mechanism while the binding to **GC** occurred mainly via its major groove for both systems (**GC12**-SLNs and **4NH₂4C₁₂**-SLNs).

The present work aimed at building an LbL assembly at the surface of calixarene-based nanoparticles to deliver genetic information into the cells. The calixarene-based nanoparticles **1NH₃⁺4C₁₂**, **1,2NH₃⁺4C₁₂**, **1,3NH₃⁺4C₁₂**, **3NH₂4C₁₂** and **4NH₂4C₁₂** and **GC12** were successfully modified with several layers of DNA-chitosan without destabilization of the system.

To go further in the study of the self-assembly properties of calix[4]arenes in the presence of DNA, lipoplexes were formed with **GC12** calixarenes. No lipoplexes could be prepared with the amino calixarene derivatives. The SLNs and lipoplexes systems were used to deliver genetic information.

The results showed that the SLNs modified by the LbL technique could not transfect DNA in the condition of the experiments conducted. On the other hand, the lipoplexes formed in pure water or in buffer were able to deliver DNA into the cell but these systems were toxic for the cells in those conditions.

The self-assembly and DNA-binding studies of calixarene nanoparticles allow a better understanding of the mechanism of interaction between the recognition moieties at the surface of the nanoparticles and the DNA molecules. Considering the broader impact of research on nanoparticle as DNA carrier system, these results might be used to optimize the design of amphiphilic molecules capable of DNA-binding by appropriate structural modifications.

7 Experimental Section

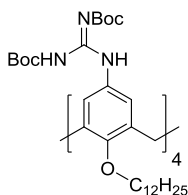
7.1 Methodology

General

All reactions were carried out under anhydrous conditions. All solvents were dried according to standard procedures and stored over molecular sieves. ^1H NMR spectra were recorded with a Bruker spectrometer 300 MHz. Mass spectra were recorded in ESI mode on a thermoquest LCQ Deca instrument. Elemental analyses were measured on a Leco CHN-900 microanalyser (C-, H-, N-detection) and are reported in mass percent.

Thin layer chromatography was performed on pre-coated silica 0.2 mm and flash column chromatography on 230–400 mesh Merck 60 silica gel. The 25,26,27,28-tetra(dodecyloxy)-calix[4]arene (**24**),¹ the 5,11,17,23-tetra(amino)-25,26,27,28-tetra(tetradodecoxy)-calix[4]arene (**4NH₂4C₁₂**),² *p*-acyl-calix[4]arene (**25**),³ dimethoxy calixarene (**28**),⁴ and *N,N'*-bis-*tert*-butoxycarbonylthiourea⁵ were produced as previously described.

Synthesis of 5,11,17,23-tetra[(bis-*N*-Boc)guanidine]-25,26,27,28-tetra(dodecyloxy)-calix[4]arene (23**)**

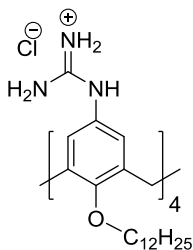


To a solution of **22** (5.13 g, 4.43 mmol) in dry CH₂Cl₂ (150 mL), *N,N'*-bis-*tert*-butoxycarbonylthiourea (5.14 g, 18.61 mmol), and Et₃N (6.73 g, 18.61 mmol) were added and the mixture was cooled in an ice bath. 2-chloro-1-methylpyridinium iodide (7.92 g, 31.01 mmol) was added and the mixture stirred 30 minutes at 0°C. The ice bath was removed and the reaction mixture was stirred overnight at 20 °C. The solvent was evaporated under reduce pressure and the residue was purified by flash column chromatography on silica gel (eluent: heptane/ethyl acetate 9:1 and 6:1) to obtain a pale yellow powder, **23** (4.14 mg, 44 %).

¹H NMR (CDCl₃-d, 300 MHz): δ_H = 11.71 (br. s., 4 H, bocNH), 10.33 (s, 4 H, ArNH), 7.30 (br. s., 4 H, ArH), 4.38 (d, *J* = 13.7 Hz, 4 H, ArCH₂Ar), 3.62 (d, *J* = 3.8 Hz, 8 H, OCH₂CH₂(CH₂)₉CH₃), 2.93 - 3.29 (m, 4 H, ArCH₂Ar), 1.85 (br. s., 8 H, OCH₂CH₂(CH₂)₉CH₃), 1.38 - 1.78 (m, 72 H, ^tBu), 1.01 - 1.38 (m, 72 H, OCH₂CH₂(CH₂)₉CH₃), 0.77 - 0.95 ppm (m, 12 H, OCH₂CH₂(CH₂)₉CH₃).

MS (ESI) m/z : $[M-8\text{boc}+\text{H}_2\text{O}+\text{H}]^+$ calcd. for $\text{C}_{80}\text{H}_{135}\text{N}_{12}\text{O}_5$, 1344.07; found, 1344.7. m/z : $[M-8\text{boc}+2\text{H}]^{2+}$ calcd. for $\text{C}_{80}\text{H}_{134}\text{N}_{12}\text{O}_4$, 663.5; found, 662.9.

Synthesis of 5,11,17,23-tetra(guanidinium)-25,26,27,28-tetra(dodecyloxy)-calix[4]arene (GC12)



Concentrated HCl (37 %) was added drop wise to a solution of **23** (2 g, 0.47 mmol) in 60 mL of 1,4-dioxane. The suspension was stirred 24h at room temperature and the solvent evaporated under vacuum. The obtained powder was triturated with ethyl acetate then filtrated, to give a beige powder in a yield of 69 %.

^1H NMR (DMSO-d_6 , 300 MHz): δ_{H} = 7.29 (br. s., 8 H, ArH), 6.55 (s, 4 H, ArNH), 4.29 (d, J = 12.5 Hz, 4 H, ArCH₂Ar), 3.84 (br. s., 8 H, OCH₂(CH₂)₁₀CH₃), 3.24 (d, J = 12.5 Hz, 4 H, ArCH₂Ar), 1.86 (br. s., 8 H, OCH₂CH₂(CH₂)₉CH₃), 1.24 (br. s., 72 H, OCH₂CH₂(CH₂)₉CH₃), 0.72 - 0.94 ppm (m, 12 H, OCH₂CH₂(CH₂)₉CH₃). MS (ESI) m/z : $[M-4\text{HCl}+2\text{H}]^{2+}$ calcd. for $\text{C}_{80}\text{H}_{134}\text{N}_{12}\text{O}_4$, 663.53; found, 662.9. TLC heptane/ethyl acetate (4:1) R_f = 0.4.

General Procedure for the Ipsso Nitration

25,26,27,28-Tetra(dodecyloxy)-calix[4]arene **24** (1 mmol) was dissolved in CH_2Cl_2 (10 mL) was added glacial acetic acid (4 mL) was added HNO_3 65 % (15eq) at 0°C. The reaction mixture was stirred at room temperature for 1h30. The reaction was stopped by addition of water (50 mL) and the product mixture was extracted with CH_2Cl_2 (3 x 50 mL).

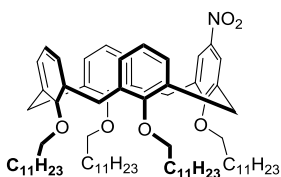
Experimental Section

The organic layer was washed with saturated sodium bicarbonate (3x50 mL) and water (3 x 50 mL) and dried over Na₂SO₄. The reaction mixture consist of **24** (9 %) and **1NO₂4C₁₂** (16 %).

The same reaction stopped after 2 h afford **1,2NO₂4C₁₂** and **1,3NO₂4C₁₂** in 4 %, 12 % yields respectively. If the reaction is stopped after 3h, the mixture is composed of **1,3NO₂4C₁₂** and **3NO₂4C₁₂** in 30 % and 33 % yields respectively. The products were separated by column chromatography.

5-Mono(nitro)-25,26,27,28-tetra(dodecyloxy)-calix[4]arene (1NO₂4C₁₂)

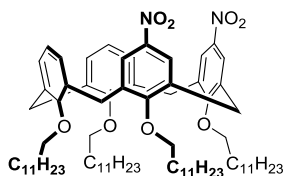
was obtained as a white powder after flash column chromatography in heptane/CH₂Cl₂ (4:1).



¹H NMR (CDCl₃-d, 300 MHz) δ_H = 7.11 (s, 2 H, ArH), 6.75 - 7.00 (m, 6 H, ArH), 6.23 (s, 3 H, ArH), 4.44 (t, *J* = 13.8 Hz, 4 H, ArCH₂Ar), 3.61 - 4.11 (m, 8 H, OCH₂(CH₂)₁₀CH₃), 3.17 (dd, *J* = 13.3, 11.8 Hz, 4 H, ArCH₂Ar), 1.77 - 1.97 (m, 8 H, OCH₂CH₂(CH₂)₉CH₃), 1.27 (br. s., 72 H, OCH₂CH₂(CH₂)₉CH₃), 0.79 - 0.93 ppm (m, 12 H, OCH₂CH₂(CH₂)₉CH₃). ¹³C NMR (CDCl₃-d, 75 MHz) δ_C = 161.4, 157.2, 155.8, 142.6, 136.6, 136.0, 134.9, 134.0, 129.4, 128.5, 127.7, 123.2, 122.4, 121.7, 75.5, 75.2, 32.0, 31.1, 31.0, 30.4, 30.2, 30.0, 29.8, 29.8, 29.4, 26.5, 26.4, 26.1, 22.7, 14.1 ppm. MS (ESI) *m/z*: [M+Na]⁺ calcd. for C₇₆H₁₁₉NO₆, 1164.89; found, 1164.9. Elemental analysis (%); calcd. C 79.88, H 10.50, N 1.23; found C 79.82, H 10.22, N 1.19. TLC heptane/ethyl acetate (10:1) R_f = 0.51.

5,11-Di(nitro)-25,26,27,28-tetra(dodecyloxy)-calix[4]arene (1,2NO₂4C₁₂)

was obtained as a white powder after flash column chromatography in heptane/ethyl acetate (20:1).

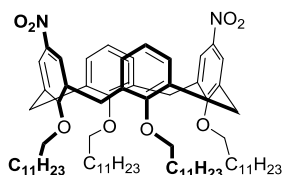


¹H NMR (CDCl₃-d, 300 MHz): δ_H = 7.49 (d, *J* = 9.3 Hz, 4 H, ArH), 6.55 (br. s., 6 H, ArH), 4.31 - 4.56 (m, 4 H, ArCH₂Ar), 3.86 (br. s., 8 H, OCH₂(CH₂)₁₀CH₃), 3.05 - 3.38 (m, 4 H, ArCH₂Ar), 1.85 (br. s., 8 H, OCH₂CH₂(CH₂)₉CH₃), 1.27 (br. s., 72 H, OCH₂CH₂(CH₂)₉CH₃), 0.79 - 0.96 ppm (m, 12 H, OCH₂CH₂(CH₂)₉CH₃).

¹³C NMR (CDCl₃-d, 75 MHz) δ_C = 162.2, 156.5, 142.5, 137.1, 135.4, 135.2, 133.5, 129.0, 128.0, 125.0, 124.4, 123.3, 122.3, 75.7, 75.3, 31.9, 31.1, 30.3, 29.9, 29.9, 29.8, 29.7, 29.4, 26.3, 26.2, 22.7, 14.1 ppm. MS (ESI) *m/z*: [M]⁺ calcd. for C₇₆H₁₁₈N₂O₈, 1187.89; found, 1187.8. Elemental analysis (%): calcd. C 76.85, H 10.01, N 2.36; found C 75.88, H 10.40, N 2.41. TLC heptane/ethyl acetate (10:1) R_f = 0.35.

5,17-Di(nitro)-25,26,27,28-tetra(dodecyloxy)-calix[4]arene (1,3NO₂4C₁₂)

was obtained as a white powder after flash column chromatography in heptane/ethyl acetate (20:1).



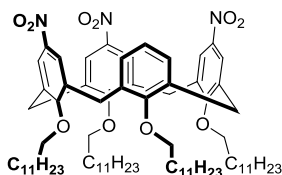
¹H NMR (CDCl₃-d, 300 MHz): δ_H = 7.43 (s, 4 H, ArH), 6.74 (s, 6 H, ArH), 4.47 (d, *J* = 13.7 Hz, 4 H, ArCH₂Ar), 3.92 (dt, *J* = 15.1, 7.4 Hz, 8 H, OCH₂(CH₂)₁₀CH₃), 3.25 (d, *J* = 13.7 Hz, 4 H, ArCH₂Ar), 1.84 - 2.01 (m, 8 H, OCH₂CH₂(CH₂)₉CH₃), 1.19 - 1.51 (m, 72 H, OCH₂CH₂(CH₂)₉CH₃), 0.80 - 0.95 ppm (m, 12 H, OCH₂CH₂(CH₂)₉CH₃).

Experimental Section

^{13}C NMR (CDCl_3 -d, 75 MHz): δ_{C} = 161.9, 156.3, 142.5, 136.3, 134.1, 128.9, 123.4, 123.0, 75.7, 75.4, 31.9, 31.1, 30.3, 30.9, 29.8, 29.7, 29.4, 26.2, 22.7, 14.1 ppm. MS (ESI) m/z : $[\text{M}+\text{Na}]^+$ calcd. for $\text{C}_{76}\text{H}_{118}\text{N}_2\text{O}_8$, 1209.88; found, 1209.7. Elemental analysis (%); calcd. C 76.85, H 10.01, N 2.36; found C 76.96, H 10.02, N 2.44. TLC heptane/ethyl acetate (10:1) R_f = 0.28.

5,11,17-Tri(nitro)-25,26,27,28-tetra(dodecyloxy)-calix[4]arene (3NO₂4C₁₂)

was obtained as a white powder after flash column chromatography in heptane/ethyl acetate (10:1).

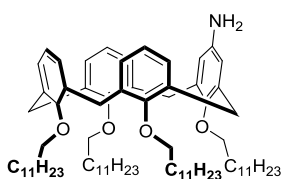


^1H NMR (CDCl_3 -d, 300 MHz) δ_{H} = 7.79 (d, J = 4.2 Hz, 4 H, ArH), 7.24 (s, 2 H, ArH), 6.37 (s, 3 H, ArH), 4.48 (t, J = 14.2 Hz, 4 H, ArCH₂Ar), 3.68 - 4.21 (m, 8 H, OCH₂(CH₂)₁₀CH₃), 3.33 (t, J = 14.6 Hz, 4 H, ArCH₂Ar), 1.87 (d, J = 6.8 Hz, 8 H, OCH₂CH₂(CH₂)₉CH₃), 1.15 - 1.53 (m, 72 H, OCH₂CH₂(CH₂)₉CH₃), 0.88 ppm (t, J = 6.4 Hz, 12 H, OCH₂CH₂(CH₂)₉CH₃). ^{13}C NMR (CDCl_3 -d, 75 MHz) δ_{C} = 162.7, 161.3, 155.8, 142.9, 142.6, 137.5, 135.8, 134.9, 132.9, 128.4, 124.7, 123.6, 122.7, 75.9, 75.6, 31.9, 31.1, 31.1, 30.4, 30.3, 29.9, 29.8, 29.8, 29.7, 29.4, 26.4, 26.3, 26.0, 22.7, 14.1 ppm. MS (ESI) m/z : $[\text{M}+\text{Na}]^+$ calcd. for $\text{C}_{76}\text{H}_{117}\text{N}_3\text{O}_{10}$, 1254.86; found, 1254.8. Elemental analysis (%); calcd. C 74.05, H 9.57, N 3.41; found C 73.93, H 9.63, N 3.42. TLC heptane/ethyl acetate (10:1) R_f = 0.17.

General Procedure for the Reduction of the Nitro Groups into Amine

Hydrazine monohydrate (20 eq per nitro groups) and catalytic amount of Pd/C (10 %) was added to a suspension of calixarene (**1NO₂4C₁₂**, **1,2NO₂4C₁₂**, **1,3NO₂4C₁₂**, or **3NO₂4C₁₂**) in ethanol. The mixture was reflux for 4 hours and then filtrated, through hot filtration. The filtrate was cool to room temperature and the desired product crystallized in ethanol.

5-Mono(amino)-25,26,27,28-tetra(dodecyloxy)-calix[4]arene (1NH₂4C₁₂) was obtained as a white powder in a yield of 84 %.

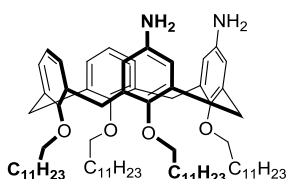


¹H NMR (CDCl₃-d, 300 MHz) δ_H = 6.50 - 6.74 (m, 9 H, ArH), 5.95 (s, 2 H, ArH), 4.44 (d, J = 13.3 Hz, 2 H, ArCH₂Ar), 4.30 (d, J = 13.3 Hz, 2 H, ArCH₂Ar), 3.85 (dt, J = 7.3, 3.9 Hz, 8 H, OCH₂(CH₂)₁₀CH₃), 3.14 (d, J = 13.3 Hz, 2 H, ArCH₂Ar), 3.02 (d, J = 13.3 Hz, 2 H, ArCH₂Ar), 1.79 - 1.96 (m, 8 H), 1.19 - 1.41 (m, 72 H, OCH₂CH₂(CH₂)₉CH₃), 0.88 ppm (t, J = 6.8 Hz, 12 H, OCH₂CH₂(CH₂)₉CH₃).

¹³C NMR (CDCl₃-d, 75 MHz) δ_C = 156.7, 140.3, 135.6, 135.2, 128.0, 121.8, 121.5, 115.4, 75.1, 32.0, 31.0, 30.3, 30.0, 29.9, 29.8, 29.8, 29.4, 26.4, 22.7, 14.1 ppm. MS (ESI) m/z: [M+H]⁺ calcd. for C₇₆H₁₂₁NO₄, 1112.94; found, 1112.7. Elemental analysis (%); calcd. C 82.06, H 10.96, N 1.26; found C 81.66, H 10.74, N 1.16. TLC CHCl₃/hexane/acetone (10:20:3) R_f = 0.55.

5,11-Di(amino)-25,26,27,28-tetra(dodecyloxy)-calix[4]arene (1,2NH₂4C₁₂)

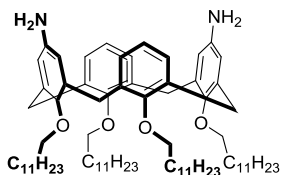
was obtained as a white powder in a yield of 87 %.



¹H NMR (CDCl₃-d, 300 MHz) δ_H = 6.46 - 6.72 (m, 6 H, ArH), 5.98 (dd, *J* = 12.1, 2.6 Hz, 4 H, ArH), 4.37 (ddd, *J* = 24.0, 13.2 Hz, 4 H, ArCH₂Ar), 3.81 (dt, *J* = 27.0, 7.3 Hz, 8 H, OCH₂(CH₂)₁₀CH₃), 3.02 (ddd, *J* = 36.6, 13.3 Hz, 4 H, ArCH₂Ar), 1.73 - 1.98 (m, 8 H, OCH₂CH₂(CH₂)₉CH₃), 1.27 (s, 72 H, OCH₂CH₂(CH₂)₉CH₃), 0.88 ppm (t, *J* = 6.7 Hz, 12 H, OCH₂CH₂(CH₂)₉CH₃). ¹³C NMR (CDCl₃-d, 75 MHz) δ_C = 156.8, 149.9, 140.2, 135.6, 135.2, 128.1, 128.0, 121.4, 115.4, 75.1, 75.1, 32.0, 31.1, 30.3, 30.3, 30.0, 29.9, 29.8, 29.8, 29.4, 26.4, 26.4, 22.7, 14.1 ppm. MS (ESI) *m/z*: [M+Na]⁺ calcd. for C₇₆H₁₂₂N₂O₄, 1149.93; found, 1149. Elemental analysis (%); calcd. C 80.94, H 10.0, N 2.48; found C 80.81, H 10.89, N 2.51. TLC CHCl₃/hexane/acetone (10:20:17) R_f = 0.45.

5,17-Di(amino(-25,26,27,28-tetra(dodecyloxy)-calix[4]arene

(1,3NH₂4C₁₂) was obtained as a white powder in a yield of 75 %.

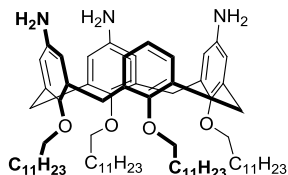


¹H NMR (CDCl₃-d, 300 MHz): δ_H = 6.51 - 6.78 (m, 6 H, ArH), 5.93 (s, 4 H, ArH), 4.37 (d, *J* = 13.3 Hz, 4 H, ArCH₂Ar), 3.59 - 3.97 (m, 8 H, OCH₂(CH₂)₁₀CH₃), 3.03 (d, *J* = 13.3 Hz, 4 H, ArCH₂Ar), 1.86 (br. s., 8 H, OCH₂CH₂(CH₂)₉CH₃), 1.08 - 1.48 (m, 72 H, OCH₂CH₂(CH₂)₉CH₃), 0.73 - 1.08 ppm (m, 12 H, OCH₂CH₂(CH₂)₉CH₃). ¹³C NMR (CDCl₃-d, 75 MHz): δ_C = 157.7, 154.2, 136.5, 135.3, 129.5, 122.6, 120.7, 75.3, 75.1, 32.0, 31.9, 31.0, 30.5, 30.1, 29.8, 29.8, 29.7, 29.4, 29.4,

26.6, 26.0, 22.7, 14.1 ppm. MS (ESI) m/z : $[M+Na]^+$ calcd. for $C_{76}H_{122}N_2O_4$, 1149.93; found, 1149.9. Elemental analysis (%); calcd. C 80.94, H 10.90, N 2.48; found C 80.46, H 10.70, N 2.39. TLC $CHCl_3$ /hexane/acetone (10:20:17) R_f = 0.40.

5,11,17-Tri(amino)-25,26,27,28-tetra(dodecyloxy)-calix[4]arene

(**3NH₂4C₁₂**) was obtained as a white powder in a yield of 54 %.

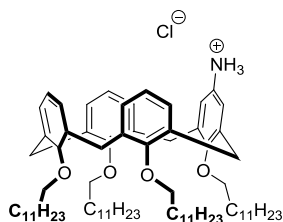


1H NMR ($CDCl_3$ -d, 300 MHz) δ_H = 6.58 - 6.75 (m, 3 H, ArH), 5.90 - 6.10 (m, 6 H, ArH), 4.37 (d, J = 13.1 Hz, 2 H, ArCH₂Ar), 4.30 (d, J = 13.3 Hz, 2 H, ArCH₂Ar), 3.65 - 3.94 (m, 8 H, OCH₂(CH₂)₁₀CH₃), 3.03 (d, J = 13.3 Hz, 2 H, ArCH₂Ar), 2.91 (d, J = 13.1 Hz, 2 H, ArCH₂Ar), 1.74 - 1.96 (m, 8 H, OCH₂(CH₂)₁₀CH₃), 1.19 - 1.45 (m, 72 H, OCH₂CH₂(CH₂)₉CH₃), 0.80 - 0.96 ppm (m, 12 H, OCH₂CH₂(CH₂)₉CH₃). ^{13}C NMR ($CDCl_3$ -d, 75 MHz) δ_C = 150.1, 150.0, 140.3, 140.1, 135.8, 135.5, 135.4, 128.1, 115.7, 115.4, 75.1, 32.0, 31.1, 30.3, 30.0, 29.9, 29.8, 29.8, 29.4, 26.4, 22.7, 14.1 ppm. MS (ESI) m/z : $[M+Na]^+$ calcd. for $C_{76}H_{123}N_3O_4$, 1164.94; found, 1164.9. Elemental analysis (%); calcd. C 79.87, H 10.85, N 3.68; found C 79.56, H 10.65, N 3.37. TLC $CHCl_3$ /hexane/acetone (10:20:17) R_f = 0.22.

General Procedure for the Protonation of the *p*-Amino Calix[4]arene Derivatives

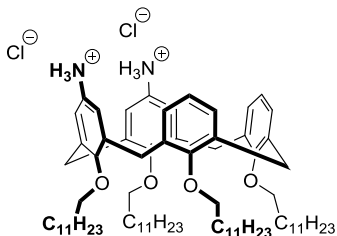
The calixarene powder was dissolved in CHCl_3 and the solution washed with HCl (0.1 N) to protonate the amine groups. The organic layer was dried over Na_2SO_4 and the solvent evaporated. The protonated calixarene were characterized by ^1H NMR.

5-Mono(ammonium)-25,26,27,28-tetra(dodecyloxy)-calix[4]arene chloride ($1\text{NH}_3^+ 4\text{C}_{12}$)



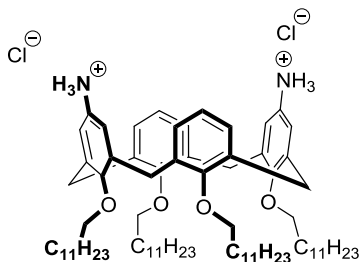
^1H NMR (CDCl_3 -d, 300 MHz) $\delta_{\text{H}} = 10.13$ (br. s., 2 H, ArNH_3^+), 6.91 (s, 2 H, *ArH*), 6.81 (s, 3 H, *ArH*), 6.45 (s, 6 H, *ArH*), 4.42 (dd, $J = 13.3$, 3.2 Hz, 4 H, ArCH_2Ar), 3.92 (t, $J = 7.6$ Hz, 4 H, $\text{OCH}_2(\text{CH}_2)_{10}\text{CH}_3$), 3.78 (m, 4 H, $\text{OCH}_2(\text{CH}_2)_{10}\text{CH}_3$), 3.15 (dd, $J = 13.5$, 6.5 Hz, 4 H, ArCH_2Ar), 1.71 - 1.90 (m, 8 H, $\text{OCH}_2\text{CH}_2(\text{CH}_2)_9\text{CH}_3$), 1.27 (br. s., 72 H, $\text{OCH}_2\text{CH}_2(\text{CH}_2)_9\text{CH}_3$), 0.88 ppm (t, $J = 6.4$ Hz, 12 H, $\text{OCH}_2\text{CH}_2(\text{CH}_2)_9\text{CH}_3$).

5,11-Di(ammonium)-25,26,27,28-tetra(dodecyloxy)-calix[4]arene dichloride (1,2NH₃⁺ 4C₁₂)



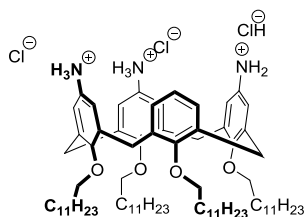
¹H NMR (CDCl₃-d, 300 MHz) δ_H = 9.79 (br. s., 5 H, ArNH₃⁺), 6.72 (br. m., 9 H, ArH), 4.28 (br. s., 4 H, ArCH₂Ar), 3.71 (br. s., 8 H, OCH₂(CH₂)₁₀CH₃), 3.00 (br. s., 4 H, ArCH₂Ar), 1.79 (br. s., 8 H, OCH₂CH₂(CH₂)₉CH₃), 1.26 (br. s., 72 H, OCH₂CH₂(CH₂)₉CH₃), 0.87 ppm (t, *J* = 6.5 Hz, 12 H, OCH₂CH₂(CH₂)₉CH₃).

5,17-Di(ammonium)-25,26,27,28-tetra(dodecyloxy)-calix[4]arene dichloride (1,3NH₃⁺ 4C₁₂)



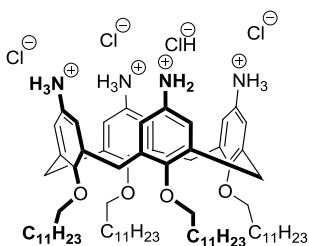
¹H NMR (CDCl₃-d, 300 MHz) δ_H = 9.41 (br. s., 6 H, ArNH₃⁺), 7.29 (d, *J* = 7.6 Hz, 4 H, ArH), 7.01 (s, 2 H, ArH), 6.24 (s, 4 H, ArH), 4.44 (d, *J* = 13.3 Hz, 4 H, ArCH₂Ar), 3.97 - 4.13 (m, 4 H, OCH₂(CH₂)₁₀CH₃), 3.67 (t, *J* = 5.9 Hz, 4 H, OCH₂(CH₂)₁₀CH₃), 3.20 (d, *J* = 13.7 Hz, 4 H), 2.31 (br. s., 4 H), 1.93 (br. s., 8 H, OCH₂(CH₂)₁₀CH₃), 1.27 (br. s., 66 H, OCH₂CH₂(CH₂)₉CH₃), 0.81 - 0.90 ppm (m, 12 H, OCH₂CH₂(CH₂)₉CH₃).

5,11,17-Tri(ammonium)-25,26,27,28-tetra(dodecyloxy)-calix[4]arene trichloride ($3\text{NH}_3^+ 4\text{C}_{12}$)



^1H NMR ($\text{CDCl}_3\text{-d}$, 300 MHz) $\delta_{\text{H}} = 6.98$ (m, 2 H, ArH), 6.86 (m, 1 H, ArH), 6.45 (br. s., 2 H, ArH), 5.96 (d, $J = 2.5$ Hz, 2 H, ArH), 5.83 (d, $J = 2.5$ Hz, 2 H, ArH), 4.17 - 4.43 (m, 4 H, ArCH_2Ar), 3.77 - 3.98 (m, 13 H, $\text{OCH}_2(\text{CH}_2)_{10}\text{CH}_3$ and ArNH_3^+), 3.62 (br. s., 4 H, $\text{OCH}_2(\text{CH}_2)_{10}\text{CH}_3$), 3.05 (d, $J = 13.9$ Hz, 2 H, ArCH_2Ar), 2.91 (d, $J = 13.5$ Hz, 2 H, ArCH_2Ar), 1.81 (m, 8 H, $\text{OCH}_2\text{CH}_2(\text{CH}_2)_9\text{CH}_3$), 1.26 (s, 72 H, $\text{OCH}_2\text{CH}_2(\text{CH}_2)_9\text{CH}_3$), 0.88 ppm (t, $J = 6.5$ Hz, 12 H, $\text{OCH}_2\text{CH}_2(\text{CH}_2)_9\text{CH}_3$).

5,11,17,21-Tetra(ammonium)-25,26,27,28-tetra(dodecyloxy)-calix[4]arene tetrachloride ($4\text{NH}_3^+ 4\text{C}_{12}$)

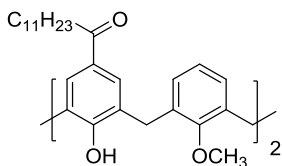


^1H NMR ($\text{CDCl}_3\text{-d}$, 300 MHz) $\delta_{\text{H}} = 6.32$ (br. s., 9 H, ArNH_3^+), 6.03 (br. s., 8 H, ArH), 4.21 (d, $J = 12.1$ Hz, 4 H, ArCH_2Ar), 3.68 (br. s., 8 H, $\text{OCH}_2(\text{CH}_2)_{10}\text{CH}_3$), 2.86 (d, $J = 11.0$ Hz, 4 H, ArCH_2Ar), 1.77 (br. s., 8 H, $\text{OCH}_2\text{CH}_2(\text{CH}_2)_9\text{CH}_3$), 1.26 (br. s., 72 H, $\text{OCH}_2\text{CH}_2(\text{CH}_2)_9\text{CH}_3$), 0.88 ppm (t, $J = 6.5$ Hz, 12 H, $\text{OCH}_2\text{CH}_2(\text{CH}_2)_9\text{CH}_3$).

General Procedure for the Diacylation

Under anhydrous nitrogen, aluminium trichloride (23.5 g, 176 mmol) and the lauroyl chloride (138 mmol) were added to nitrobenzene (200 mL) and the mixture was stirred for 10 minutes. The solution became dark brown; to this was added calixarene **28** (9.7 g, 23 mmol). The resultant solution was stirred at room temperature for 4 hours. Pouring onto ice for one hour stopped the reaction. The organic phase was extracted with chloroform (800 mL), washed with 1 M HCl (2 × 400 mL), 1 M NaCl (2 × 400 mL), water (4 × 400 mL) and dried under anhydrous MgSO₄. The chloroform was removed under reduced pressure, and the nitrobenzene distilled off under vacuum (10⁻² T) to give a volume of 100 mL. Compounds were precipitated as white solids by the addition of methanol (300 mL). The products were recrystallized from acetone to yield the pure compounds.

5,11,17,21-Diacyl-25,27-di(methoxy)-calix[4]arene (**29**)



¹H NMR (CDCl₃-d, 300 MHz): δ_H = 8.47 (s, 2 H), 7.76 (s, 4 H), 6.91 (d, *J* = 7.4 Hz, 4 H), 6.71 - 6.81 (m, 2 H), 4.29 (d, *J* = 13.3 Hz, 4 H), 4.00 (s, 6 H), 3.49 (d, *J* = 13.3 Hz, 4 H), 2.90 (t, *J* = 7.5 Hz, 4 H), 1.72 (t, *J* = 6.9 Hz, 4 H), 1.26 (br. s., 32 H), 0.88 ppm (t, *J* = 6.6 Hz, 6 H).

General Procedure for the *o*-Alkylation

Under anhydrous nitrogen, the relevant para acyl calixarene was stirred in dry DMF for 30 minutes, prior the carefully addition of NaH (2.3 equivalents per OH group). The mixture was stirred for 1 h at room temperature and N-(3-bromoethyl)phthalimide (2.3 equivalents per OH group) was added. The reaction was quenched by HCl solution 1 N.

Langmuir Monolayer Experiments

Prior to experiments, the Langmuir trough (Nima 112D) and the barriers were cleaned with analytical grade chloroform and nanopure water (resistivity $\geq 18 \text{ M}\Omega \text{ cm}$). The microbalance was calibrated before each series of runs using a weighing pan and a calibration weight. Buffer solutions, at defined concentration in nanopure water, were prepared extemporaneously. The absence of surface-active molecules was controlled by closing the barriers in the absence of **GC12**; no relevant change in surface tension was observed. 10 μL of **GC12** solution in chloroform (1 mg mL^{-1}) was spread on the liquid subphase using a gastight microsyringe. Fifteen minutes was allowed for solvent evaporation and monolayer equilibration; barriers were closed in continuous mode at a speed rate of $5 \text{ cm}^2 \text{ min}^{-1}$.

Spectroscopic Ellipsometry

Ellipsometry measurements were carried out using an imaging and spectroscopic system (EP³ Ellipsometer, Accurion, Germany) in a nulling PCSA (polarizer-compensator-sample-analyzer) set-up mounted on the Langmuir trough; the BAM images are coded in gray level. To determine the thickness of the layer at the air-water interface, the calibration procedure of the manufacturer (EP3 View V252) was used to determine the linear function between the reflectance and the gray level. In this system, the incident beam that is elliptically polarized with a linear polarizer (P) and a quarter-wave plate (C) is reflected from the sample (S) to the analyzer (A) and finally imaged with a CCD camera using a 10x objective. The nulling conditions, related to the optical properties of each sample, were obtained by tuning the angles of P, C and A. In the thickness model, the minimum and maximum refractive index values were set to 1.44 and 1.46 respectively.

Nanoparticules Preparation and Characterization

SLNs Preparation

The SLNs suspensions were prepared by dissolving 15 mg of **calixarene** in 5 mL THF. After 1 minute stirring, a volume of 50 mL of nanopure water was added and the solution was stirred one more minute. The THF was subsequently evaporated under reduced pressure at 40°C and the volume adjusted to 50 mL with nanopure water to obtain a final concentration of 300 µg mL⁻¹.

Lipoplexes Preparation

First method: The lipoplexes suspensions were prepared by mixing 1 mg of **calixarene** in 1 mL of the appropriate aqueous solution (nanopure water, HEPES buffer, cacodylate buffer, phosphate buffer or Tris-HCl buffer) 120 minutes at 40°C. The clear suspension was then cool down to room temperature and mixed with DNA 1.6 µg during 20 minutes at room temperature.

Second method: The lipoplexes suspensions were prepared by mixing 1 mg of **calixarene** and 1.6 µg of DNA in 1mL of the appropriate aqueous solution (nanopure water, HEPES buffer, cacodylate buffer, phosphate buffer or Tris-HCl buffer) during 20 minutes at 40°C. The clear suspension was then cool down to room temperature.

Critical Micellar Concentration (CMC)

A Krüss K100 tensiometer was used to measure the surface tension of **GC12** suspensions by the du Noüy ring detachment method, at room temperature. Solutions of **GC12**-based SLNs in nanopure water were prepared at different concentrations ranging from 2.0×10^{-7} M to 7.0×10^{-4} M. Measurements were made after an equilibration time of 10 minutes in triplicate to ensure reproducibility.

Dynamic Light Scanning (DLS) and ζ -potential Measurements

The particles size and zeta potential were measured using a Zetasizer Nano ZS system (Malvern Instruments). The SLNs suspensions were diluted to a concentration of 50 $\mu\text{g mL}^{-1}$ in nanopure water. All values were measured three times. The system was thermostated at 25°C.

Atomic Force Microscopy (AFM)

A solution SLNs at a final concentration 100 $\mu\text{g mL}^{-1}$ was deposited on freshly cleaved mica. Imaging was performed in non-contact mode in air using a NTegra Prima system (NT-MDT) equipped with diamond rectangular cantilevers (NT-MDT). The image is presented unfiltered.

DNA-Binding Experiments and Characterization

Ethidium bromide and sodium cacodylate were purchased from Sigma-Aldrich. The following oligonucleotides (30-mer) were purchased from Microsynth.

Table S1. DNA sequences used

Name	Sequence
AT	d(5'-AAA AAA AAA AAA AAA AAA AAA AAA AAA AAA-3') d(5'-TTT TTT TTT TTT TTT TTT TTT TTT TTT TTT-3')
GC	d(5'-CCC CCC CCC CCC CCC CCC CCC CCC CCC-3') d(5'-GGG GGG GGG GGG GGG GGG GGG GGG GGG GGG-3')
ATGC	d(5'-GTG GCT AAC TAC GCA TTC CAC GAC CAA ATG-3') d(5'-CAT TTG GTC GTG GAA TGC GTA GTT AGC CAC-3')

Double-Stranded DNA Preparation

The lyophilized oligonucleotides were resuspended in nanopure water (300 μM) and stored at -20°C . Double-stranded oligonucleotides 30-mer were prepared by mixing the same volume of the two complementary single stranded oligonucleotide in HEPES buffer (20 mM HEPES, 100 mM NaCl, pH 7.1).

The solutions were heated 5 minutes at 95°C , slowly cooled down to room temperature and the volume of the solution was adjusted to a final concentration of 54 μM . Double-stranded DNA samples used for circular dichroism experiments were prepared following the same protocol with a sodium cacodylate buffer solution (20 mM sodium cacodylate, 100 mM NaCl, pH 6.8).

Layer-by-Layer Technique

Prior the preparation of SLNs coated with several DNA-chitosan layers, the amount of DNA or chitosan needed to fully cover the SLNs was measured by following the change in zeta potential. SLNs at a concentration All CD experiments were recorded on an Applied of $50 \mu\text{g mL}^{-1}$ in nanopure water were mixed with increasing concentration of DNA ($100 \mu\text{g mL}^{-1}$). Then SLNs/DNA/chitosan complex was formed by adding increasing concentration of chitosan ($100 \mu\text{g mL}^{-1}$) to the SLN/DNA complex. SLNs coated with several layer of DNA/chitosan was prepared by mixing the SLNs in water ($50 \mu\text{g mL}^{-1}$) with DNA then incubated with chitosan.

Ethidium Bromide Displacement Assay

Fluorescence measurements were carried out in a 96-well plate (flat bottom, black) at room temperature (excitation at 510 nm, emission at 595 nm) with a Tecan Infinite M200 reader. Ethidium bromide (0.5 equivalents per base pair) was incubated with DNA (1 mg mL^{-1} , $54 \text{ }\mu\text{M}$) in a buffer solution (20 mM HEPES, 100 mM NaCl, pH 7.1) during 15 minutes prior to titration by SLNs. Increasing volumes of the stock solution ($300 \text{ }\mu\text{g mL}^{-1}$) of SLNs in a buffer solution (20 mM HEPES, 10 mM NaCl, pH 7.1 or 20 mM HEPES, 100 mM NaCl, pH 7.1) were mixed with the premixed DNA-EtBr solution (final concentration of oligonucleotide $40 \text{ }\mu\text{g mL}^{-1}$) 30 minutes prior to measurement. Standard calibration curves were fitted to a linear curve using Origin software.

Circular Dichroism (CD)

Photophysics[®] Chirascan circular dichroism spectrometer using a quartz cell with a 1 cm path length. Volumes of SLNs stock solution ($300 \text{ }\mu\text{g mL}^{-1}$, $204 \text{ }\mu\text{M}$, in buffer 20 mM Sodium Cacodylate, 100 mM NaCl, pH 6.8) were added to a solution of oligonucleotide ($650 \text{ }\mu\text{L}$, $2.72 \text{ }\mu\text{M}$, in the same buffer), the spectra were recorded from 200 to 350 nm at 20°C and data recorded in 0.5 nm increments with an average of 2 seconds.

Isothermal Titration Calorimetry (ITC)

Isothermal titration calorimetry measurements were conducted at 20°C on a MicroCal ITC₂₀₀. Volumes of 1.5 µL of oligonucleotide (147 µM in 20 mM HEPES, 100 mM NaCl, pH 7.1) were injected at 20°C into an isothermal sample chamber containing SLNs (400 µL, 7.37 µM in 20mM HEPES, 100 mM NaCl, pH 7.1) via a 40 µL rotary syringe (500 rpm). The interval time between each injection was 240 s. The initial delay prior to the first injection was 60 seconds. Injections of oligonucleotide solutions at the same concentration in buffer solution were used as a blank. The experimental data were fitted to a theoretical titration curve using the software supplied by MicroCal (OriginLab).

Transfection Protocol

CHO (Chinese Hamster Ovary) cells were grown in Dubelbecco's Modified Eagle Medium: Nutrient Mixture F-12 medium with 10 % FBS (Foetal Bovine Serum, Invitrogene) and 1 % P/S (Pennicillin/Streptomycin, Invitrogen). One day before transfection, cells were plated in the appropriate amount of medium so that they reached 80-90 % confluence on the day of the transfection experiment. Transfections were performed in 12 well plates, adding 50 µL of the appropriate nanoparticles suspensions. Transfection positive controls were obtained using LipofectamineTM 2000 (Invitrogen) following the manufacturer's procedure. Negative controls were obtained by adding the pure plasmid DNA.

7.2 Results

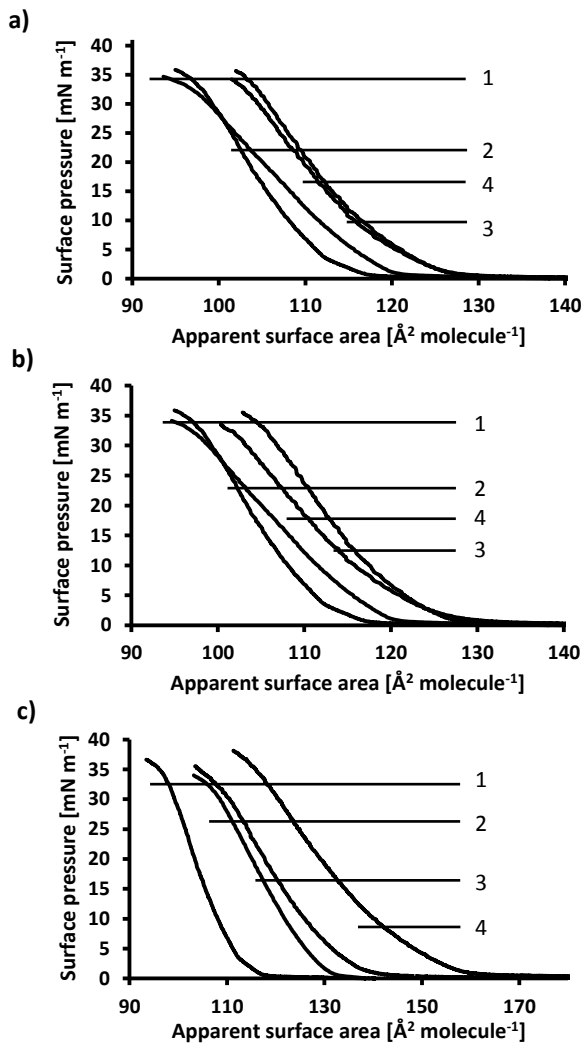


Figure S1. Π -A isotherms of GC12 monolayer in the presence of pure water (1), ATGC (2), AT (3) or GC (4) in the subphase at a concentration of a) 10^{-6} g L^{-1} , b) 10^{-5} g L^{-1} , and c) 10^{-4} g L^{-1} .

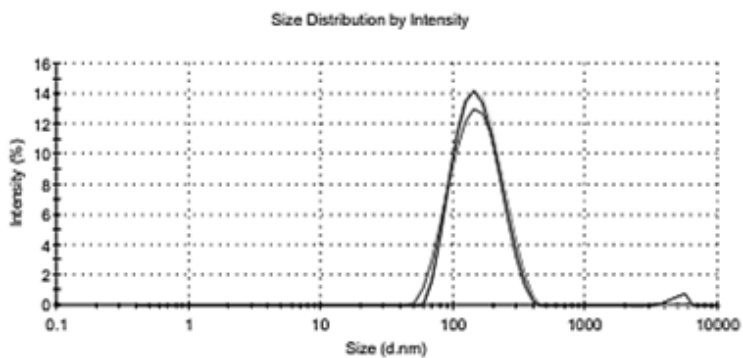


Figure S2. DLS size-distribution intensity measurements of **GC12-SLNs** ($6 \mu\text{g mL}^{-1}$) in nanopure water.

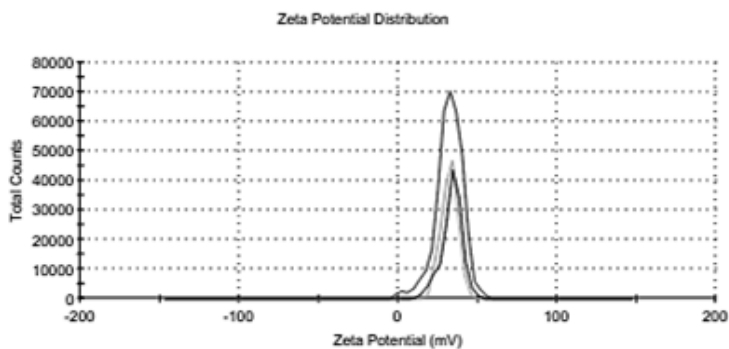
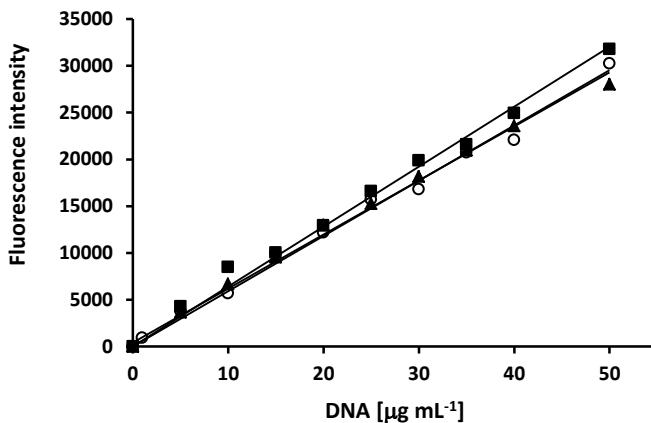
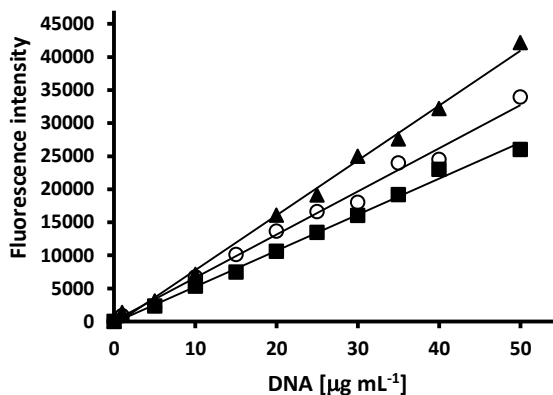


Figure S3. ζ -potential measurements of **GC12-SLNs** ($6 \mu\text{g mL}^{-1}$) in nanopure water.



Equation	F = A + B*[DNA]			R ²
		Value	Standard Error	
AT	A	0	0	0.99129
	B	640.47	10.48	
GC	A	0	0	0.99254
	B	590.07	9.51	
ATGC	A	0	0	0.9924
	B	590.79	9.03	

Figure S4. Standard calibration curve of **AT**-EtBr (square), **GC**-EtBr (circle) and **ATGC**-EtBr solution (triangle) fluorescence intensity as function of the oligonucleotide concentration ($\mu\text{g mL}^{-1}$) in a buffer solution (20 mM HEPES, 10 mM NaCl, pH 7.1) after 15 minutes of incubation with EtBr 0.5 equivalents per base pair; Table values of the parameters fitting the linear equation.



Equation	F = A + B*[DNA]			
		Value	Standard Error	R ²
AT	A	0	0	
	B	539.460	7.23	
GC	A	0	0	0.99199
	B	655.51	11.15	
ATGC	A	0	0	0.99621
	B	814.27	10.33	

Figure S5. Standard calibration curve of AT-EtBr (square), GC-EtBr (circle) and ATGC-EtBr solution (triangle) fluorescence intensity as function of the oligonucleotide concentration ($\mu\text{g mL}^{-1}$) in a buffer solution (20 mM HEPES, 100 mM NaCl, pH 7.1) after 15 minutes of incubation with EtBr 0.5 equivalents per base pair; Table values of the parameters fitting the linear equation.

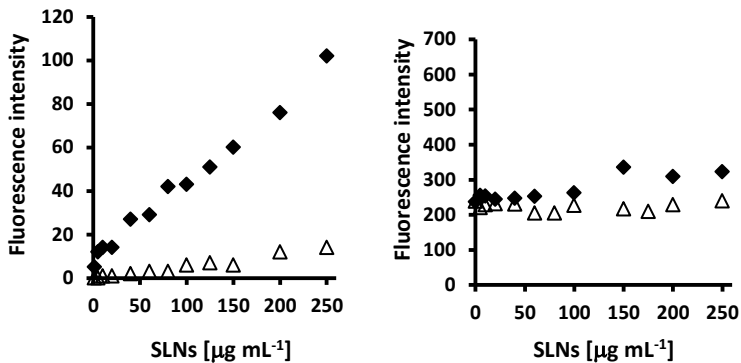


Figure S6. Fluorescence intensity of calixarene-based SLNs, **GC12** (\blacklozenge) and **4NH₂C₁₂** (\triangle) measured in nanopure water (left) and after 15 minutes of incubation with EtBr in buffer solution (20 mM HEPES, 100 mM NaCl, pH 7.1) (right).

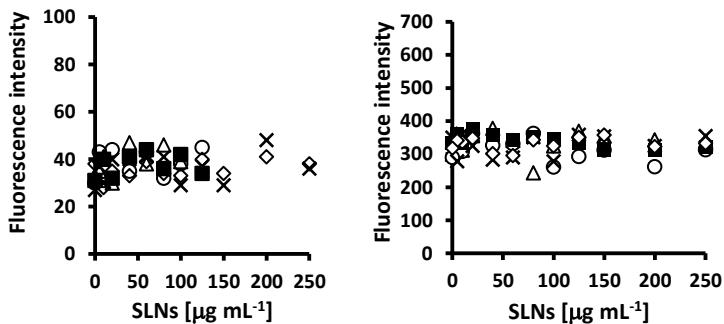


Figure S7. Fluorescence intensity of (\triangle) **1NH₃⁺4C₁₂**-SLNs, (\circ) **1,2NH₃⁺4C₁₂**-SLNs, (\blacksquare) **1,3NH₃⁺4C₁₂**-SLNs, (\diamond) **3NH₂4C₁₂**-SLNs and (\times) **4NH₂4C₁₂**-SLNs, in HEPES buffer (20mM HEPES, 10 mM NaCl, pH 7.1) (left) and in the presence of EtBr in HEPES buffer (20mM HEPES, 10 mM NaCl, pH 7.1) (right).

Experimental Section

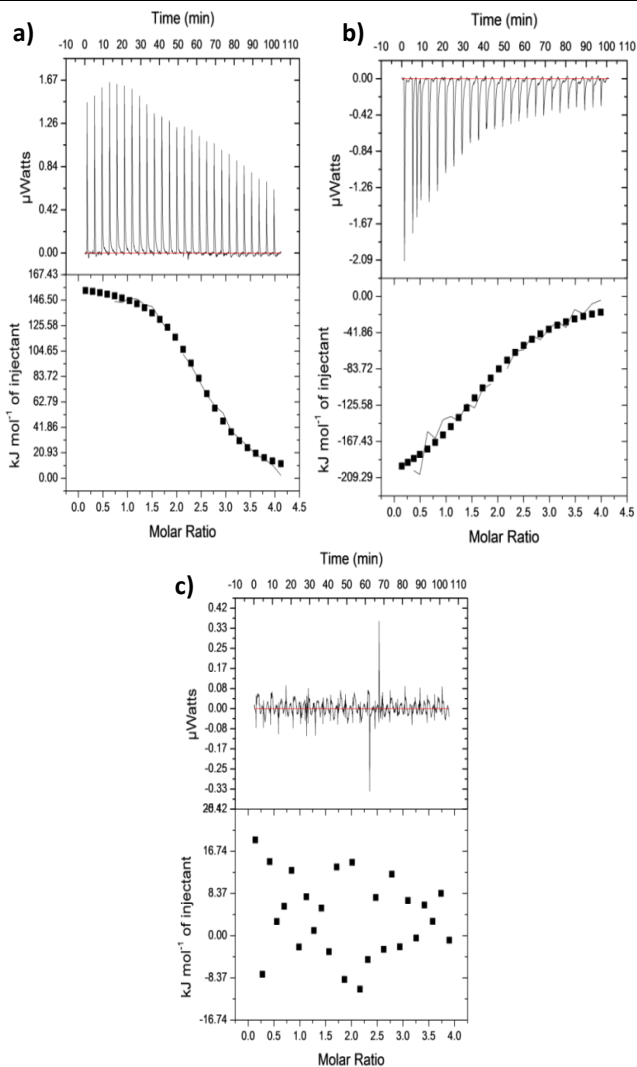


Figure S8. Isotherm titration calorimetry profiles for the binding of **GC12-SLNs** at 20°C in buffer solution (20 mM HEPES, 100 mM NaCl, pH 7.1) with a) **AT**; b) **GC** and c) **ATGC**.

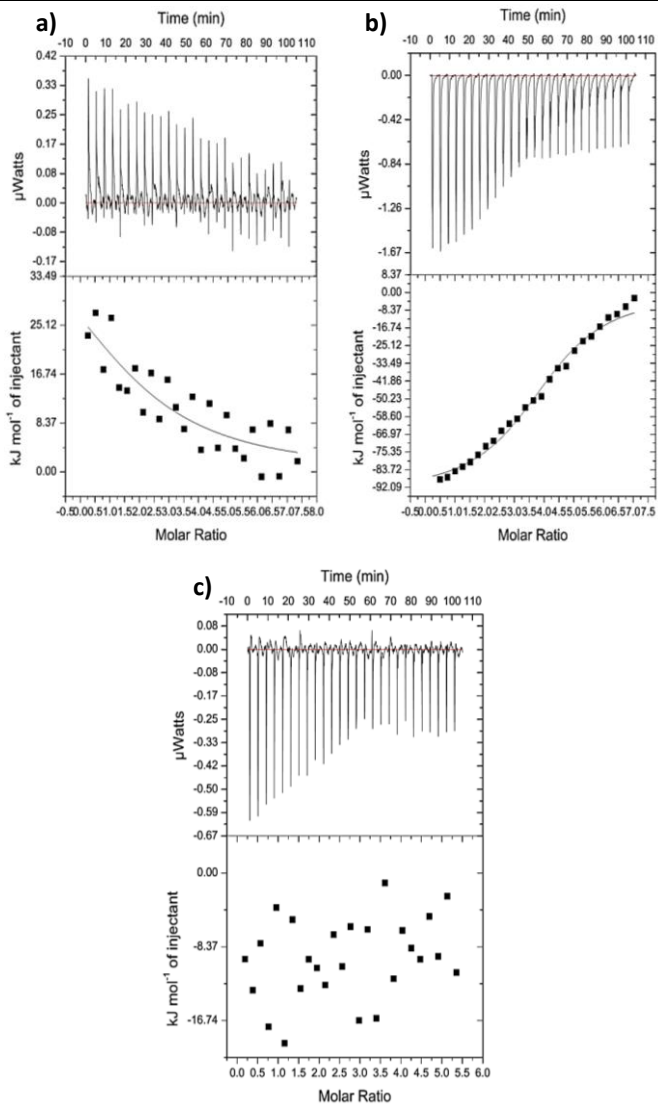


Figure S9. Isotherm titration calorimetry profiles for the binding of 4NH₂4C₁₂-SLNs at 20°C in buffer solution (20 mM HEPES, 100 mM NaCl, pH 7.1) with a) AT; b) GC and c) ATGC.

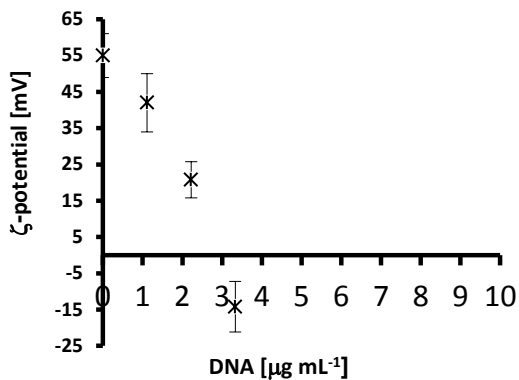


Figure S10. Variation of the ζ -potential of the the $1\text{NH}_24\text{C}_{12}$ nanoparticles as function of DNA concentration.

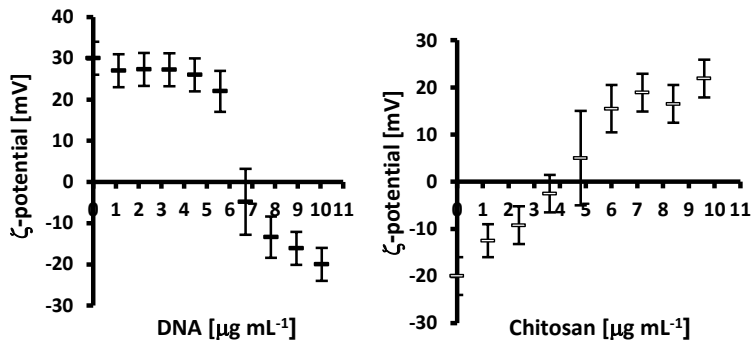


Figure S11. Variation of the ζ -potential of the $1,2\text{NH}_24\text{C}_{12}$ nanoparticles as function of DNA concentration (right) and variation of the ζ -potential of the $1,2\text{NH}_24\text{C}_{12}$ -DNA as function of the chitosan concentration (left).

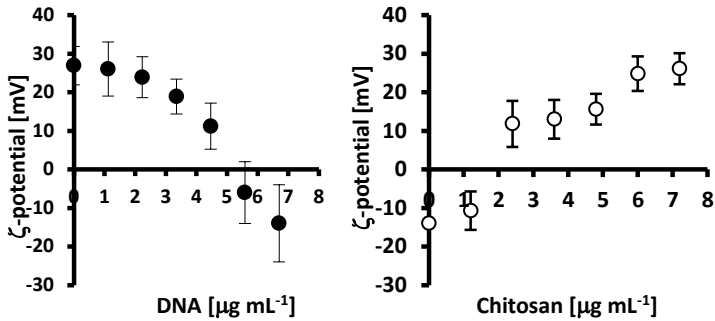


Figure S12. Variation of the ζ -potential of the $1,3\text{NH}_24\text{C}_{12}$ nanoparticles as function of DNA concentration (right) and variation of the ζ -potential of the $1,3\text{NH}_24\text{C}_{12}$ -DNA as function of the chitosan concentration (left).

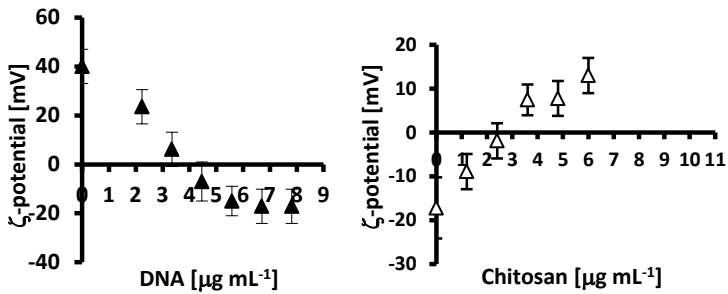


Figure S13. Variation of the ζ -potential of the $3\text{NH}_24\text{C}_{12}$ nanoparticles as function of DNA concentration (right) and variation of the ζ -potential of the $3\text{NH}_24\text{C}_{12}$ -DNA as function of the chitosan concentration (left).

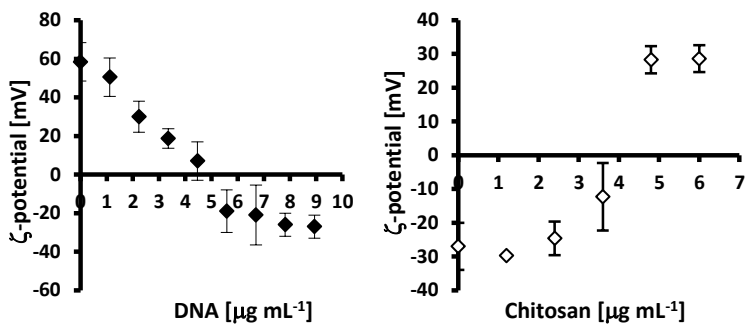


Figure S14. Variation of the ζ -potential of the $4\text{NH}_24\text{C}_{12}$ nanoparticles as function of DNA concentration (right) and variation of the ζ -potential of the $4\text{NH}_24\text{C}_{12}$ -DNA as function of the chitosan concentration (left).

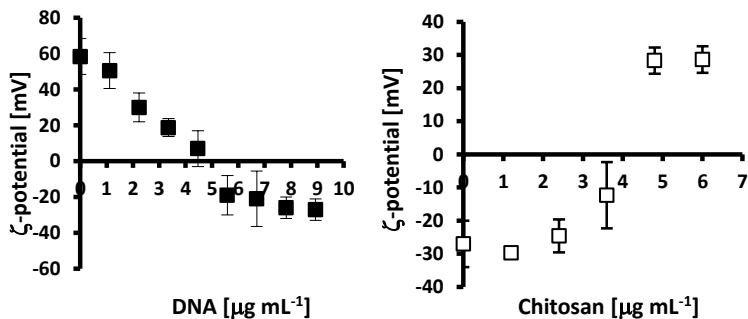


Figure S15. Variation of the ζ -potential of the GC_{12} nanoparticles as function of DNA concentration (right) and variation of the ζ -potential of the GC_{12} -DNA as function of the chitosan concentration (left).

References

1. Shahgaldian, P.; Coleman, A. W.; Kuduva, S. S.; Zaworotko, M. J., Amphiphilic behavior of an apparently non-polar calixarene. *Chem. Commun.* **2005**, (15), 1968-1970.
2. Shahgaldian, P.; Sciotti, M. A.; Pielles, U., Amino-Substituted Amphiphilic Calixarenes: Self-Assembly and Interactions with DNA. *Langmuir* **2008**, 24 (16), 8522-8526.
3. Shahgaldian, P.; Coleman, A. W.; Kalchenko, V. I., Synthesis and properties of novel amphiphilic calix-[4]-arene derivatives. *Tetrahedron Lett.* **2001**, 42 (4), 577-579.
4. Arduini, A.; Casnati, A., *Macrocyclic Synthesis: A Practical Approach*. Oxford University Press: 1996.
5. Bianco, A.; Brufani, M.; Dri, D. A.; Melchioni, C.; Filocamo, L., Design and Synthesis of a New Furanosic Sialylmimetic as a Potential Influenza Neuraminidase Viral Inhibitor. *Lett. Org. Chem.* **2005**, 2 (1), 83-88.

8 Acknowledgements

First and foremost, I would like to express my gratitude and my special thanks to my supervisor Prof. Dr. Patrick Shahgaldian for giving me the opportunity to do a PhD in his group. Notably, I am grateful for his scientific guidance, encouragement and advices he provided at key moments in my work while also allowing me to work.

I am also grateful to Prof. Dr. Thomas Ward to act as “Doctor Father”.

I would also like to thank Prof. Dr. Uwe Pieles and all the members of his group, whom I worked with. Special thanks to J.B. for the great time during my PhD thesis and for the relaxing lunch breaks.

Acknowledgements

I would like to thank René Prétôt for his time and knowledge on the transfection experiments, Markus Neuburger for trying to elucidate the crystal structures of my molecules.

Further thanks go to my lab colleagues, Mohamed, Negar, Ludovico, Rita, Sabine and Alessandro and all the former members of the group for contributing to the pleasant working ambiance. If you know the “banana position” well then, we went together up to 4000 m to skydive, and I thank you for this amazing experience!!!

Finally, I would like to thank the SNSF, not only for providing the funding which allowed me to undertake this research, but also for giving me the opportunity to attend conferences and meet so many interesting people.

9 Curriculum Vitae

PERSONNAL

Name	Vanessa Rullaud
Address	Luftstrasse 24, 8820 Wädenswil (Switzerland)
Email	rullaud.vanessa@gmail.com

EDUCATION

2010-2014	PhD. in Organic chemistry, <i>University of Applied Sciences, ICB, Muttenz, Switzerland.</i>
2008-2010	M.Sc. in Organic chemistry, <i>Université de Bourgogne, Dijon, France.</i>
2005-2007	B.Sc. in Chemistry, <i>Université de Bourgogne, Dijon, France.</i>

RESEARCH EXPERIENCE

- 2010-2014 *University of Applied Sciences, ICB, Muttenz, Switzerland.*
“Calixarene-based amphiphiles: Synthesis, Self-assembly and Interaction with DNA”.
- 2009-2010 *Université de Bourgogne, ICMUB, Dijon, France.* “New phosphoniums ligands for selective hydrogenation of nitroarenes in ionic liquids”.
- 2010 *Eberhard Karls Universität, Tübingen, Germany.* “Imidazolium ligands synthesis”.
- 2009 *Erasmus student, Nottingham Trent University, Nottingham, England.* “Silk – Mineral Binding Peptides Chimera: Chemical Synthesis and Biomineralisation”.

TECHNICAL SKILLS

Chemistry

Multi-steps synthesis of supramolecules, organic/organometallic synthesis under inert atmosphere (Shlenk lines and glove boxes)
Chemical separation and purification: titration, extraction, distillation, column chromatography and crystallization
Supramolecular self-assembly as nanoparticles
Monolayer self-assembly: Langmuir monolayer at the air-water interface and Langmuir-Blodgett film

Analytical method

Nuclear Magnetic Resonance Spectroscopy (NMR)

Mass spectroscopy: Electrospray (ESI-MS) and MALDI-TOF

Chromatography: High Performance Liquid Chromatography (HPLC),

Thin Layer Chromatography (TLC)

UV-Vis Absorption and fluorescence Spectroscopy, Fourier transformed infrared (FTIR)

Physico-chemical analysis

Dynamic Light Scattering (DLS) and ζ -potential

Atomic force microscopy (AFM)

Basic knowledge of electronic microscopy characterization and analysis (SEM and TEM)

Ellipsometry, Brewster angle microscopy

Circular dichroism, Isothermal titration calorimetry (ITC)

Biology

Fluorescence displacement assay

Electrophoresis

Solid-phase peptide synthesis

IT

MS Office, ChemDraw, Mercury, Origin, Scifinder, Reaxys, Endnote,

Blender

PUBLICATIONS

“DNA surface coating of calixarene-based nanoparticles: a sequence-dependent binding mechanism” V. Rullaud, M. Siragusa, A. Cumbo, D. Gygax and P. Shahgaldian, **Chem. Commun.**, 2012, **48**, 12186-12188.

“Langmuir-Blodgett Monolayer Stabilization Using Supramolecular Clips” N. Moridi, C. Wäckerlin, V. Rullaud, R. Schelldorfer, Thomas A. Jung and P. Shahgaldian, **Chem. Commun.**, 2013, **49**, 367-369.

“Sequence-Specific DNA Interactions with Calixarene-Based Langmuir Monolayers” V. Rullaud, N. Moridi and P. Shahgaldian, **Langmuir**, 2014, **30** (29), 8675-8679.

TALKS AND POSTERS

European Winter School on Physical Organic Chemistry-on Supramolecular Chemistry in water (E-WISPOC 2013), Bressanone, Italy, Jan 27-Feb 1, 2013, **Poster and oral presentation.**

SwissNanoconvention 2013, Basel, May 23-24, 2013, **Poster.**

The 8th International Symposium on Macrocyclic and Supramolecular Chemistry (8-ISMSC), Arlington VA, USA, July 7-11, **Poster.**

12th International Conference on Calixarenes (Calix 2013), St-John's NL, Canada, July 14-17, 2013, **Poster and oral presentation.**

SwissNanoconvention 2014, Brugg, May 21-22, 2014, **Poster.**

The 9th International Symposium on Macrocyclic and Supramolecular Chemistry (ISMSC-9), Shanghai, China, June 7-11, **Poster**.

TRAVEL GRANT

COST action 1005 (Supramolecular chemistry in water)

ADDITIONAL INFORMATIONS

Languages: French (Mother tongue)
 English (Fluent *written* and *spoken*)
 German (Basic knowledge)